A FIELD STUDY OF THE VISIBLE AND NEAR-INFRARED SPECTRAL REFLECTANCE AND ATTENUATION OF SOLAR RADIATION BY SNOW

by

Anil Vishnupant Kulkarni

A Thesis Submitted to the Faculty of Graduate Studies and Research in Partial Fulfillment of the Requirements for the Degree of Master of Science

Department of Geography

McGill University

December, 1986

ABSTRACT

Snow cover spectral reflectance and attenuation characteristics were observed using a Li-1800 portable spectroradiometer at Schefferville, Quebec. A specially designed fiber optic probe was used for measurements in the snow cover. A Radio Shack TRS-80 model 100 portable computer was used to transfer data from the spectroradiometer to 3.5 inch microdisks in the field. This greatly increased the throughput of the field instrumentation and made it possible to collect data at high spectral resolution in the wavelengths between 400 to 1100 nm.

The effect of liquid water content of snow on its spectral reflectance was investigated by measuring the change in spectral reflectance associated with changes from a melting to non-melting and again to melting condition of the snow cover. A drop in reflectance of 18 per cent was observed around 960 nm when the snow changed from dry to wet. A rise of 9 per cent was observed at the same wavelength for a change from wet to dry. The study shows that the ratio between wavelengths 580-600 and 960-980 nm is generally greater than 1.34 for melting snow and less than 1.30 for dry snow. These observations suggest that the wavelengths around 960 nm could be more indicative of the liquid water content of snow than other regions of the electromagnetic spectrum between 400 to 1100 nm.

Spectral attenuation of solar radiation was measured by

multi-level observations of solar radiation intensity in the snow cover. The lowest attenuation was observed around 580 nm and the maximum from 990 to 1100 nm. The extinction coefficient varied depending on the depth of observation inside the snow pack. The attenuation was greater in winter than in spring. The maximum penetration depth was observed around 580 nm, where radiation can penetrate up to 140 cm in spring. The minimum penetration of only a few millimeters occurs in the wavelengths between 1000 to 1100 nm.

RESUME

La réflectance spectrale et les caractéristiques d'atténuation du manteau nival ont été observées à Schefferville, Nouveau-Québec, à l'aide d'un spectroradiomètre portatif Li-1800. Une sonde de fibre optique spécialement créée a été utilisée pour la prise de mesures dans le manteau nival. Un ordinateur portatif Radio Shack TRS-80, modèle 100, a servi sur le terrain à transférer les données fournies par le spectroradiomètre vers des microdisques de 3.5 pouces. Ceci a permis d'augmenter largement le rendement des instruments sur le terrain et de rendre possible l'enregistrement de données d'une haute résolution spectrale, pour des longueurs d'onde variant de 400 à 1100 nm.

On a étudié l'effet de la teneur en eau liquide de la neige sur sa réflectance spectrale en comparant cette dernière aux changements survenant lorsque le manteau nival passe de l'état de fusion à l'état gelé, puis lorsque la neige se remet à fondre. On a noté une baisse de réflectance de 18% autour de 960 nm lorsque la neige sèche devint mouillée. De plus, une augmentation de 9% a été observée à la même longueur d'onde lors de l'assèchement de la neige mouillée. L'étude indique que le rapport entre les bandes 580-600 nm et 960-980 nm dépasse généralement 1.34 pour la neige en fusion et n'excède pas 1.30 pour la neige sèche. Ces observations suggèrent que les longueurs d'onde voisines de 960 nm pourraient indiquer la teneur

en eau liquide de la neige mieux que n'importe laquelle autre région du spectre électromagnétique entre 400 et 1100 nm.

L'atténuation spectrale du rayonnement solaire a été mesurée en observant l'intensité du rayonnement solaire à plusieurs niveaux dans le manteau nival. La plus faible atténuation a été notée aux environs de 580 nm alors que l'atténuation maximale se situait entre 990 et 1100 nm. Les coefficients d'extinction variaient suivant la profondeur du point d'observation dans le manteau nival. Aussi, l'atténuation était plus élevée en hiver qu'au printemps. La plus grande pénétration a été observée autour de 580 nm; à cette longueur d'onde, au printemps, le rayonnement peut pénétrer jusqu'à une profondeur de 140 cm. Par contre, on a enregistré une pénétration de quelques millimètres seulement pour les longueurs d'onde entre 1000 et 1100 nm.

TABLE OF CONTENTS

ABSTRACT .....Page I

TABLE OF CONTENTS V

LIST OF FIGURES IX

LIST OF TABLES XIV

ACKNOWLEDGEMENTS .....X V

CHAPTER I: INTRODUCTION 1

1.1 Research objective 1

1.2 Background 1

1.3 Organizations of the thesis 3

1.4 Study area and field work 4

CHAPTER II: LITERATURE REVIEW AND
THEORETICAL BACKGROUND 7

2.1 Definitions 7

2.2 Spectral reflectance of snow 9

2.3 Spectral attenuation of solar radiation
by a snow pack 13

2.4 Different techniques to estimate liquid water
content of snow 15

2.4.1 The centrifugal method 17

2.4.2 The capacitance method 18

2.4.3 The solution method 18

2.4.4 The calorimetric method 19

2.5 Techniques to estimate grain size 22

CHAPTER III: METHODS OF DATA ACQUISITION 24

3.1 Introduction 24

3.2 Data acquisition system 24

3.2.1 Radiation measurements 24

3.2.1.1 Reflectance measurements 26

3.2.1.2 Attenuation measurements 28

3.2.1.3 Sources of error 30

3.2.2 Measurements of liquid water content of snow 30

3.2.2.1 The freezing calorimeter equipment 30

3.2.2.2 Estimation of the calorimetric constant..32

3.2.2.3 Field procedure 33

3.2.3 Grain size measurements 34

3.2.4 Other data 35

CHAPTER IV: THE INFLUENCE OF CHANGE IN LIQUID WATER CONTENT AND GRAIN SIZE ON ITS SPECTRAL REFLECTANCE 36

4.1 Introduction 36

4.2 Effects of liquid water content 36

4.2.1 Liquid water content of snow pack 35

4.2.2 Change in reflectance from dry to wet snow...39

4.2.3 Change in reflectance from wet to dry snow...43

4.2.4 Repeatability of the results 43

4.3 Effect of grain size of snow on

spectral reflectance 53
4.3.1 Repeatability of the results 55
4.4 Grain size vs. liquid water content 58
4.4.1 Repeatability of the results 58

CHAPTER V: ATTENUATION OF SOLAR RADIATION BY THE SNOW COVER 63
5.1 Introduction 63
5.2 Differential attenuation of solar radiation with wavelength 63
5.2.1 Repeatability of the results 66
5.3 Variations in the extinction coefficient with depth 66
5.4 Depth of penetration in winter and spring 68
5.4.1 Depth of penetration of solar radiation in winter 68
5.4.2 Depth of penetration of solar radiation in spring 72
5.4.2 Comparison of the penetration of solar radiation in winter and spring 74
5.5 Maximum penetration depth of solar radiation 77
5.5.1 Variations in penetration depth with wavelength 78
5.5.2 Variations in the penetration depth due to variations in the extinction coefficient..78
5.5.3 Changes in maximum penetration depth from winter to spring 80

CHAPTER VI: CONCLUSIONS AND RECOMMENDATIONS 85

6.1 Conclusions 85

6.1.1 Spectral reflectance 85

6.1.2 Spectral attenuation 87

6.1.3 Additional conclusions 88

6.2 Some recommendations for future research 88

REFERENCES 90

APPENDIX A GRAPHS SHOWING SPECTRAL ATTENUATION AND EXTINCTION COEFFICIENT AT SITE 2 100

LIST OF FIGURES

1.1. A. Location map showing Schefferville.
B. Location map showing Field site 1
and Field site 2 5

2.1. Variation of snow spectral reflectance
with wavelength.....10

2.2. Effects of grain size of snow on the planetary
reflectance of a snow surface.....11

2.3. Effect of soot on snow albedo.....14

2.4. Extinction coefficient of diffuse radiation for
different wetness and foreign matter content.....16

3.1. Field set up for spectral reflectance
data collection.....27

3.2 Field set up for spectral attenuation
data collection.....29

4.1 Temperature Vs. Time graphs in the calorimeter.....37

4.2 Temperature Vs. Time graphs in the calorimeter.....38

4.3 Spectral reflectance curves for snow pack.....41

4.4 Changes in reflectance due to variation in liquid water content of snow cover.....42

4.5 Spectral reflectance curves for snow cover.....45

4.6 Changes in reflectance due to variation in liquid water content of snow pack.....46

4.7 Histogram showing change in reflectance after ratio.....51

4.8 Spectral reflectance of snow for different grain sizes.....54

4.9 Effect of change in grain size from 0.5-1 to 2-4 mm on spectral reflectance.....54

4.10 Effect of changes in grain size on spectral reflectance.....56

4.11 Effect of changes in grain size from (A) 0.25-0.5 to 0.5-1; (B) 0.25-0.5 to 1.0-2.0; (C) 0.25-0.5 to 2.0 to 4.0 mm on spectral reflectance.....56

4.12 Histogram showing change in ratio due to variation in grain size. Classes explained in Table 4.5.....56

4.13 Variation in spectral reflectance of snow due to change in (A) grain size from 0.5-1 to 1-2 mm; (B) snow condition from dry to wet and (C) snow condition from wet to dry.....59

4.14 Variation in spectral reflectance of snow due to change in (A) grain size from 0.25-0.5 to 1-2 mm; (B) snow condition from dry to wet and (C) snow condition from wet to dry.....61

4.15 Histogram showing changes in ratio due to variation in grain size and liquid water content. Classes explained in Table 4.5.....62

5.1 Measured solar radiation (A), attenuation (B) and extinction coefficient (C) at 0 cm (1), 10 cm (2), 20 cm (3) and 30 cm (4) in a snow pack.....64

5.2 Measured solar radiation (A), attenuation (B) and extinction coefficient (C) at 0 cm (1), 10 cm (2), 20 cm (3), 30 cm (4) in a snow pack..... 67

5.3a Variations in extinction coefficient due to

depth of observation in snow pack. Measured solar radiation (I) and extinction coefficient (II) from 2 (A1) to 18 (A8) cm depth at intervals of 2 cm.....69

5.3b Variations in extinction coefficient due to depth of observation in a snow pack. Measured solar radiation (I) and extinction coefficient (II) from 18 (1) to 30 cm (4) at intervals of 4 cm.....70

5.4 Attenuation of solar radiation in winter (A) Measured solar radiation at 0 cm (1), 10 cm (2), 20 cm (3) and 40 cm (4); (B) attenuation and (C) extinction coefficient.....71

5.5 Attenuation and extinction coefficient of solar radiation in spring. (A) Measured solar radiation at 0 (1), 10 (2), 20 (3) and 30 cm (4); (B) attenuation and (C) extinction coefficient....73

5.6a Comparision of attenuation and extinction coefficient between winter (DA3) and spring (SR).....75

5.6b Comparision of attenuation and extinction coefficient between winter (DA3) and spring SR).....76

5.7 Variations in penetration depth with wavelength...79

5.8 Variations in penetration depth due to extinction coefficient. Depths of observation from 10 (1) to 60 cm (6) at intervals of 10 cm....81

5.9 Variation in penetration depth due to extinction coefficient Depths of observation from 10 (1) to 60 cm (6) at intervals of 10 cm.....82

5.10 Maximum penetration depth in (A) winter and (B) spring.....84

LIST OF TABLES

Table — Page

1.1. Data collection schedule..... 6

4.1. Liquid water content of snow samples..... 40

4.2. Drop in spectral reflectance from dry to wet snow..... 47

4.3. Rise in spectral reflectance from wet to dry snow..... 48

4.4. Ratios between visible and near infrared radiation for dry and wet snow..... 49

4.5. Difference in ratio due to variation in liquid water..... 52

ACKNOWLEDGEMENTS

I would like to thank my supervisor, Dr. H.B. Granberg, now at CARTEL, University of Sherbrooke, for his encouragement, guidance and helpful discussions during all stages of this study. I also wish to thank Messrs. C.A. Nadeau, D.T. Desrochers and C.M. Kingsbury for their help during field investigations and suggestions during writing of this thesis.

I wish to thank Dr. J.E. Lewis for lending me a Li-1800 portable spectroradiometer. The fiber optics probe was designed and manufactured by Dr. H.B. Granberg. I am also thankful to the the Canadian Commonwealth Scholarship and Fellowship Administration, Ottawa for their scholarship support. Partial funding for development of the field data acquisition system came from NSERC and EMR grants to Dr. H.B. Granberg. Logistical support for field operations was provided by the McGill Subarctic Research Station, Schefferville, Quebec.

I also thank to the Indian Space Research Organization for sanctioning study leave to complete this thesis.

Last, but not least, I would like to express my gratitude to my wife Vinda for her understanding and patience during the completion of this thesis.

1. INTRODUCTION

1.1 Research objective

The objective of this investigation is twofold; First, it aims to document the spectral reflectance and attenuation of solar radiation by a natural snow cover. Secondly, it aims to develop a better understanding of the effects of liquid water and grain size on the spectral reflectance and attenuation of solar radiation by snow in the visible and near-infrared region of the electromagnetic spectrum.

1.2 Background

The rapidly growing population of the world has increasingly imposed demands upon water resources. In order to meet these additional demands, existing water supplies must be managed efficiently. Runoff from melting snow contributes considerably to stream flow. The knowledge of snow pack characteristics and runoff relationships is important in efficient and overall management of water resources.

One of the tools in water resources management is hydrologic modelling of river basins. Information generated from satellite images can be used in these models (Rango, 1985). However, in order to derive the proper information from satellite images, it is essential to understand the effects of the changing

physical properties of snow on its spectral reflectance and attenuation of solar radiation. Two important physical properties are the free water content of the snow pack and its grain size. Grain size is important, because the albedo of snow decreases with an increase in grain size (Dozier et al. 1981; Warren 1982).

The liquid water content of snow provides pertinent information, since it may be used to distinguish between a melting and non melting snowcover. This information can be incorporated in snow-melt runoff models. In satellite images a reduction in the near-infrared spectral reflectance of a snowcover has been observed due to melting of a snow pack (Barnes et al., 1975; Kulkarni and Navalgund, 1982). Using an albedo model, Dozier et al. (1981) predicted that the lowering of reflectance is not caused by an increase in liquid water content, but rather by an increase in grain size. This prediction was supported by laboratory observations of O'Brian and Munis (1975), who reported that an increase in spectral reflectance was not observed after refreezing of snow. However, Staenz and Haefner (1981) did observe a distinct increase in the ratio between Landsat 4 MSS bands (500 to 600 nm) and 7 (800 to 1100 nm) due to melting snow, (i.e. a greater drop in near infrared reflectance than in visible reflectance due to melting snow).

In order to interpret satellite images and understand the

spectral reflectance characteristics of snow, it is important to know more about the mechanisms involved in the attenuation of solar radiation by snow. If a significant amount of solar radiation can penetrate through the snow pack, then the characteristics of the substrate can affect the reflectance of the snow surface and influence the runoff processes at the snow-soil interface. Even though a significant amount of theoretical work has been done to understand the penetration of solar radiation through snow (Giddings and LaChapelle, 1961; Barkstrom and Querfeld, 1975; Wiscombe and Warren, 1981), not many field investigations have been conducted to verify these models.

1.3 Organization of the thesis

The organization of the present thesis reflects the planning and execution of the investigation. A literature review and theoretical background is given in Chapter II. The chapter is subdivided into five subsections dealing with (i) general theory of radiative transfer, (ii) factors affecting the spectral reflectance of snow, (iii) factors affecting the penetration of solar radiation through snow, (iv) techniques used to estimate the liquid water content of snow and (v) techniques used to estimate grain size.

Chapter 3 concerns field methods. The data acquisition system, the techniques to collect radiometric data, measurements of

liquid water content and grain size of snow and acquisition of other data are discussed.

Field observations on the effects of liquid water and grain size of snow on its spectral reflectance are discussed in Chapter 4. In Chapter 5 measurements relating to the attenuation of solar radiation by snow are discussed. In Chapter 6 the conclusions of this study and some recommendations for future work are given.

1.4 Study area and fieldwork

The present investigation was conducted at a site near Schefferville, Quebec, Canada (54° 48'N, 66° 49'W). The locations of the field sites are indicated in Figure 1.1. Site 1 was used in May 1985 and Site 2 in February and April 1986. These sites are well protected from wind causing admixture of foreign matter and were selected for easy access.

Reconnaissance field work was conducted in February, 1985. In May 1985, field data were collected to study effects of liquid water and grain size on spectral reflectance of the snow pack. The fieldwork relating to spectral attenuation of solar radiation by the snow cover was undertaken in February and April, 1986. The data collection schedule is given in Table 1.1. A complete set of plots of the attenuation data is given in Appendix A.

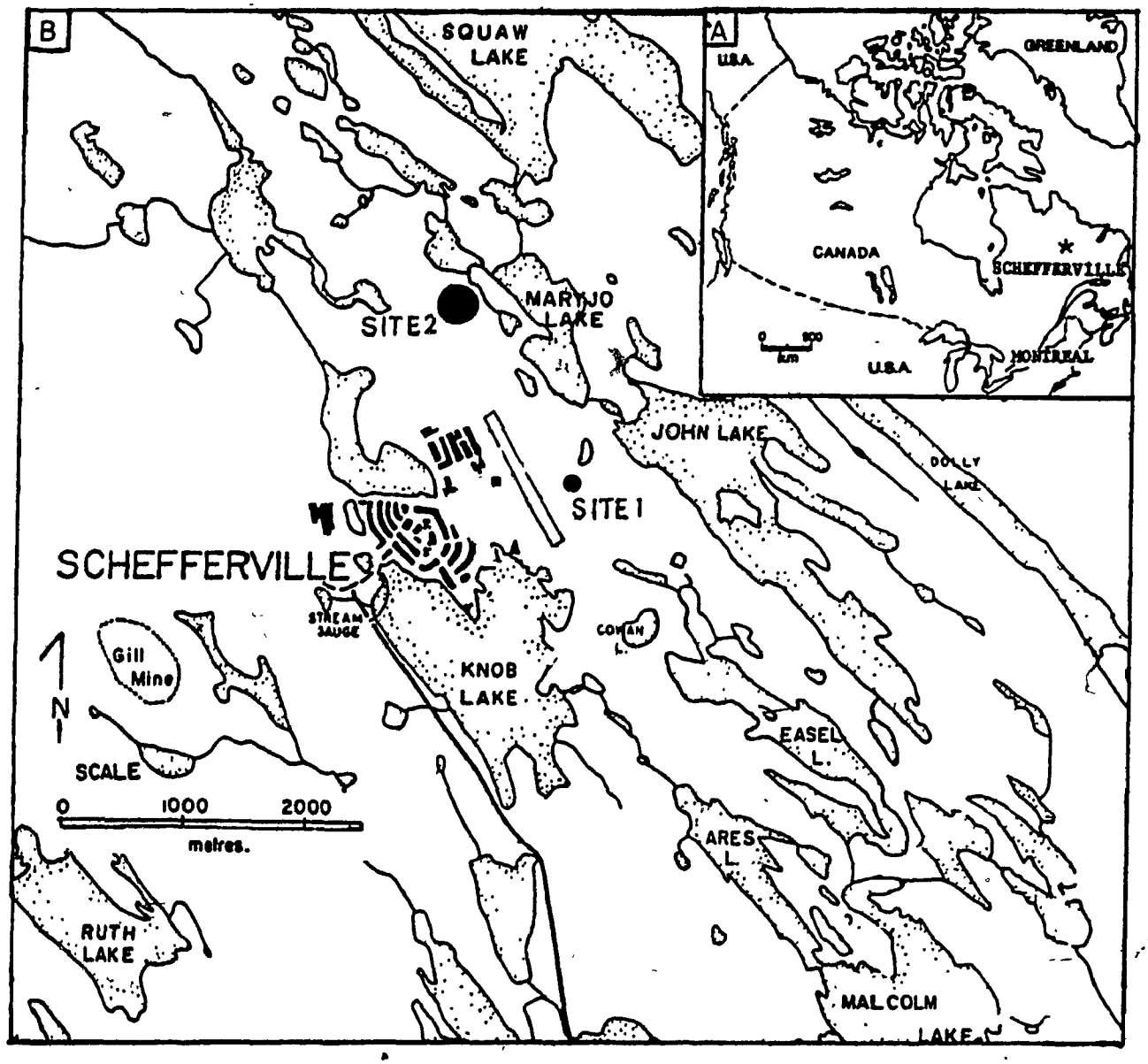

Figure 1.1: A. Location map showing Schefferville. B. Location map showing Field site 1 and Field site 2.

Date	Files/ profile	Date	Files/ profile	Date	Files/ profile
4/25/85	DI25 DI26 DI27	5/03/85	DI39 DI40	5/07/85	DI41 DI42
5/08/85	DI43 DI45	5/12/85	DI51	5/13/85	DI53 DI54 DI55 DI56
5/14/85	DI57 DI58 DI59	2/13/86	DA25 DA26 DA27 DA28	2/18/86	DA1 DA2
2/20/86	BC CD SE	4/21/86	MO1 MO2	4/23/86	WE1 WE2
4/26/86	SR	4/29/86	TU1 TU2 TU3		

Table 1.1: Data collection schedule

2. LITERATURE REVIEW AND THEORETICAL BACKGROUND

2.1 Definitions

The radiation balance at a snow surface can be described by the following equation:

$$Qn = G - So + Li - Lo \qquad (2.1)$$

where Qn = Net all wave radiation at snow surface

G = Incoming or global shortwave radiation

So = Reflected or outgoing shortwave radiation

Li = Incoming longwave radiation

Lo = Outgoing longwave radiation

Reviews of this topic are given by Petzold (1974) and Male and Granger (1981).

The global radiation consists of direct and diffuse solar radiation. The diffuse radiation component is produced by atmospheric scattering. Both components are reflected, absorbed and transmitted by the snow cover.

The ability of snow to reflect solar radiation is generally referred to as its albedo (A), which is defined as

$$A = R / I \qquad (2.2)$$

where R is the reflected and I is the incident radiation. The albedo of snow varies with wavelength, angle of incidence of the incoming radiation and character of the surface (Sauberer, 1938; Trainor, 1947; Barkstrom, 1972; Barkstrom and Querfeld, 1975 and O'Brian and Munis, 1975). Therefore, the reflectance, r of a snow surface is usually defined for narrow spectral intervals. The albedo may then be defined as (Mantis, 1951; Male and Gray, 1981)

$$A = \int_{\lambda_1}^{\lambda 2} r\lambda \; I\lambda \; d\lambda \; / \int_{\lambda_1}^{\lambda 2} I\lambda \; d\lambda \qquad (2.3)$$

The limits of integration are $\lambda 1$ and $\lambda 2$ and represent the lower and upper spectral limits of the measuring instrument.

For a homogeneous snow pack the attenuation of solar radiation may be approximated by the Bouguer-Lambert law (Trainor, 1947; Mantis, 1951; Dunkle and Bevans, 1956 and Giddings and La Chapelle, 1961):

$$Iz = Io \exp(-bz) \qquad (2.4)$$

where Iz = Radiation intensity at any depth z (W/m2),

Io = Radiation intensity at the snow surface (W/m2),

b = Extinction coefficient (1/cm) and

z = Depth (cm).

The magnitude of the extinction coefficient depends on such factors as wavelength, particle size, snow density and depth

of snow (Mellor, 1966; Bohren and Barkstrom 1974; O'Neill and Gray, 1972). In addition, radiation penetration is extremely sensitive to foreign matter in the snow (Manz, 1974).

2.2 Spectral reflectance of snow

In general, the reflectance of snow is high in the red end of the visible spectrum (600 to 700 nm). It tends to decline in the near infrared region until 1090 nm (Figure 2.1), where a slight gain in reflectance occurs and gives a minor peak at approximately 1090 to 1100 nm (Trainor, 1947; O'Brian and Munis, 1975; Bolsenga and Kistler, 1982). The reflectance also shows minor peaks around 1830 and 2240 nm with a strong depression of the reflectance around 1950 and 2050 nm (O'Brian and Munis, 1975).

The reflectance of snow decreases with increasing grain size. Bohren and Barkstrom (1974) predicted that the albedo under diffuse illumination is independent of density and proportional to the square root of grain size. Dozier (1984) predicted that snow reflectance is sensitive to grain size in Band 4 of the Thematic Mapper (TM4) (780-900 nm) but not in the TM1 (450-520 nm) or TM2 (530-610 nm) bands (Fig. 2.2). A delta-Eddington radiative transfer model and Thematic Mapper data from Landsat 4 were used.

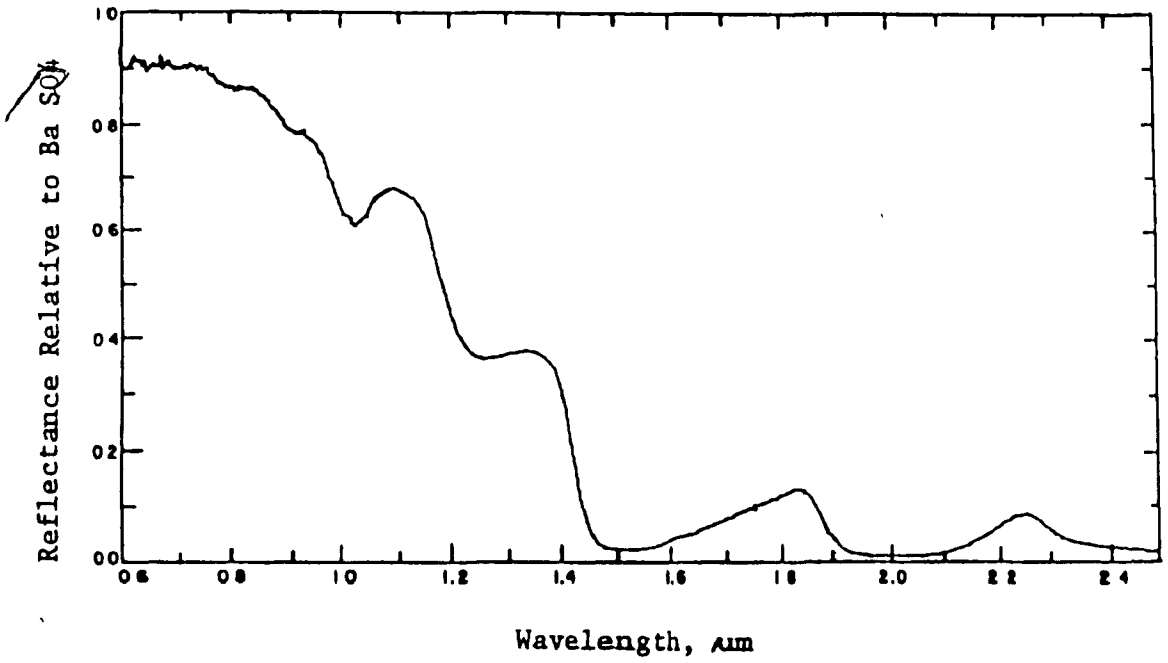

Fig. 2.1: Variation of snow spectral reflectance with wavelength (after O'Brian and Munis, 1975).

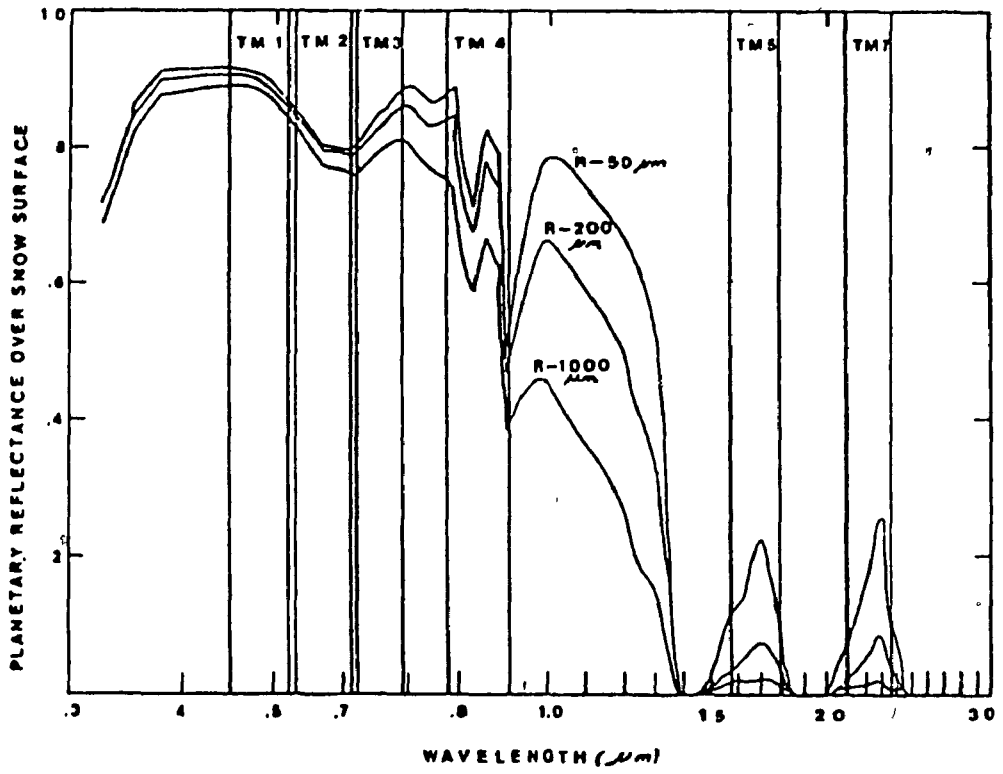

Fig 2.2: Effect of snow grain size on the planetary reflectance of a snow surface. TM 1, TM 2 etc. are the Thematic Mapper spectral bands and R is grain size (after Dozier, 1984).

The natural aging processes of snow can significantly transform snow grain size, shape and cohesion (Colbeck, 1982). Therefore, aging can in a general way influence reflectance. Dunkle and Bevans (1956) predicted that the albedo of snow should decrease with increased age. This general prediction was supported by the laboratory observations of O'Brian and Munis (1975). They observed a significant decrease in reflectance in the near infrared but a small increase in the red region of the spectrum.

Staenz and Haefner (1981) observed that the albedo of snow decreased due to an increase in liquid water content. Such a decrease may be due to an effective increase in grain size because of clustering of two or three snow crystals under wet snow conditions (Colbeck, 1979; Dozier et al., 1981). For wavelengths less than 1000 nm, the spectral refractive index of ice is very close to that of snow (Irving and Pollack, 1968). Therefore, a decreased albedo may be due to the increased crystal size rather than the liquid water content (Dozier et al., 1981; Wiscombe and Warren, 1981). This prediction was further supported by O'Brian and Munis (1975), who observed negligible increases in reflectance (except near 1400 and 2100 nm) after refreezing of snow.

The effect of snow contaminants such as atmospheric aerosols or carbon soot is at a maximum in the visible region and declines with increasing wavelength. The drop in reflectance

is at a maximum between 300 and 700 nm and declines up to 1300 nm (Figure 2.3). The effect of contaminants is negligible beyond 1300 nm (Warren and Wiscombe, 1981).

Mellor (1966) observed that 20 to 60 percent of the reflected intensity from dense dry snow in the visible spectrum were due to subsurface backscattering. The thickness of snow therefore influences its reflectance. Giddings and La Chapelle (1966) reported that if the grain size of snow is greater than 0.5 mm and the snow depth is greater than 10 to 20 cm, then the spectral reflectance becomes effectively independent of snow thickness. By using an extinction coefficient, Barkstrom and Querfeld (1975) predicted that the spectral reflectance is independent of thickness beyond 5.3 mm.

On the other hand, Wiscombe and Warren (1981), by using a delta-Eddington approximation for multiple scattering, and Mie theory for single scattering predicted an effectively semi-infinite snow depth for a melting snow pack of a water equivalent of 20 cm. Observations of O'Brian and Koh (1981) agree with this prediction.

2.3 Spectral attenuation of solar radiation by a snow pack

A variety of techniques have been used to study the transmission of solar radiation through a snow pack.

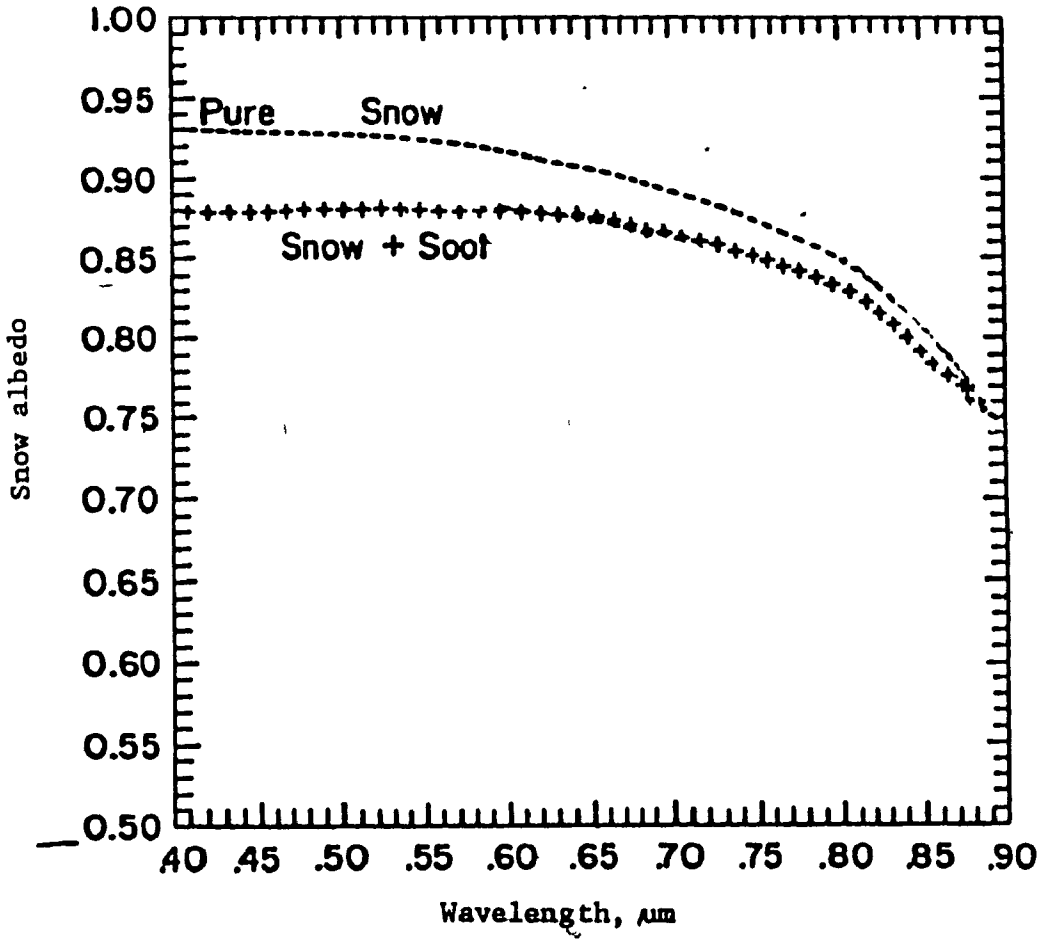

Fig. 2.3: Effect of soot on snow albedo (after Warren and Wiscombe, 1981).

Sauberer (1938), using a photoelectric cell and a variety of filters, observed that more energy was transferred in the blue and violet and that a large percentage of radiation was absorbed at 800 nm for wet snow. Manz (1974) reported that radiation penetration is extremely sensitive to the foreign matter content of the snow. The extinction coefficient between 450 and 950 nm is more sensitive to foreign matter than to variations in wetness or density of the snow (Fig. 2.4; Male and Gray, 1981). Weller (1969) reported that in a ripening snowpack the extinction coefficient decreases as the grain size of the snow increases (O'Neill and Gray, 1972).

Schwerdtfeger and Weller (1977) observed the extinction of the allwave radiation flux in clean and dry snow on the Antarctic Plateau. Warren (1982) using this data set observed that the exponential decay does not apply in the top 40 cm or so due to rapid change in the spectral composition of the downward flux. In addition, he predicted that visible radiation can penetrate up to 100 cm and that blue light around 460 nm can penetrate more than 100 cm due to a low absorption coefficient at these wavelengths.

2.4 Different techniques to estimate the liquid water content of snow

The liquid water content of snow is generally expressed as a

	Condition	Density kg/m³	Foreign Matter mg/Litre	Particle Size (cm)
Test 1	Wet	284	51	0 302
Test 2	Wet	338	29 8	0 475
Test 3	Dry	284	50 5	0 259
Test 4	Wet	160	15 5	0 167

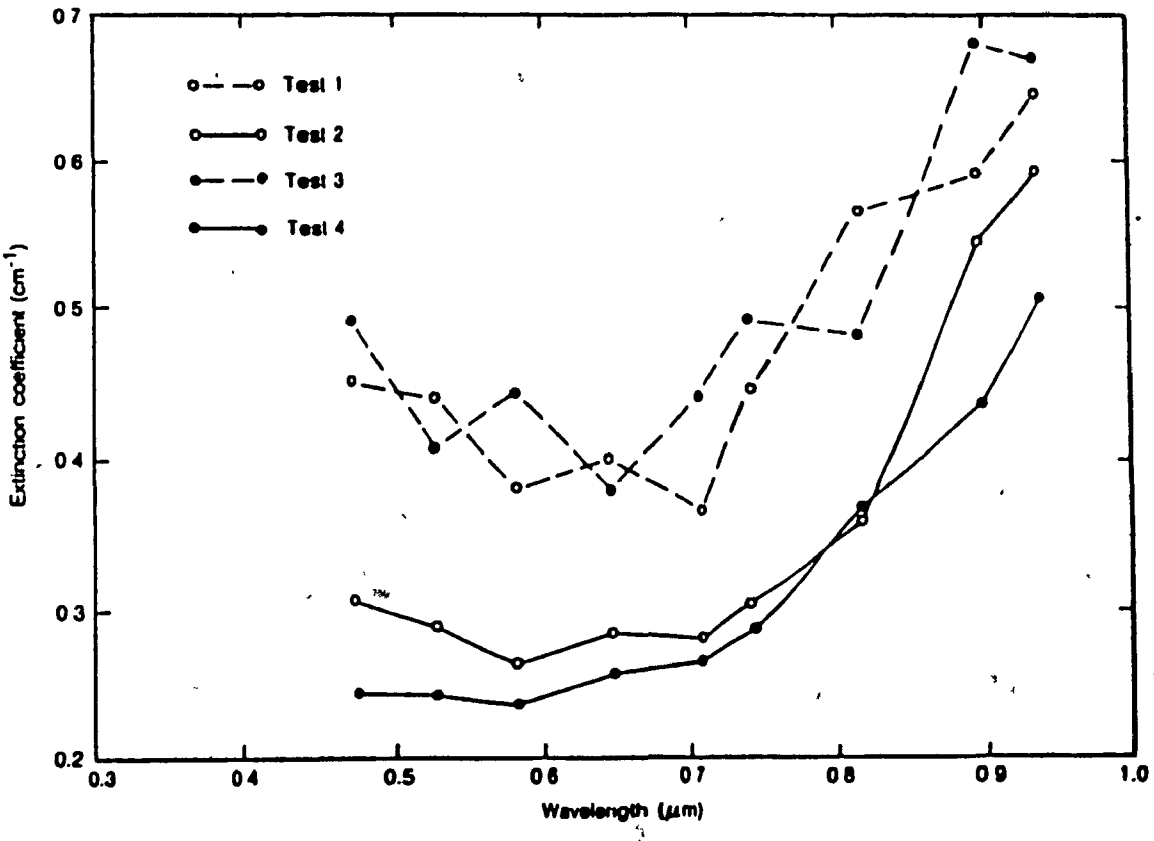

Fig. 2.4: Extinction coefficient of diffuse radiation for different snow wetness and foreign matter contents (after Manz,. 1974).

percentage of liquid water either by weight or by volume of the sample. Existing methods to estimate liquid water content are based on the centrifugal, the capacitive, the solution and the calorimetric principles. There are other possible methods which have not yet been applied to snow, such as nuclear magnetic resonance, time-domain reflectometry, Raman scattering and acoustic methods (Colbeck, 1978; Miller, 1972). In the following section, only those methods are discussed which have actually been employed for an estimation of the liquid water content of snow.

2.4.1 The centrifugal method

In this method, wet snow samples are centrifuged to extract the water. Unfortunately some melting of the samples can occur and, therefore, measurements obtained using this technique may not represent a true water content (Langham, 1973). This error may be accounted for by spinning samples several times in the centrifuge and plotting a graph of successive measurements of extracted water. The graph can be extrapolated back to the origin before centrifuging started. However, errors are introduced by variations in the grain size (Wakahama, 1968). Yosida (1967) and LaChapelle (1956) have noted a partial retention of water by centrifuged samples.

2.4.2 The capacitance method

This method was first tested by Linlor (1975). The free water content of a snow sample is estimated by measuring its dielectric constant. The dielectric constant is a linear function of snow wetness. Snow structural properties may introduce errors in the measurements. Therefore, the change in dielectric constant as the snow sample is frozen by dry ice is measured. Colbeck (1978) noted that even though the dielectric constant of snow is very sensitive to small changes in the volume of liquid water present, it is difficult to interpret the liquid water content from the dielectric constant of the solid-liquid-gaseous mixture. This difficulty arises from the importance of shape factors to the contribution of each phase to the dielectric constant of the mixture.

2.4.3 The solution method

This method was first proposed by Bader (1948) and was based on measuring the concentration changes of a sodium hydroxide solution when mixed with wet snow. A variety of different solutions have been used by different workers including fluorescent dye (Davis and Dozier, 1984), india ink (Grenfell, 1986) and hydrochloric acid (Davis et. al., 1985),

2.4.4 The calorimetric method

The calorimetric method is based on measurement of the amount of energy required to melt or freeze a known quantity of snow (Leaf, 1966; Stiles and Ulaby, 1980). The calorimeter is generally a thermos bottle where provision has been made for measurement of temperature. The free water content is estimated by monitoring the heat required to melt or freeze the snow samples. The melting calorimetric technique has inherent disadvantage because wetness values are generally small while large amounts of heat are required to melt the sample. Therefore, it is necessary to take small differences between large numbers. Hence large errors are possible (Radok, et al., 1961; Colbeck, 1978).

A new calorimeter has been developed by Fisk (1986). The calorimeter uses methanol to dissolve snow samples. This produces a temperature depression which can be linearly related to the liquid water content of the snow sample.

The freezing calorimeter method was used in this study. This method was selected because Jones et al. (1981) have shown that consistent results can be obtained by using the freezing calorimeter. If a calorimeter is assumed to be without loss, then

$$Hi = Hf \qquad (2.5)$$

Where Hi = Initial heat content of all constituents and

Hf = Final heat content of all constituents.

The initial and final heat content are obtained by following equations:

$$Hi = Ti\ [Wi+Ec]Cti + L\ Wf + Ts\ Wd\ Cs + Ts\ Wf\ Cw \quad (2.6)$$

$$Hf = Tf\ (Wi + Ec\ )\ Ctf + Tf\ Ws\ Csf \quad (2.7)$$

Where Ti = Initial temperature of the freezing agent (degrees C),

Wi = Weight of the freezing agent (g),

Cti = Specific heat of the freezing agent at Ti (J/g degree C),

L = Latent heat of fusion of water (J/g),

Wf = Weight of free water in snow (g),

Wd = Weight of dry snow (g),

Cs = Specific heat of snow at Ts (J/g degree C),

Cw = Specific heat of water at Ts (J/g degree C),

Tf = The final equilibrium temperature (degrees C),

Ctf = Specific heat of the freezing agent at Tf (J/g degree C),

Csf = Specific heat of snow at Tf (J/g degree C).

By using the above mentioned equations and solving for the fraction of free water

$$mw/100=Wf/Ws=(Wi+Ec)(Tf\ Ctf-Ti\ Cti)/Ws(Ts\ Cw+Lf)+$$
$$(Tf\ Ws\ Csf-Tf\ Wd\ Cs)/Ws(Ts\ Cw+Lf) \qquad (2.8)$$

and by making the following approximations

$$Ctf = Cti \qquad (2.9)$$
$$Cs = Csf \qquad (2.10)$$
$$Ts = 0 \qquad (2.11)$$

the final equation can be written as:

$$mw/100 = (Wi + Ec)\ (Tf - Ti)\ Ct/\ Ws\ L +$$
$$Tf\ Cs/\ L \qquad (2.12)$$

During this study a temperature gradient inside the calorimeter was observed. Therefore, to get the final temperature of the snow-toluene mixture, the temperature changes inside the calorimeter were monitored at two different levels. The final temperature was obtained by averaging the temperature at the two levels. Therefore, in this experiment the initial (Ti) and final (Tf) temperatures are obtained by

$$Ti = (Tti + Tbi)/2 \qquad (2.13)$$

where Tti = Initial temperature of the top thermistor and

Tbi = Initial temperature of the bottom thermistor.

Similarly, the final temperature can be obtained by:

$$Tf = (Ttf + Tbf)/2 \qquad (2.14)$$

Where Ttf = Final temperature of the top thermistor and Tbf = Final temperature of the bottom thermistor. By adding equations 2.13 and 2.14 the final equation can be written as:

$$mw/100 = [Wi+Ec][((Ttf+Tbf)/2)-((Tti+Tbi)/2)Ct/Ws\ L + [(Ttf+Tbf)/2]Cs/L \qquad (2.15)$$

2.5 Techniques for estimating grain size

A variety of techniques have been used to estimate the grain size of snow. They vary from simple manual to sophisticated computerized methods. One commonly used method is visual estimation of grain size. This method is convenient to use in the field but leads to large errors.

O'Brian and Koh (1981) used Formvar replicas to measure grain size. These replicas were made by pressing a Formvar-coated microscope slide against the side of a sharply cut snow pit. A Millipore particle measurement computer was used to determine the size characteristics of the replicated snow granules.

A third method, sieve analysis, has been used successfully for cold and friable snow in the estimation of grain size distributions (Keeler, 1969; Granberg, 1984). However, sieve analysis is not successful in warm snow, where the snow tends to agglomerate in the sieves, or in fine grained, well bonded tundra snow (Granberg, 1984).

The sieve technique was used for grain size determination in this study as the temperature conditions were such that good results could be obtained. The sieve technique was also used in the preparation of snow samples of uniform grain size.

3. METHODS OF DATA ACQUISITION

3.1 Introduction

Field data were collected during spring 1985, winter 1986 and spring 1986. In spring 1985 data were collected to study the effect of grain size and liquid water content on spectral reflectance. In winter of 1986 the data were collected to study the effect of grain size on spectral reflectance and attenuation of solar radiation by the snowpack. In the spring of 1986 data were collected to study the attenuation of solar radiation by the snowpack.

3.2 Data Acquisition System

3.2.1 Radiation measurements

A LI-1800 spectroradiometer was used for all field measurements. The instrument utilizes a holographic grating and a stable, high quantum efficiency silicon detector. The light passes through a filter wheel before it enters the monochromator. Each filter in the wheel corresponds to a particular wavelength range. The LI-1800 automatically selects the appropriate filter. The light enters into the holographic grating monochromator which is used to disperse light into individual wavebands. The monochromator has three components: (i) the entrance slit, (ii) the grating and (iii) the exit

slit. The radiation from the entrance slit strikes the grating. The grating diffracts and reflects light towards the exit slit. By changing the angle between the entrance slit and the face of the grating, selected wavelengths of light can be passed through the exit slit. The light that passes through the exit slit strikes a silicon detector. This generates a current which is amplified, converted into a voltage and passed to an analog-to-digital converter which is sampled by the computer.

The above mentioned operations are controlled by the computer. The LI-1800 has two interface connectors: a terminal port for control and data transfer and an output port for data transfer. The output port can function in one of three modes: RS-232, audio cassette tape and analog millivolt. The memory capacity of the spectroradiometer is 16 K. Therefore, it can only hold data from six measurements at full spectral resolution. The spectroradiometer can be equipped with a tape recorder for dumping of memory contents in the field. However, the necessary equipment for data retrieval from the tape is costly and was not available to the author. This severely limited the quantity of field data that could be collected in one field visit. An improvement was introduced in the winter of 1986. Data were then transferred from the radiometer to a TRS-80 model 100 portable computer, from which the data were transferred to cassette tapes. During spring 1986, this method was further improved. After acquiring a portable 3.5 inch disk drive, data could be stored on microdisks rather than cassette tapes. This

greatly increased the throughput of the field data acquisition system. In the laboratory the data were transferred from the TRS-80 model 100 computer to a Hewlett Packard computer system.

3.2.1.1 Reflectance measurements

The LI-1800 was used for all field measurements. A remote cosine receptor was attached to the extension arm of a photographic tripod. This arm was rotated to get reflectance readings from a barium sulfate plate and from the snow surface without changing the view angle of the cosine receptor (Figure 3.1).

During the spring of 1986, data to study the effects of grain size and liquid water content on reflectance were collected in intervals of 10 nm from 300 to 1100 nm. The output from the radiometer was converted into reflectance values using the following relationship:

$$Rb = Lr,t \; / \; Lr,s \qquad (3.1)$$

Where Rb = Reflectance compared to barium sulfate,
Lr,t = Reflected radiation of the snow into a finite solid angle and
Lr,s = Reflected radiation of the barium sulfate plate into the same solid angle.

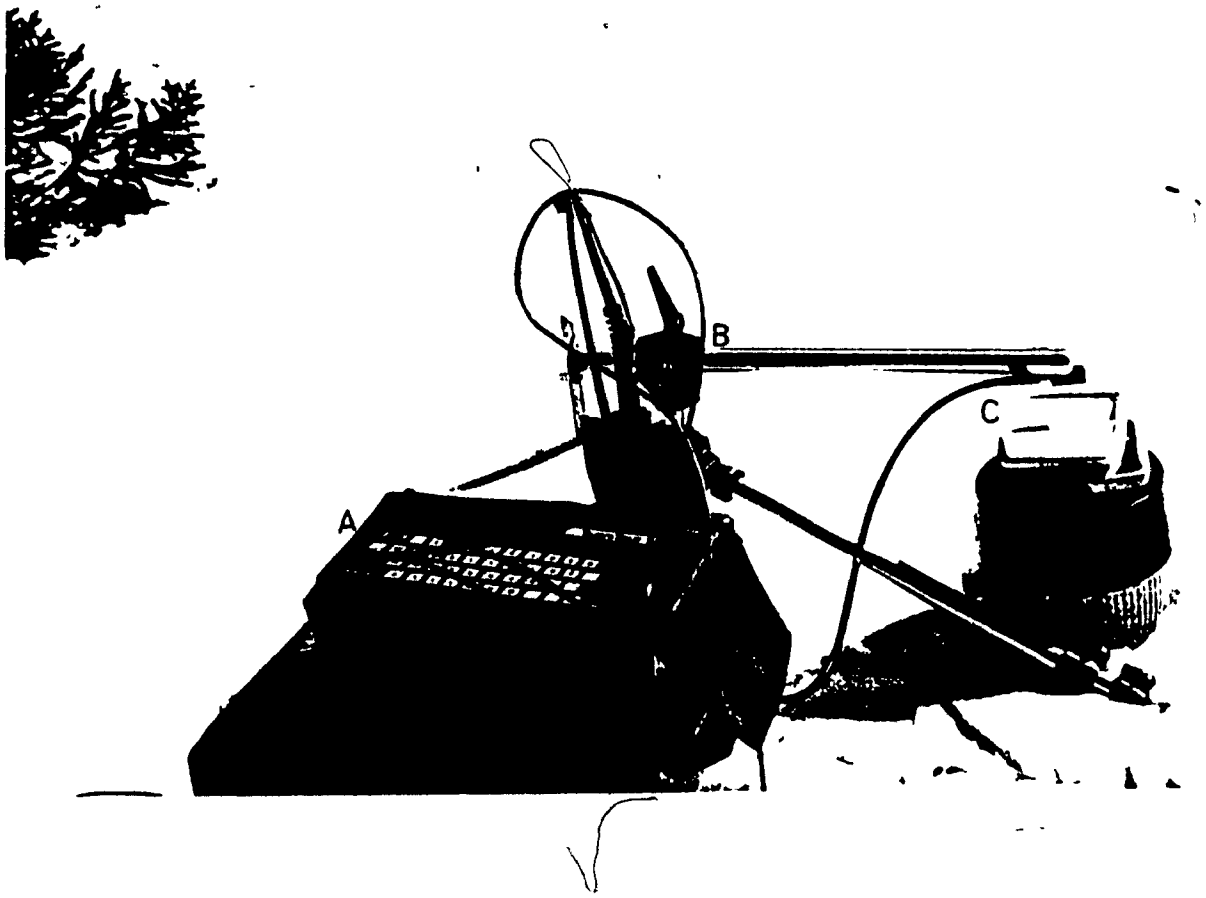

Fig. 3.1: Set up for spectral reflectance data collection, (A) Li-1800 spectroradiometer, (B) photographic tripod, (C) barium sulfate plate.

3.2.1.2 Attenuation measurements

A new fiber optics probe was designed to measure the attenuation of solar radiation at different depths in a snowpack (Granberg, in prep.). This probe was designed and supplied by Dr. H.B. Granberg. The first 70 cm of a 1.2 m fiber optics cable is enclosed in a hard plastic tube, forming a rigid probe. The other end is connected to the fiber optics light conductor supplied by the manufacturer of the LI-1800 radiometer. The optically polished, flat end of the fiber optics cable (4 mm in diameter) was used directly as light collector. The probe was attached to a specially designed stand, enabling the probe to be inserted into the snow to precisely determined depths to measure the upwelling radiation (Figure 3.2).

The spectral distribution of solar radiation was measured at 2 or 10 cm depth intervals by lowering the probe along with the extension arm of the stand. The data was collected at a spectral resolution of 2 nm and at 10 cm depth intervals, during the winter of 1986. Improvements in the field data acquisition system permitted data to be collected at a spectral resolution of 1 or 2 nm and at 2 cm depth intervals during the spring of 1986.

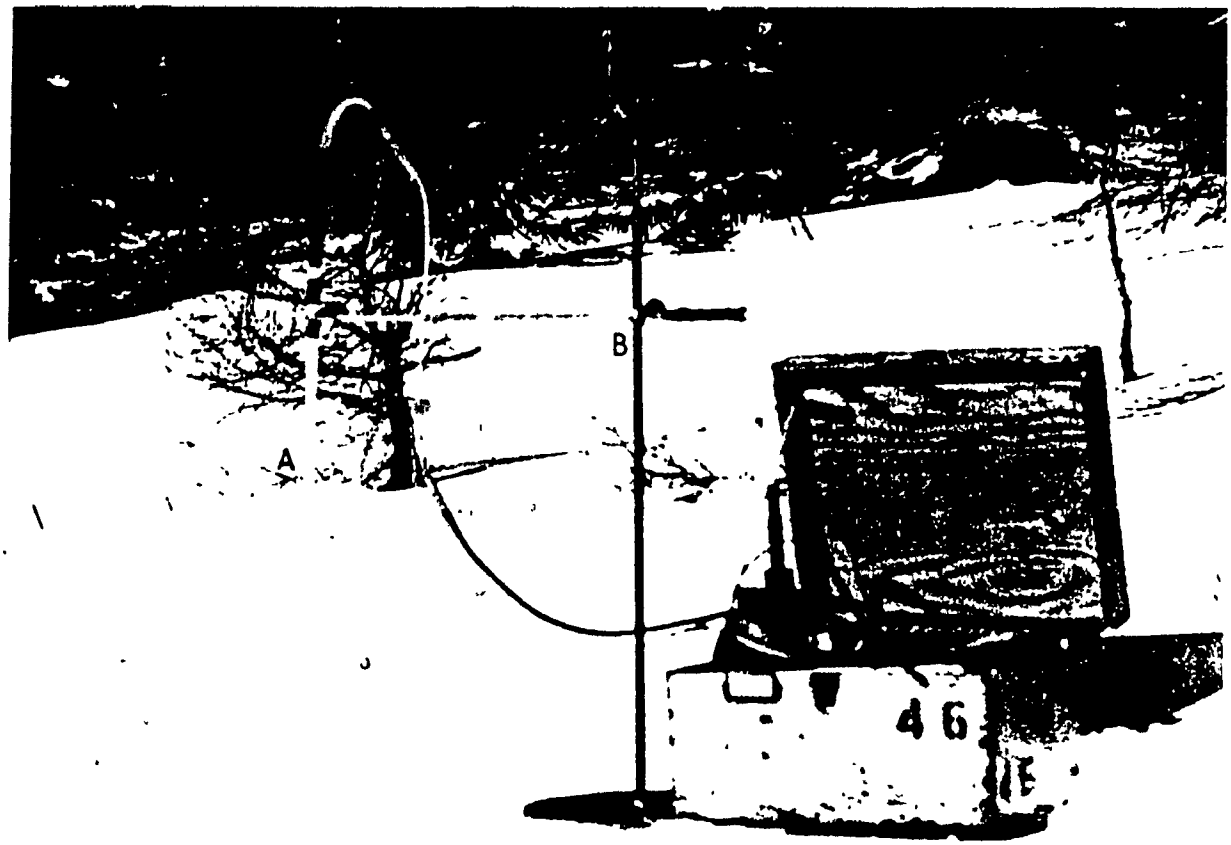

Fig. 3.2: Set up for spectral attenuation data collection, (A) fiber optics probe, (B) stand, (C) Li-1800 spectroradiometer.

3.2.1.3 Sources of error

The stability of a silicon detector beyond 850 nm degenerates markedly under extreme temperature conditions. It can affect the relationship between detector signal and spectral irradiance. This is not a problem when the temperatures of calibration and measurement are the same (Li-cor Instructional manual, 1982). In this investigation the sample and reference scans were taken at the same temperature. Therefore, the error from this source is considered negligible. Another possible source of error is variation in solar zenith angle. Staenz and Haefner (1981) observed for old and moist snow that the variation in sun zenith angle from 24 to 49 degrees had negligible effect on the spectral reflectance. Most of the measurements of the present investigation were made under relatively similar sun zenith angles (excepting the winter measurements). Therefore, errors from this source are also considered negligible.

3.2.2 Measurements of the liquid water content of snow

3.2.2.1. The Freezing Calorimeter Equipment

The different parts of the equipment required for freezing calorimeter measurements are:

a. Calorimeter: The calorimeter was constructed from a wide mouth vacuum thermos bottle made of stainless steel.

b. Temperature probes: Thermistors were used to monitor the temperature inside the calorimeter. The temperatures were measured to the nearest 0.01 degree C using a digital multimeter. A Campbell Scientific CR7 datalogger was used to measure temperatures during the determination of the calorimetric constant.

c. Scale: A Mettler 1000 electronic balance was used to measure weights with an accuracy of 1 mg.

d. The freezing agent: A freezing agent was used to freeze the liquid water of the snow samples. The freezing agent should have a low viscosity and a high flash point. Silicon oil was used by Jones et.al. (1981), but in order to reduce costs, toluene was used in this investigation.

e. Material to cool the freezing agent: The freezing agent was cooled using a mixture of calcium chloride and snow. The eutectic composition of the calcium chloride-water system is approximately 68% water and 32% calcium chloride by weight (Keyser, 1981). The temperature of the mixture at the eutectic composition is -52 degrees C.

f. Snow sampler: Snow was collected and placed into the

calorimeter using a cylindrical sampler, made from a syringe. The sampler was 5 cm in diameter and 15 cm in length.

3.2.2.2: Estimation of the calorimetric constant

The calorimetric constant is used to compensate the heat balance equation for the amount of energy absorbed by the calorimeter due to temperature changes during the mixing process. For the convenience of use in the equation, the calorimetric constant is generally expressed in terms of the equivalent weight of freezing agent. The constant was determined by using the following equation (Jones and Rango, 1981).

$$Wt1\,[(Csw + Cs2)/2]\,(Tw - T2) = (Wt2 + E)\,[(Cs1 + Cs2)/2]\,(T2 - T1) \qquad (3.2)$$

where Wt1 = Weight of the warm fluid (g),
Wt2 = Weight of the cold fluid (g),
E = The calorimetric constant expressed in the equivalent weight of fluid (g),
Tw = Initial temperature of the warm fluid before mixing (degrees C),
T1 = Initial temperature of the cold fluid before mixing (degrees C),
T2 = The final temperature of the fluid mix (degrees C),

Csw = The specific heat of the fluid at the temperature of the warm fluid (J/g degrees C),

Cs1 = The specific heat of fluid at the temperature of the cold fluid (J/g degrees C) and

Cs2 = The specific heat of the fluid at the final temperature of the mix (J/g degrees C).

To determine the calorimeter constant, calorimeter temperatures were monitored at one-minute intervals using copper-constantan thermocouples and a Campbell CR-7 data logger. The temperatures at the bottom and the top of the calorimeter were recorded for a period of ten minutes prior to insertion of the cold fluid and 30 minutes after the insertion.

3.2.2.3 Field procedure

1. A known volume of toluene was stored in a glass bottle. The bottle was immersed in the snow and calcium chloride mixture for half an hour to reduce the temperature of its contents to -20 degrees C.

2. The thermistors were inserted at two levels inside the calorimeter and their resistance monitored.

3. The toluene was poured into the calorimeter and the entire contents were shaken. Temperature changes were monitored for ten minutes to get the initial temperature of the toluene.

4. The snow sample was inserted into the calorimeter and the entire contents were shaken. The temperature was monitored at the top and bottom of the calorimeter for an hour at one minute intervals.

5. The weight of the total mixture was measured.

3.2.3 Grain Size Measurements

The sieve technique was used to fractionate snow into samples of uniform grain size in the study of the effects of grain size variations on spectral reflectance. The reproducibility of sieve analysis results in cold condition have been discussed by Granberg (1984). The same procedure was used in the present investigation. A stack of standard sieves (4, 2, 1, .5, .25 and .125 mm) was used with an automatic sieve shaker. Analyses were conducted when air temperatures were between -20 to -30 degrees C in an unheated, well ventilated porch of the McGill Subarctic Research Station in Schefferville. This gave a low ambient temperature and also protection from wind and drifting snow. The sieved snow samples of uniform grain size were stored in cardboard boxes. Three boxes for grain sizes from .5 to 1, 1 to 2 and 2 to 4 mm respectively were filled. The spectral reflectances of these samples were measured the next day.

3.2.4 Other Data

Other data like depth and density of snow and maximum, minimum and ambient air temperatures were collected during scanning. These parameters were measured using equipment such as a snow ruler, a Swedish snow density sampler (Granberg and Kingsbury, 1984) and mercury thermometers respectively. The maximum and minimum temperatures were taken from the Schefferville meteorological station.

4. THE INFLUENCE OF CHANGE IN LIQUID WATER CONTENT AND GRAIN SIZE OF SNOW ON SPECTRAL REFLECTANCE

4.1 Introduction

This section is divided into three subsections. In the first and second subsections the effects of change in liquid water content and grain size are discussed separately. In the third subsection their combined effects are discussed.

4.2 Effects of Liquid Water Content

In order to study the effects of liquid water content on spectral reflectance, the change in reflectance from non-melting to melting, and from melting to dry snow conditions were observed. In the present analysis reflectance measurements from May 12, 1985 to May 14, 1985 are used. These days were selected because of clear and sunny weather conditions and because of ideal changes in night (below freezing) and day (above freezing) temperatures.

4.2.1 Liquid Water Content of Snowpack

The liquid water content of snow was estimated using equation 2.15. The initial (Ti) and final (Tf) temperatures of the freezing agent and the snow-freezing agent mixture respectively were estimated from graphs of temperature vs. time (Figures

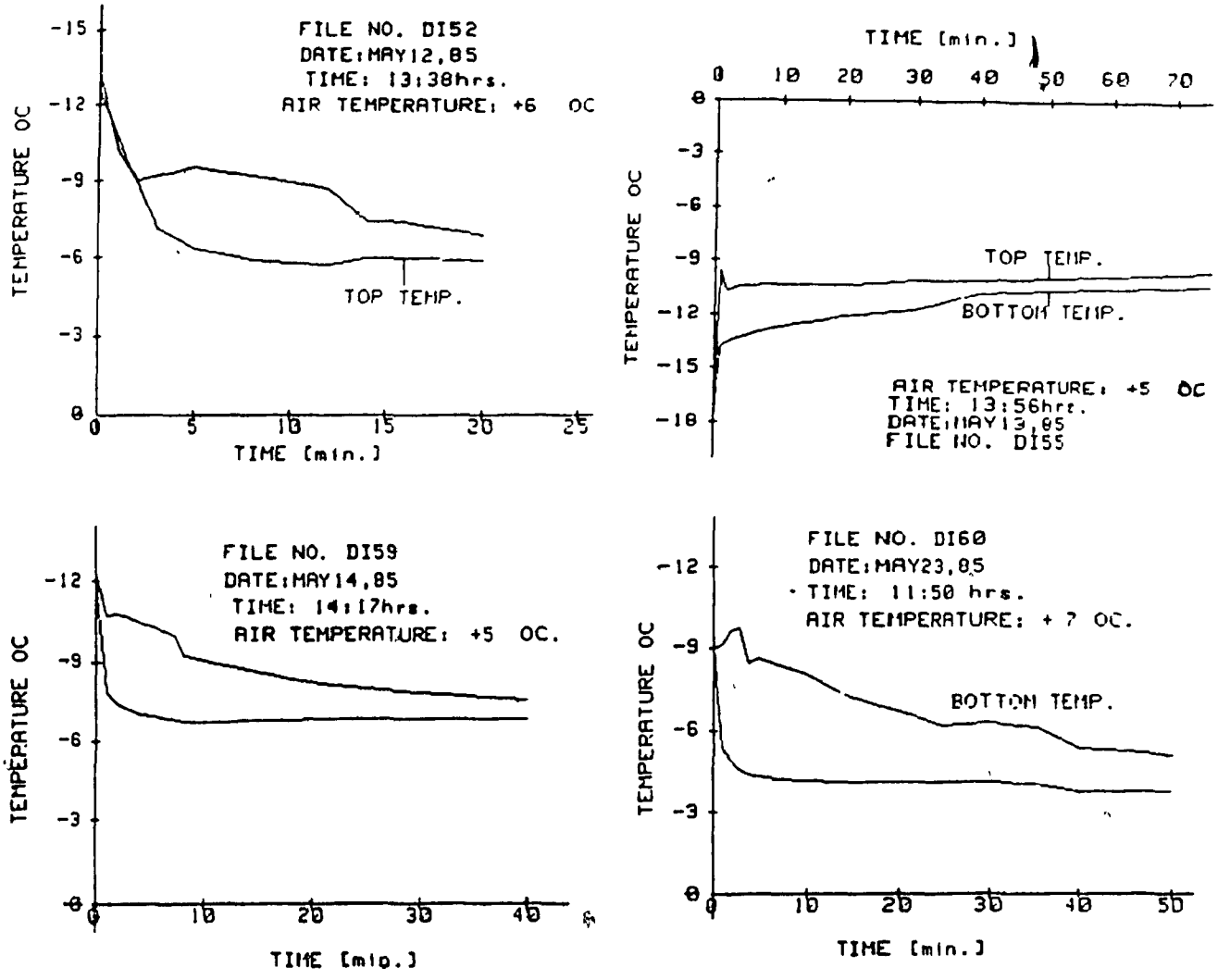

Fig. 4.1: Temperature vs. Time graphs for the calorimeter.

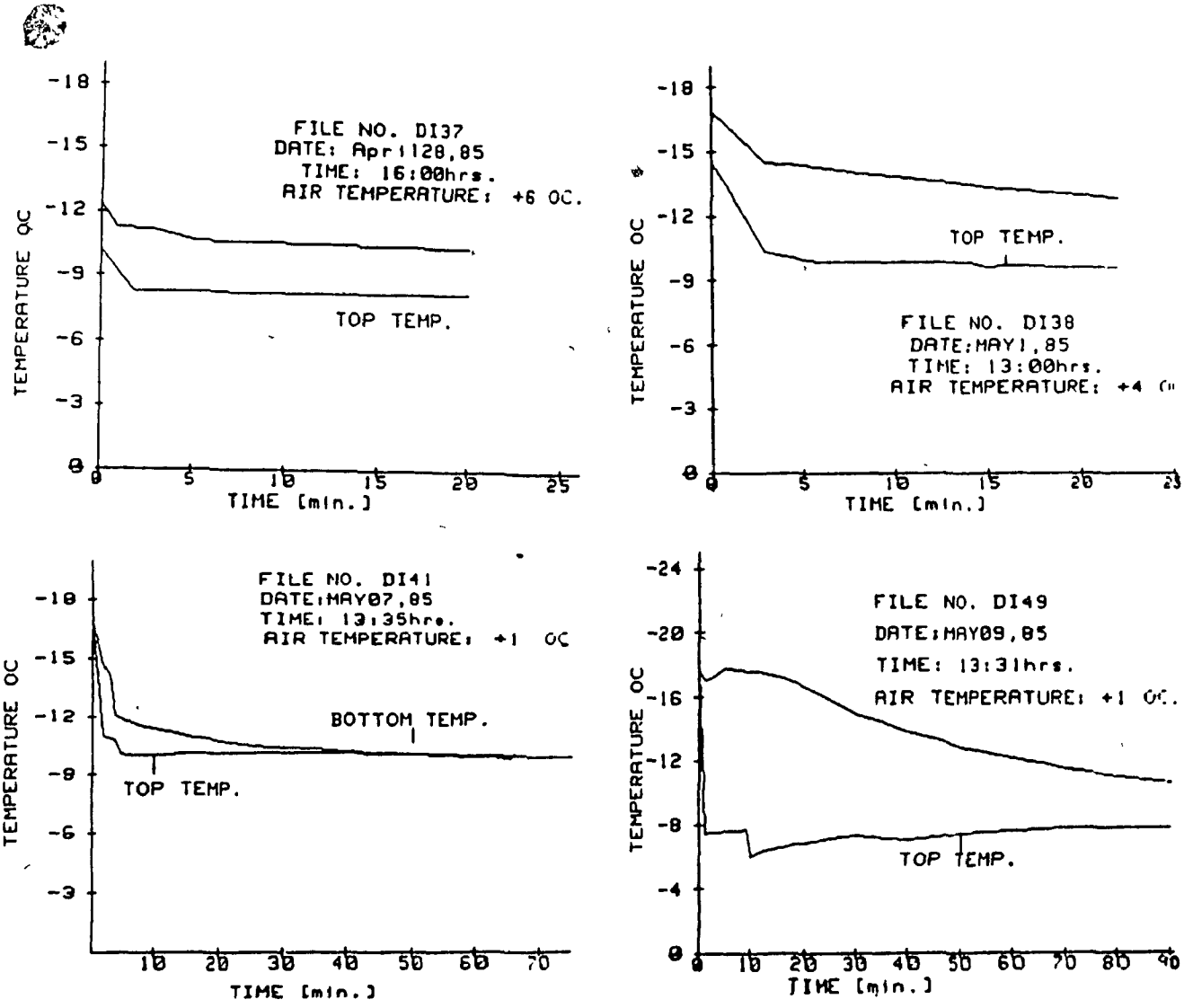

Fig. 4.2: Temperature vs. Time graphs for the calorimeter.

4.1 and 4.2). The liquid water content, expressed in per cent by weight, is given in Table 4.1.

4.2.2 Change in reflectance from dry to wet snow.

A comparison was made between the reflectance measured at 9:30 and 13:56 respectively on May 13, 1986 (Figure 4.3). The minimum temperature recorded at the McGill Subarctic Research Station was -11.6 degrees C. At the experimental site, during scanning, a temperature of -3.0 degrees C was recorded. The liquid water content of the snow pack at 9:30 on May 13, 1986 is therefore assumed to be zero percent. The temperature at 13:56 on the same day was +5 degrees C. A liquid water content of 13% by weight was estimated using the freezing calorimeter technique (Table 4.1).

The reflectance values observed at 13:56 were subtracted from those observed at 9:30 (DI53 - DI55) to get the change in reflectance. The differences were converted into a percentage of maximum possible reflectance (i.e. 1). The results are plotted in Figure 4.4.

The smallest drop in reflectance (8%) was observed in the visible band around 600 nm. The change increases with wavelength up to 970 nm, where a maximum of 17% occurs. The change in reflectance decreases from 970 to 1100 nm.

Table 4.1
Liquid water content of snow samples.

Date of invest.	Initial Temp. Tti	Tbi	Final Temp. Ttf	Tbf	snow weight	% Liquid water
May 7,85	-16.98	-16.79	-10.00	-10.00	97.9	12.3
May 8,85	-08.69	-08.86	-06.04	-02.78	77.6	09.1
May 9,85	-18.06	-17.82	-07.78	-10.66	198.5	07.7
May 12,85	-12.59	-13.37	-05.89	-06.87	88.00	13.3
May 13,85	-17.15	-18.13	-09.81	-10.51	98.7	13.3
May 14,85	-12.12	-12.36	-06.86	-07.58	86.7	10.5

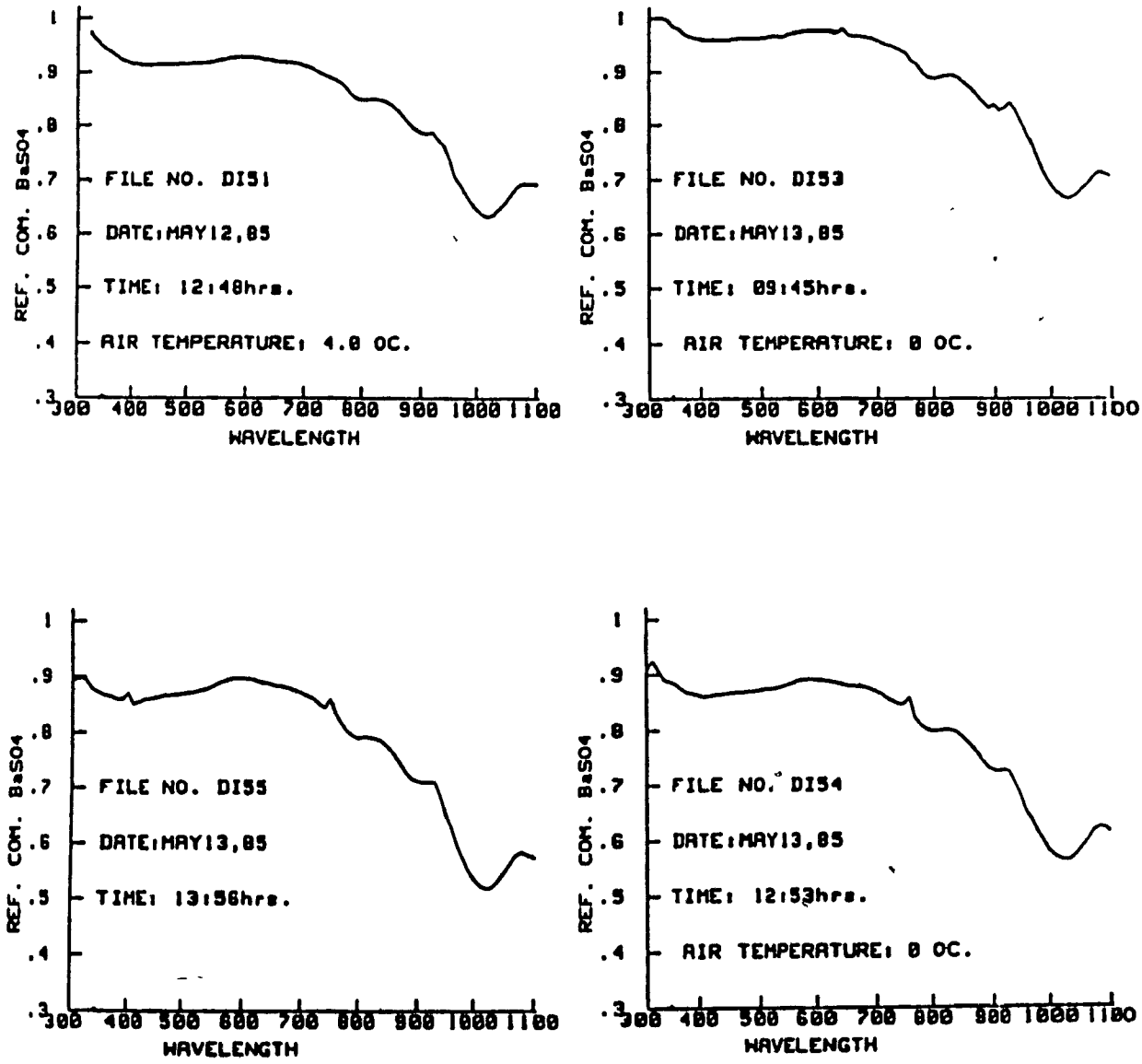

Fig. 4.3: Spectral reflectance curves for snow cover.

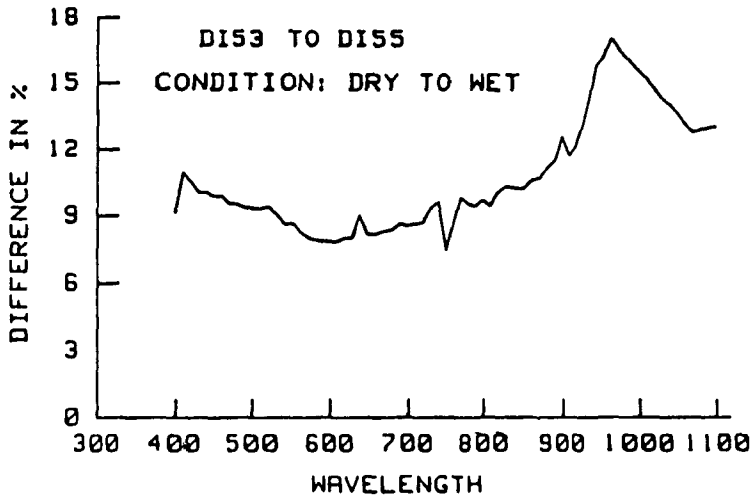

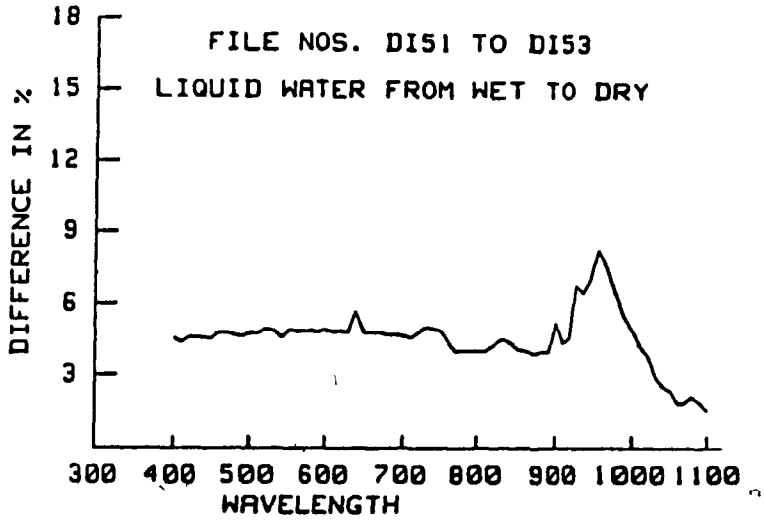

Fig. 4.4: Changes in reflectance due to variation in liquid water content of snow cover.

4.2.3 Change in reflectance from wet to dry snow

To study this condition, spectral reflectance of snow at 12:48 on May 12, 1985 and 9:30 on May 13, 1985 were compared (DI51 and DI53 respectively; Figure 4.3). The free water content of the snow pack at 9:30 on May 13 is assumed to be zero percent. On May 12, 1985 at 12:48, the air temperature at the site was +4 degrees C. The liquid water content was estimated at 13:47 the same day and indicated 13 per cent by weight. Therefore, the snow condition at 12:48 was considered wet. A similar procedure to that mentioned above was used to estimate the difference in reflectance between May 12 and May 13, 1985 (Figure 4.4).

The graph shows that from 400 to 900 nm, the rise in reflectance was between 4 and 5 percent. From 900 nm onward the difference increases and a maximum of 8.3 percent is observed at 960 nm. The difference decreases from 960 to 1100 nm. The peak difference around 960 nm possibly occurs because the difference between the absorption coefficient of ice and water is greater at 970 nm (0.34) than at any other wavelength between 400 and 1100 nm (Irving and Pollack, 1968; Grenfell and Perovich, 1981).

4.2.4 Repeatability of the results

The results showing changes in reflectance from dry to wet and

wet to dry conditions are plotted in Figures 4.5 and 4.6 respectively. The numerical values are given in Table 4.2 and 4.3. On May 8, 1985 the peak loss is shifted from 960 to 1030 nm (dry to wet) (Table 4.2). The difference in loss between 950 and 1030 is small; however, on the same day the maximum rise in reflectance from wet to dry was observed at 950 nm (Table 4.3). These results support the earlier observations that the spectral region around 960 nm is sensitive to changes in the liquid water content.

It can also be seen from Figures 4.5 and 4.6 that although the maximum drop in reflectance from dry to wet was 17%, the maximum rise after refreezing was only 8%. To further investigate this phenomenon the ratio between reflectances in 580 to 600 nm (which are least strongly affected by the liquid water content) and 960 to 980 nm (which are most strongly affected by the liquid water content) were computed and tabulated (Table 4.4). The ratios are less than 1.3 for dry snow and greater than 1.34 for wet snow. For dry snow, it varies from 1.22 to 1.29, for wet snow it varies from 1.35 to 1.64. For dry snow, the minimum value of 1.22 was observed for fresh snow. This ratio tends to increase as the snow goes through several freeze and thaw cycles. Even after many freeze and thaw cycles; however, a significant difference is noticed between the ratios for wet and dry snow.

On May 14, 1985, it was observed that as the air temperature

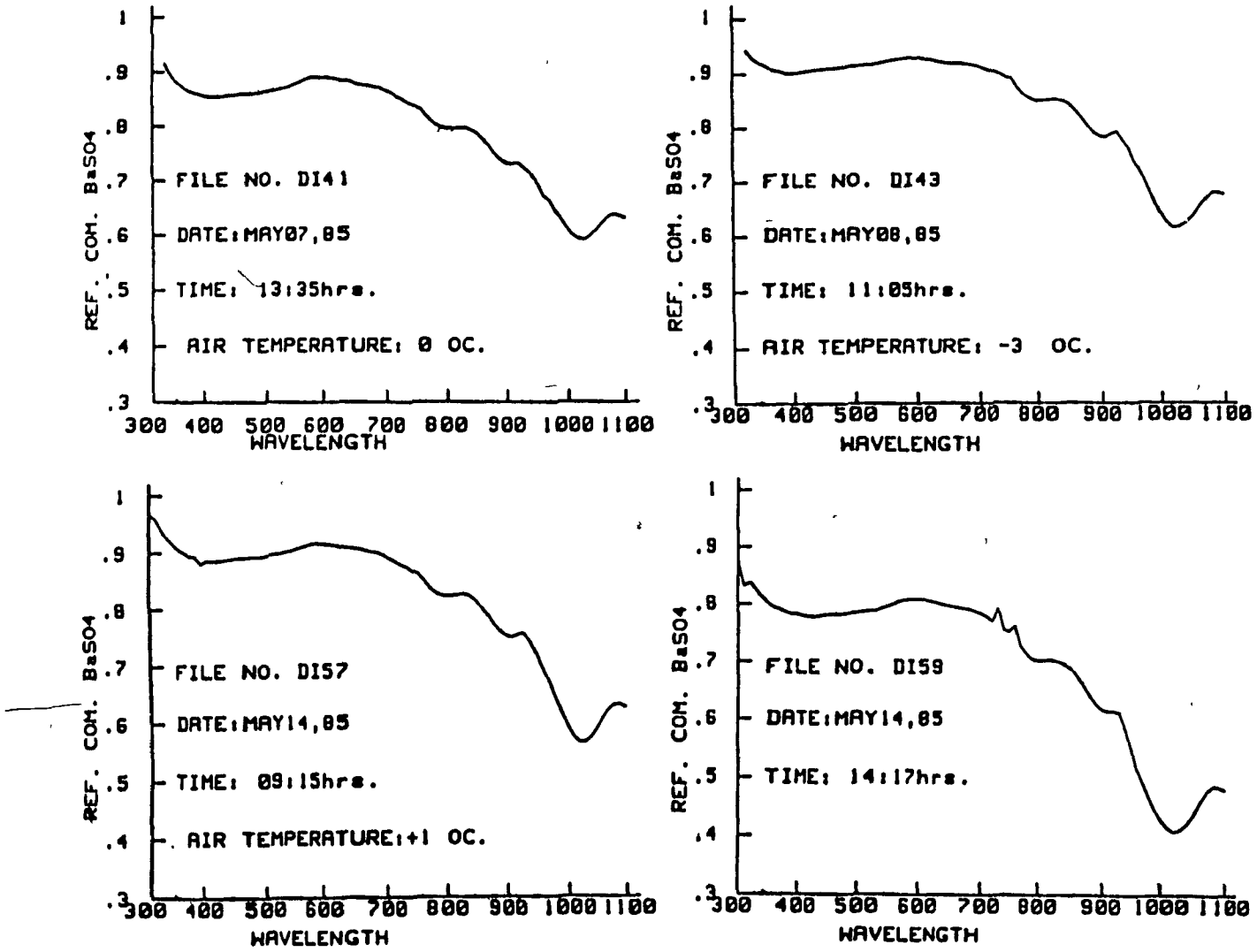

Fig. 4.5: Spectral reflectance curves for snow cover.

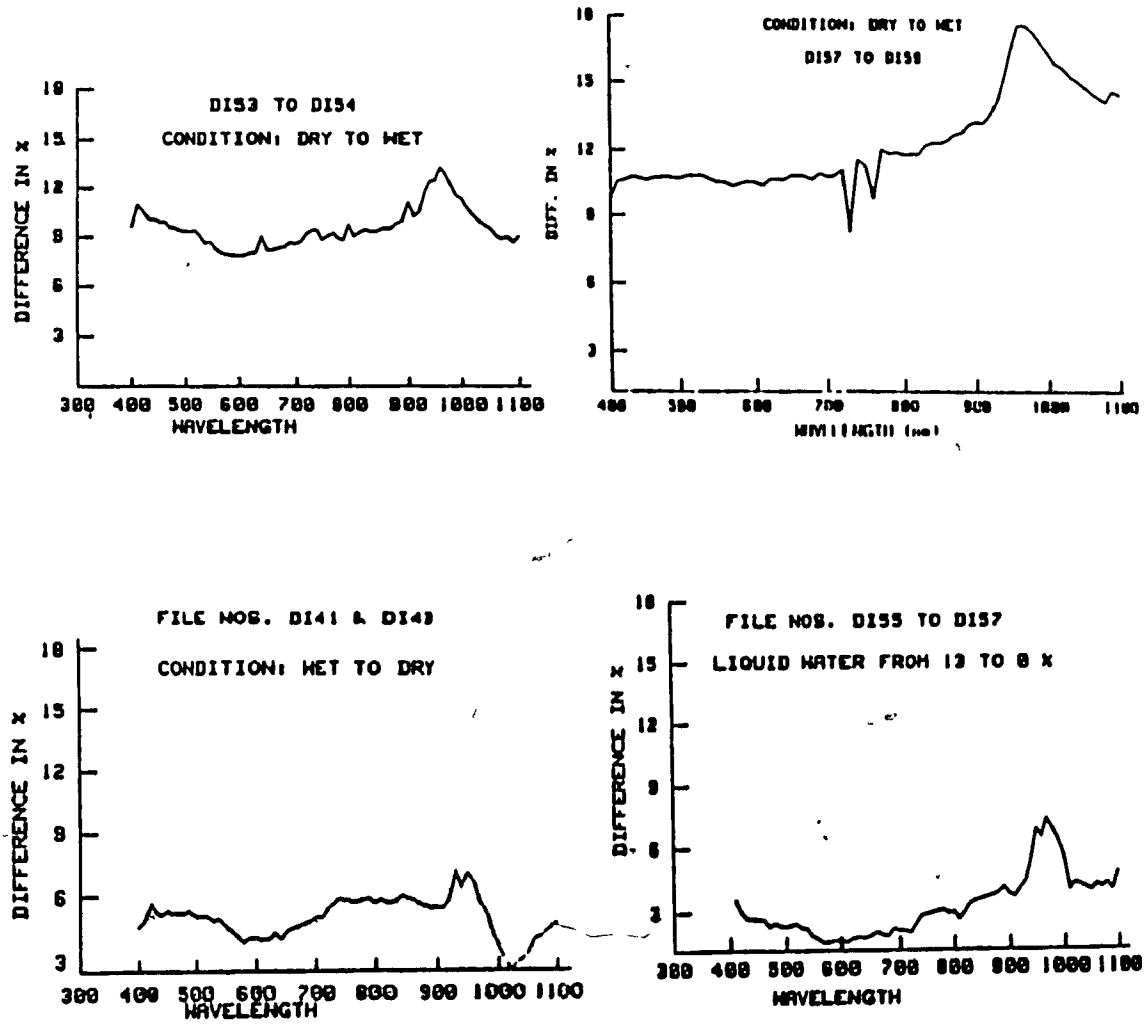

Fig. 4.6: Changes in reflectance due to variations in liquid water content of snow pack.

Table 4.2
Drop in spectral reflectance from dry to wet snow.

Drop in reflectance		Air temp.		% liq. water		Average differ.
From A	To B	A	B	A	B	950 to 980 nm
May 8 11:01	May 8 12:10	-5	+1	dry	wet	13.07
May 8 11:11	May 8 12:10	-3.5	+1	dry	wet	13.1
May 13 09:50	May 13 12:53	-3	+2	dry	wet	12.9
May 13 09:50	May 13 13:56	-3	+5	dry	wet	16.3
May 14 09:12	May 14 14:17	0	+5	dry	wet	17.3

Table 4.3
Rise in spectral reflectance from wet to dry snow

Drop in reflectance		Air temp.		% liq. water		Average differ.
From A	To B	A	B	A	B 950	to 980 nm.
May 7 13:35	May 8 11:01	+1	-3.5	12.2	dry	6.1
May 12 12:48	May 13 09:50	+4	-3	13.3	dry	7.3
May 13 13:56	May 14 09:12	+5	0	13.1	almost dry	6.8

Table 4,4
Ratios between the visible and near infrared radiation for dry and wet snow.

Date of reading	File number	Time of reading	Air temp.	Snow condition	% liquid water	Ratio 580-600/ 960-980
April 25	DI26	12.00	-7	Dry	---	1.22
May 3	DI39	10:10	-2	Dry	---	1.28
May 7	DI41	13:35	+1	Wet	---	1.35
May 7	DI42	14:35	+1	Wet	---	1.35
May 8	DI43	11.05	-2	Dry	---	1.29
May 12	DI51	12:48	+4	Wet	---	1.34
May 13	DI53	09:50	-3	Dry	----	1.28
May 13	DI54	12:53	+2	Wet	----	1.40
May 13	DI55	13:56	+5	Wet	13.1	1.49
May 13	DI56	15:12	+3.5	Wet	----	1.46
May 14	DI58	13:06	+4	Wet	10.4	1.63
May 14	DI59	14:17	+5	Wet	----	1.64

increased from +1 to +5 degrees C, the ratio increased from 1.37 to 1.64. Similarly, on May 14, 1985, as the air temperature increased from -3 to +5 degrees C, the ratio increased from 1.28 to 1.49. However, later on the same day as the air temperature decreased from +5 to +3.5 degrees C, the ratio decreased from 1.49 to 1.46.

To assess the best ratio for detection of melting snow, different ratio techniques were attempted. The results are shown in Figure 4.7 and Table 4.5. The differences between files DI57 and DI59 were plotted in two ways. In the first example the ratio between wavelengths 1000-1030 nm and 600-630 nm were computed for wet and dry snow reflectance. The ratio of wet snow was subtracted from that of the dry snow condition and multiplied by 100 to get the difference in per cent. This technique was used for positions 1 to 5 in Table 4.5 and Figure 4.7. In the second example the reflectance of dry snow in wavelength 1000-1030 and 600-630 was subtracted from that of the wet snow. The ratios of the difference were calculated and multiplied by 100 to obtain the difference in percent. This method was used for positions 6 and 7 in Table 4.5. The differences range from 11.3 to 164.5 per cent. The maximum difference of 164.5 was obtained when the second procedure was used and wavelengths of 960 to 990 and 600 to 630 were used.

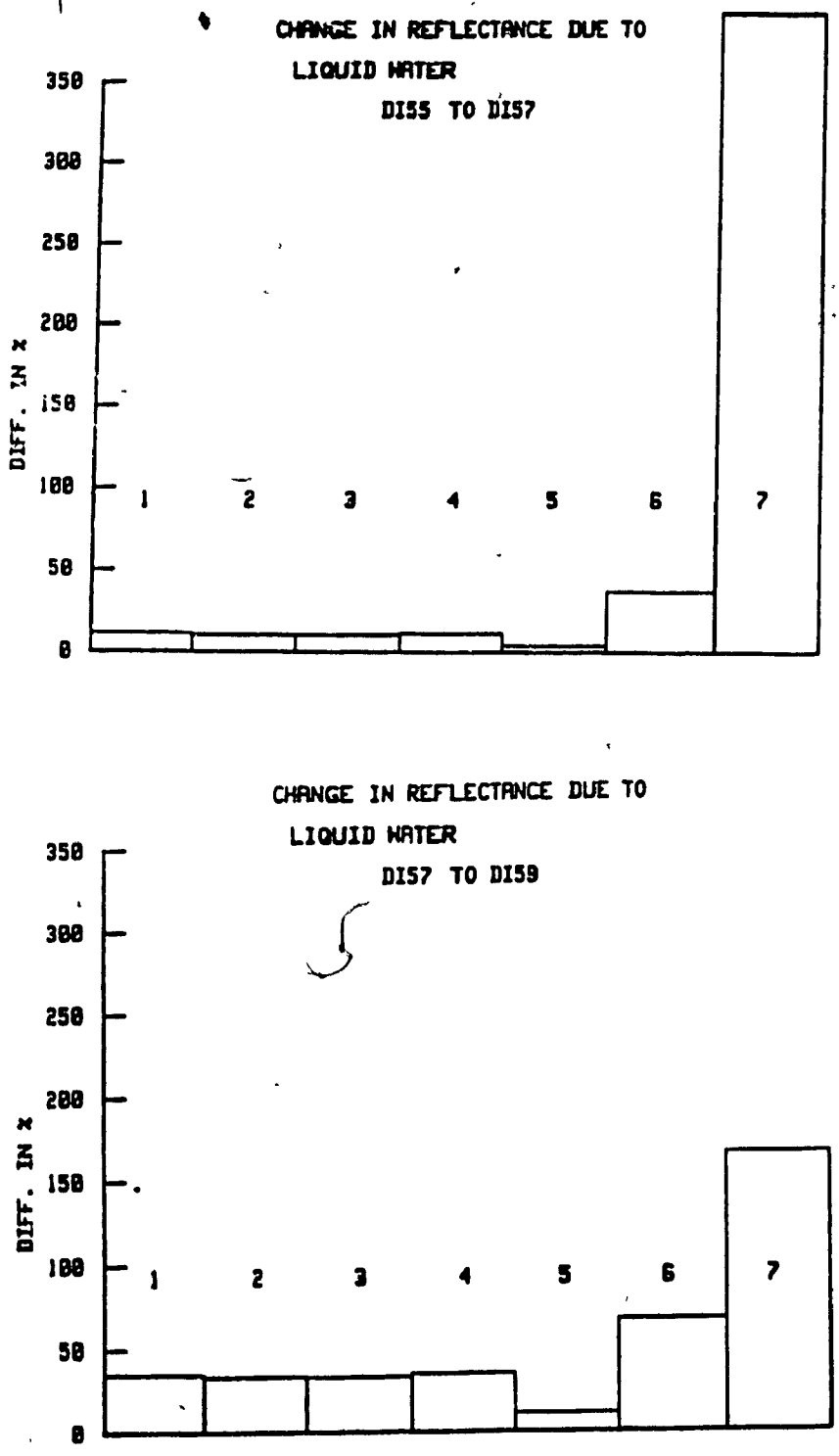

Fig. 4.7: Histogram showing change in reflectance after taking ratios. Classes explained in text and Table 4.5.

Table 4.5
Difference in ratio due to variation in liquid water.

Ratio (wavelength in nm)	Position in figure	% differ.
1000 to 1030/600 to 630	1	11
600 to 630/1000 to 1050	2	35
550 to 580/1000 to 1030	3	35
550 to 600/1000 to 1050	4	30
600 to 650/1000 to 1050	5	33
$\frac{DI57(600 \text{ to } 630)-DI59(600 \text{ to } 630)}{DI57(1000 \text{ to } 1030)-DI59(1000 \text{ to } 1030)}$	6	149
$\frac{DI57(960 \text{ to } 990)-DI59(960 \text{ to } 990)}{DI57(600 \text{ to } 630)-DI59(600 \text{ to } 630)}$	7	164
$\frac{DI57(1000 \text{ to } 1030)-DI59(1000 \text{ to } 1030)}{DI57(600 \text{ to } 630)-DI59(600 \text{ to } 630)}$	8	--

4.3 Effect of grain size of snow on spectral reflectance

To study the effect of grain size on spectral reflectance, snow samples of different, uniform grain sizes were obtained as described in Section 3.2.3. The spectral reflectance of each snow sample with reference to barium sulfate was plotted (Figure 4.8).

In all grain sizes, the maximum reflectance occurs between 400 nm and 700 nm. The reflectance decreases from 700 to 1010 nm, with minor peaks around 730 and 910 nm. The lowest reflectance occurs around 1010 nm and then it increases up to 1090 nm, giving a minor peak at 1090 nm. As the grain size increases from 0.5-1 mm to 2-4 mm, the general trend remains as given above, but a significant drop in reflectance is observed. The decline in reflectance may vary from wavelength to wavelength but it is noticed in all wavelengths from 400 to 1100 nm with increasing grain size.

The drop in spectral reflectance (in percent) due to increase in grain size from 0.5-1 mm to 2-4 mm was plotted (Figure 4.9). The graph was computed by subtracting the spectral reflectance values for 2-4 mm from those measured over the 0.5-1 mm sample. The values were converted into percent of maximum possible reflectance (i.e. 1). The difference in percent was then plotted against wavelength. The difference is at a minimum and almost constant from 400 to 750 nm. From 750 nm onward the

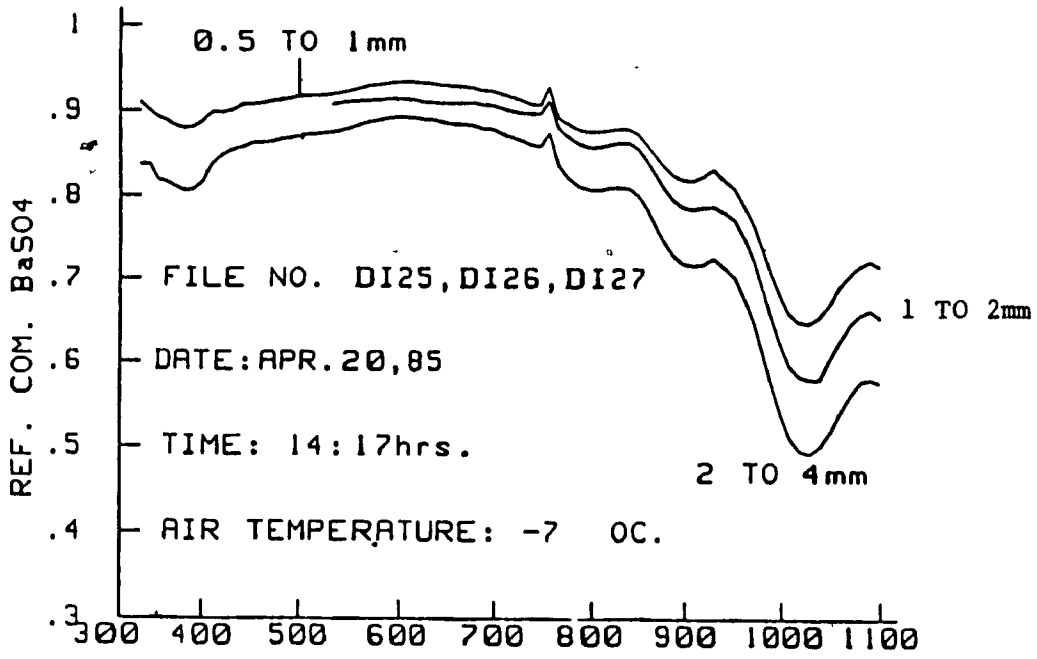

Fig. 4.8: Spectral reflectance of snow for different grain sizes.

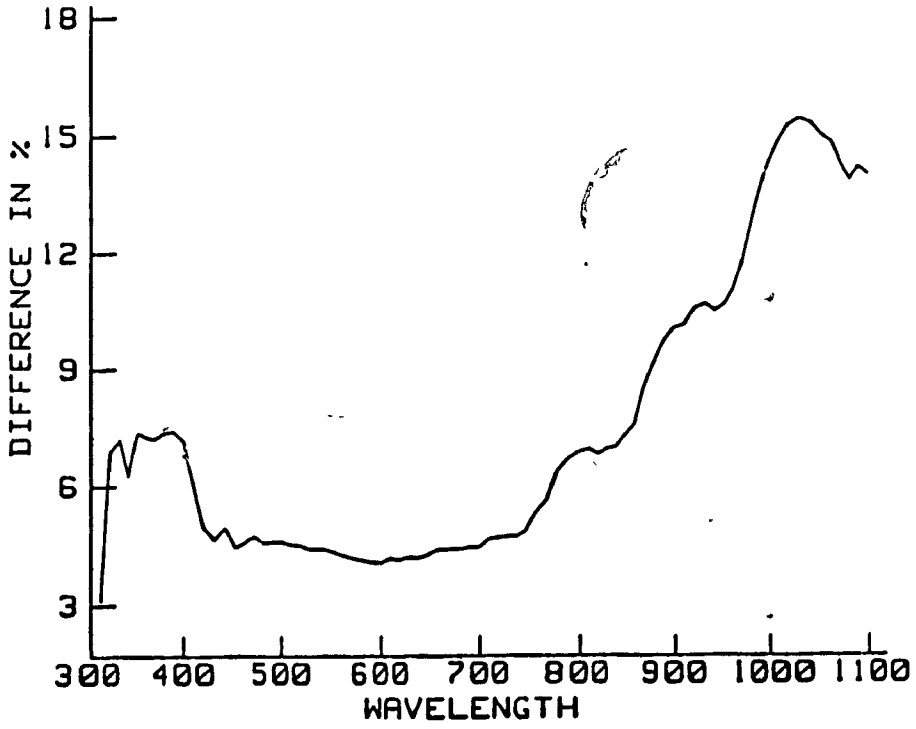

Fig. 4.9: Effect of change in grain size from 0.5-1 to 2-4 mm on spectral reflectance.

difference increases with increasing wavelength until 1020 nm. The maximum difference of 16 per cent was obtained around 1020 nm. After 1030 nm a minor decrease was noticed up to 1100 nm, with minor peaks near 790 and 940 nm. Similar results were obtained when the grain size was increased from 0.5-1 to 1-2 mm, except the amount of change in reflectance was smaller.

4.3.1 Repeatability of the Results

Similar experiments were repeated in February, 1986. These results are plotted in Figure 4.10. The figure shows a clear trend of successive change in reflectance for a change in grain size from 0.25-0.5 to 0.5-1(A); 1-2(B); 2-4(C) mm. The reflectance decreases with an increase in grain size in all wavelengths. The reduction in reflectance is almost constant for wavelengths between 400 and 750 nm. After 750 nm, the difference increases with increasing wavelength. The peak is observed around 1020 nm and after that there is a decline to 1100 nm. Figure 4.11 (graphs A, B, C) also shows that as grain size increases the difference between visible and near infrared reflectance also increases.

To assess the best ratio for detection of grain size variations, different ratios were attempted as shown in Figure 4.12 and Table 4.5. The procedure to compute these ratios is similar to that given in section 4.3. The analysis shows that the ratio between wavelengths 1000-1030 and 600-630 nm is the

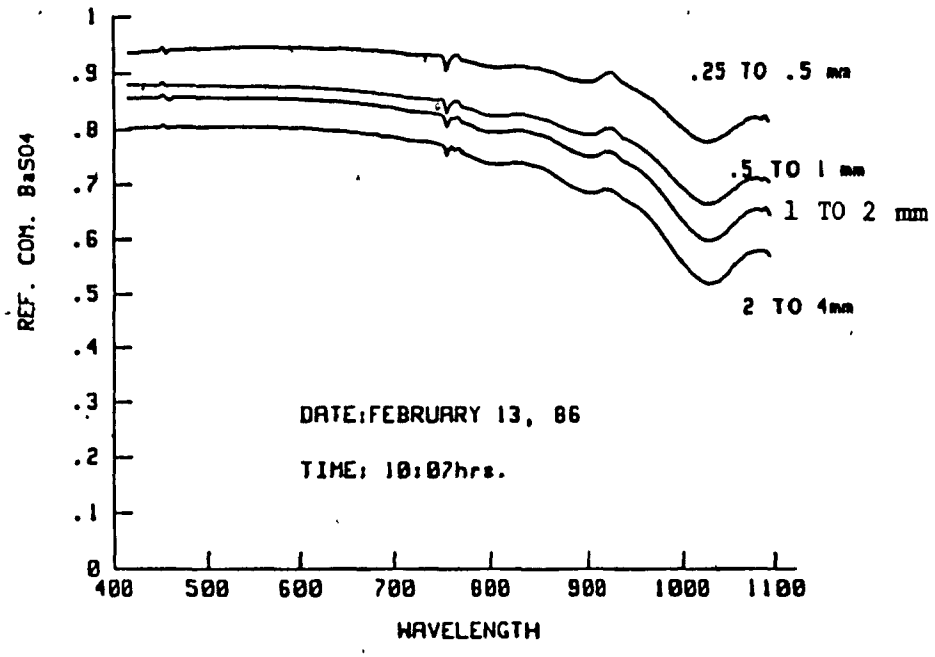

Fig. 4.10: Effect of changes in grain size on spectral reflectance

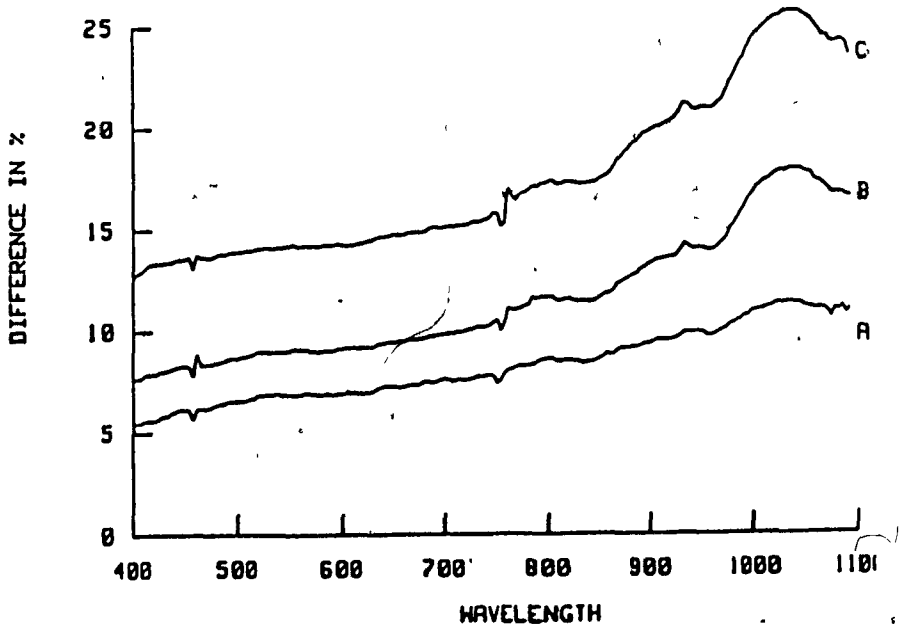

Fig. 4.11: Effect of changes in grain size from (A) 0.25-0.5 to 0.5-1 mm; (B) 0.25-0.5 to 1.0-2.0 mm; (C) 0.25-0.5 to 2.0-4.0 mm on spectral reflectance.

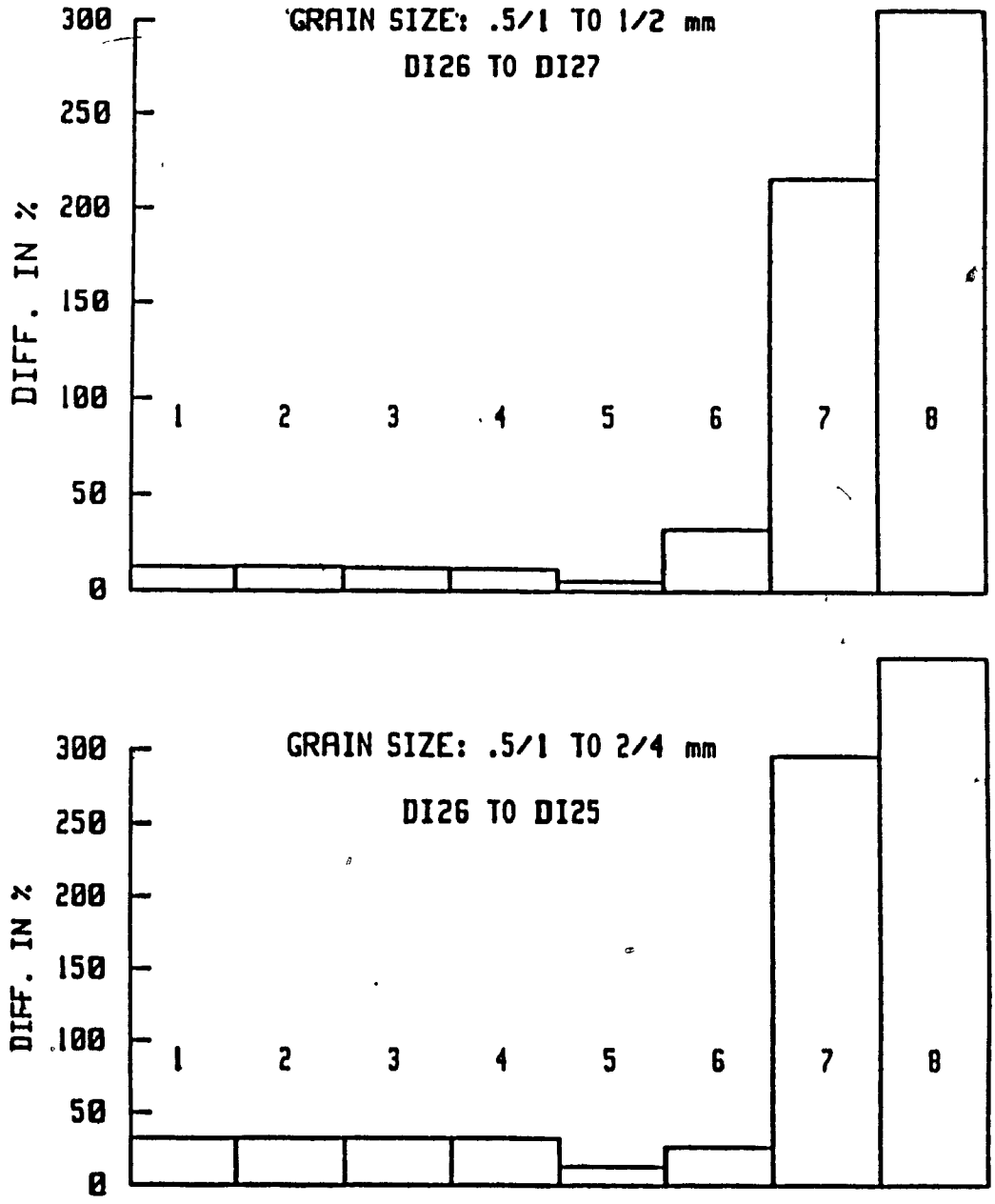

Fig. 4.12: Histogram showing change in ratio due to variation in grain size. Classes explained in Table 4.5.

one that is most sensitive to variations in grain size.

4.4 Grain size vs. liquid water content

One of the important objectives of this investigation is to assess, whether or not the effects of grain size and liquid water content can be differentiated. Therefore, the change in reflectance due to liquid water content and grain size are plotted in Figure 4.13. The graph A shows difference in reflectance between grain size 0.5-1 and 1-2 mm. The graph B shows change in reflectance due to change in snow condition from dry to wet snow (DI53 to DI55) and graph C due to change in snow condition from wet to dry (DI55 to DI57) (Figure 4.13).

Figure 4.13 shows that the maximum change in reflectance due to change from dry to wet and wet to dry snow condition occurs around 960 nm. The maximum difference due to variations in the grain size of the snow is observed around 1020 nm. Therefore, differentiation of effects of grain size and liquid water content appears possible.

4.4.1 Repeatability of the Results

In order to assess the repeatability of the above mentioned results additional, similar cases were investigated. The change in reflectance between dry to wet condition (DI57 to DI59), wet

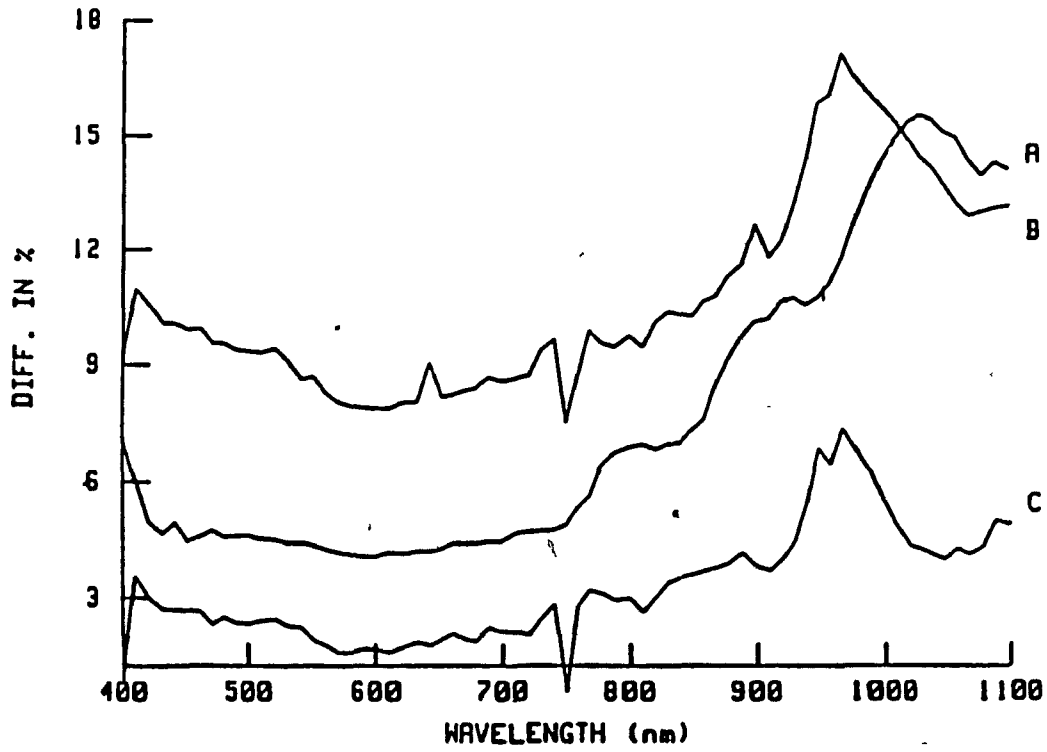

Fig. 4.13: Variation in spectral reflectance of snow due to change in (A) grain size from 0.5–1 to 1–2mm; (B) snow condition from dry to wet and (C) snow condition from wet to dry.

to dry condition (DI51 to DI53) and change in grain size from 0.25-0.5 to 1-2 mm (DI29 to DI31) were plotted in Figure 4.14. It shows that above mentioned results are repeated.

Further, the ratio between reflectances at 580-600 and 960-980 was computed (Table 4.4). The ratio between 580-600/960-980 is more than 1.31 for melting snow and less than 1.31 for non-melting snow of different grain size (File numbers DI26 and DI27 in Table 4.4). On the other hand the ratio between 600-630/1010-1030 is more sensitive to variations in grain size than to variations in the liquid water content (Bar number 8 in Figure 4.15). This phenomenon was observed during and after many freeze and thaw cycles. Therefore, contrary to earlier predictions (Dozier et al. 1981), the reflectance in this region of the electromagnetic spectrum is not only sensitive to grain size variations but is also significantly sensitive to variations in the liquid water content.

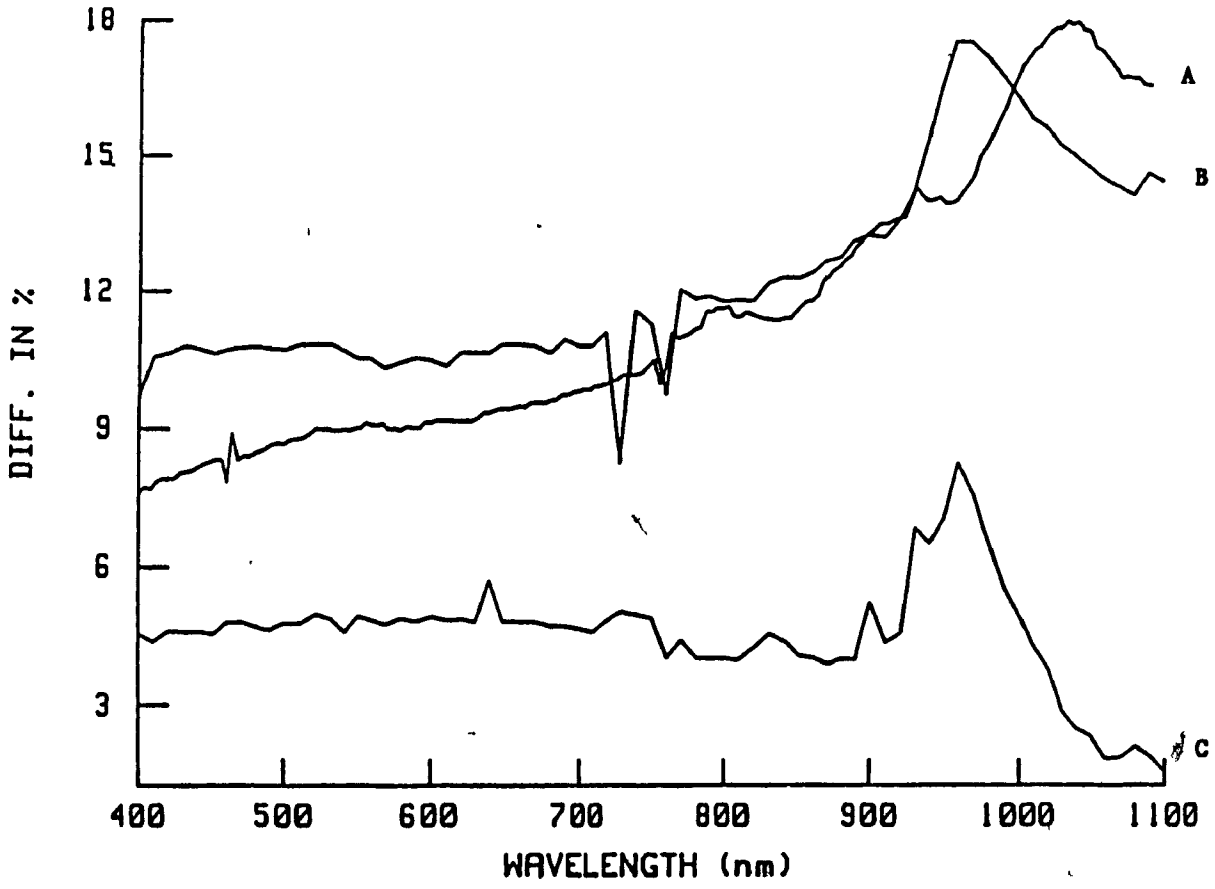

Fig. 4.14: Variation in spectral reflectance of snow due to change in (A) grain size from 0.25-0.5 to 1-2 mm; (B) snow condition from dry to wet and (C) snow condition from wet to dry.

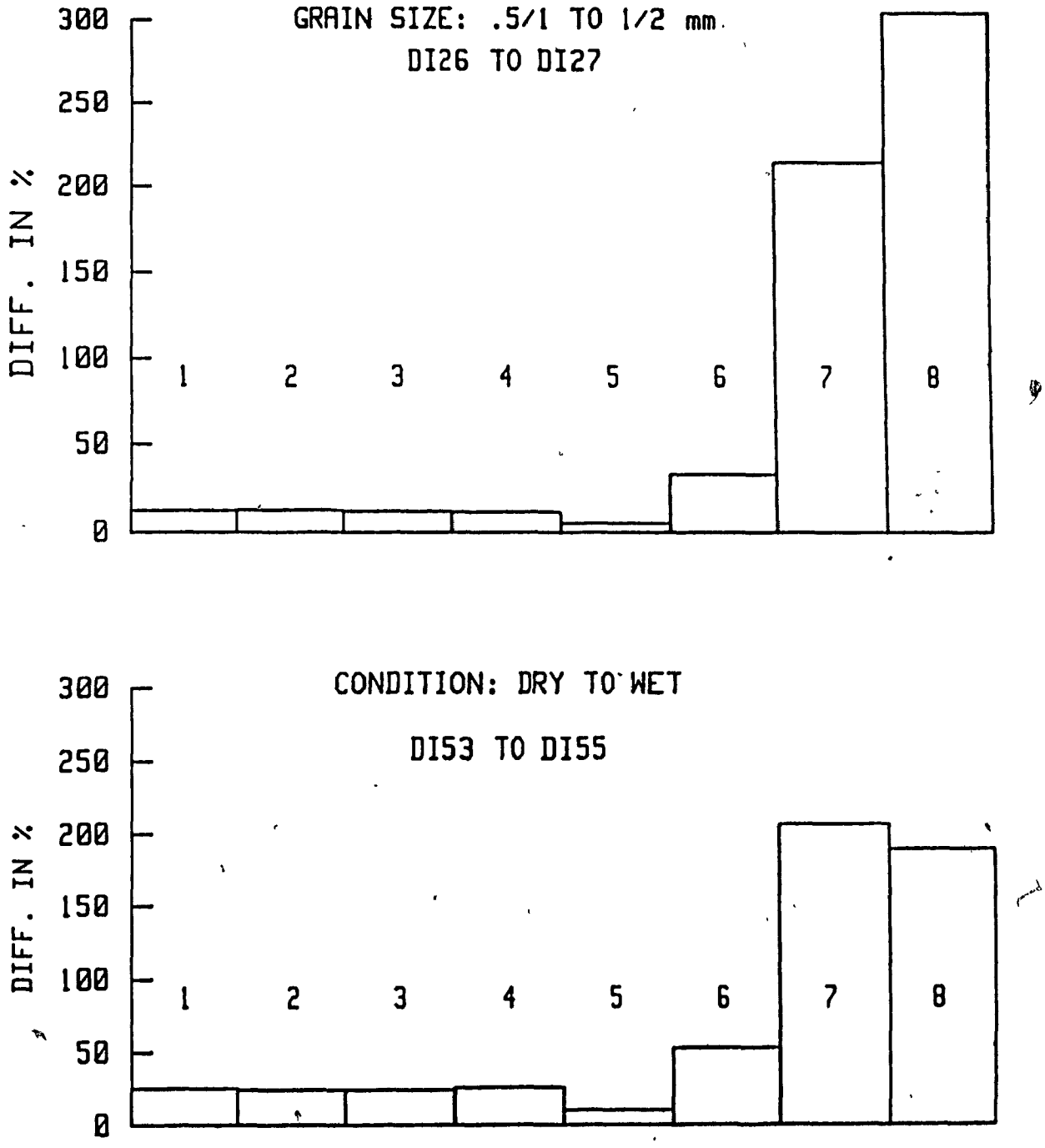

Fig. 4.15: Histogram showing changes in ratio due to variation in grain size and liquid water content. Classes explained in Table 4.5.

5. ATTENUATION OF SOLAR RADIATION BY THE SNOW COVER

5.1 Introduction

In this section, field measurements conducted during the winter and spring of 1986 to study the attenuation of solar radiation by the snow cover are analysed and discussed. The chapter deals with four main topics: (i) variations in the attenuation of solar radiation with wavelength, (ii) variations in the extinction coefficient with depth, (iii) changes in the extinction coefficient from winter to spring and (iv) variations in the depth of penetration with wavelength in winter and spring.

5.2 Differential attenuation of solar radiation with wavelength

In order to examine the spectral attenuation of solar radiation in the wavelengths from 400 to 1100 nm, both the attenuation of solar radiation in percent of incoming solar radiation and the extinction coefficient were plotted in Figure 5.1. The data were collected in April, 1986 (Profile SR), at a spectral interval of 2 nm.

In section A of Figure 5.1, the top graph represents the incoming solar radiation, expressed in mV. It was obtained by measuring the reflected radiation from a barium sulfate plate

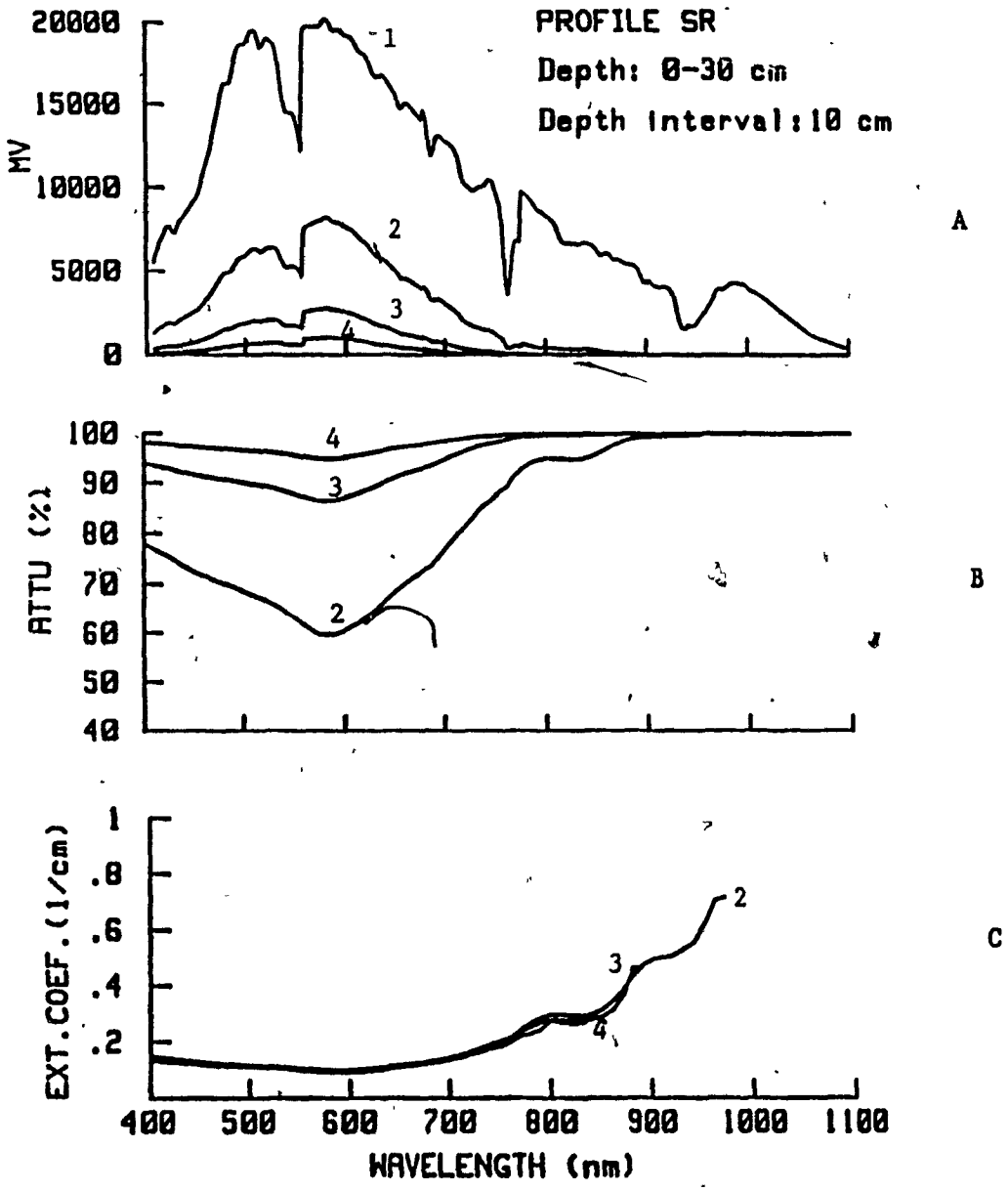

Fig. 5.1: Measured solar radiation (A), attenuation (B) and extinction coefficient (C) at 0 cm (1), 10 cm (2), 20 cm (3), 30 cm (4), in a snow pack.

and then dividing it by the absolute reflectance of barium sulfate (Grum and Luckey, 1968). Each successive graph in section A of Figure 5.1 represents the spectral variations in solar radiation (Iz) measured at depth intervals of 10 cm.

In section B of Figure 5.1, the attenuation of solar radiation was plotted at 10, 20 and 30 cm depths. The attenuation was obtained by subtracting the solar radiation measured at individual depths from the incoming radiation at each wavelength. These values were converted into percent of incoming solar radiation.

In section C of Figure 5.1, the spectral extinction coefficients were plotted against wavelength. The top graph represents the extinction coefficients obtained from radiation data collected at 10 cm intervals starting at a depth of 10 cm. The extinction coefficients for individual wavelengths were estimated using equation 2.4.

About 60 percent of the incoming solar radiation at 400 nm was attenuated at a depth of 10 cm (section B, Fig. 5.1). The attenuation decreases up to 580 nm. The lowest attenuation of 38 per cent was observed around 580 nm. After 580 nm, the attenuation increases with increasing wavelength. Almost 100 per cent attenuation was observed at 990 nm. These results are also reflected by the extinction coefficient, where the lowest value was observed near 580 nm and the maximum value was found

between 990 and 1100 nm (Fig. 5.1). The patterns of attenuation and extinction are repeated at greater depths in the snow cover. In general, the green part of the solar spectrum shows the maximum and the near infrared region the minimum penetration.

5.2.1 Repeatability of the results

To assess the repeatability of the results, the attenuation of solar radiation and the extinction coefficient were plotted in Figure 5.2. This data set was collected in February 1986 at intervals of 10 cm (Profile BC). The graphs show that the results observed in the earlier section were repeated in February, 1986 (See also plots in Appendix A).

5.3 Variations in the extinction coefficient with depth.

The extinction coefficient was determined using equation 2.4. This equation is generally applicable to a homogenous snow pack. However, a natural snow pack is rarely homogenous and the attenuation of solar radiation is therefore not necessarily uniform throughout its depth.

To study the variation in extinction coefficient with depth in the snow pack, the radiation intensity was measured at an interval of 2 cm from the top of the snow pack down to 18 cm and then at an interval of 4 cm from 18 cm to 30 cm. This data

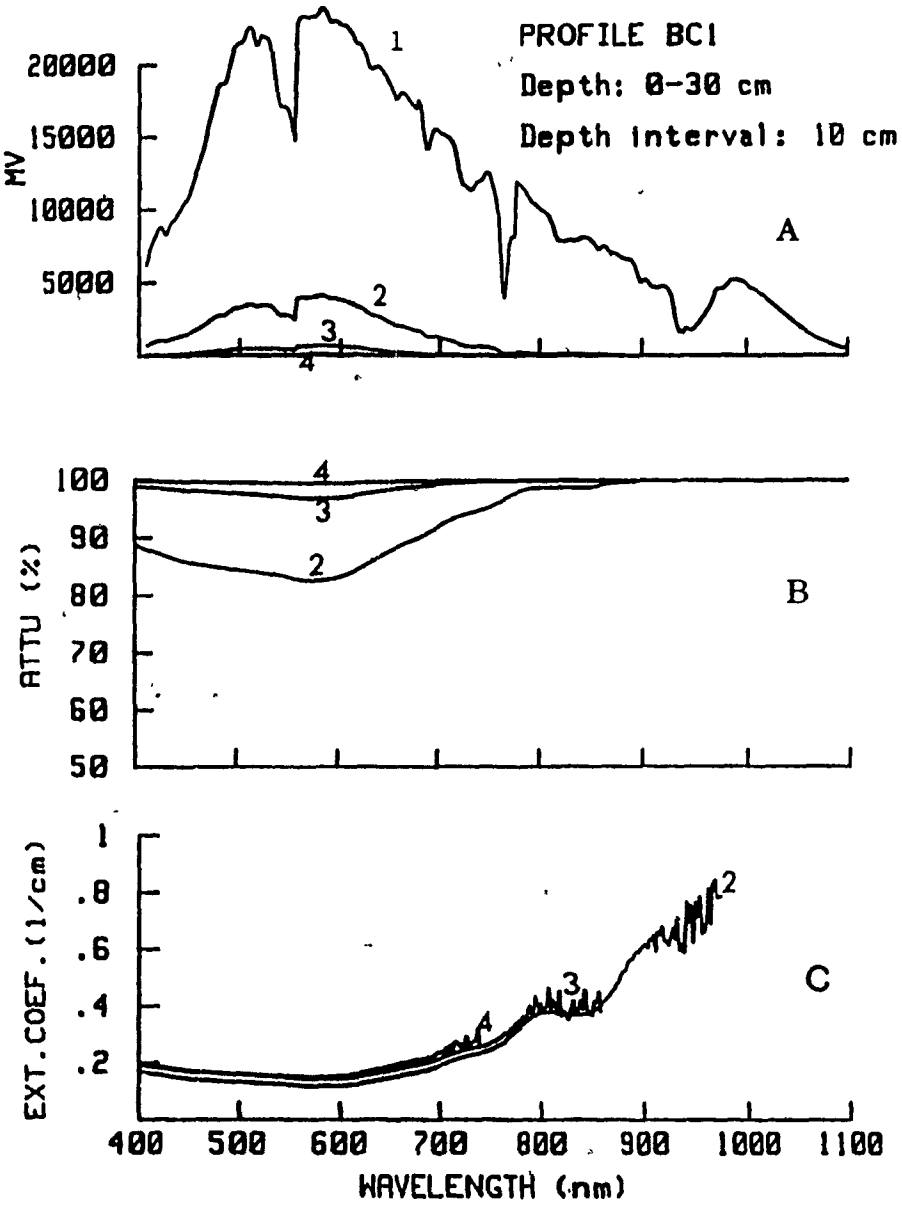

Fig. 5.2: Measured solar radiation (A), attenuation (B) and extinction coefficient (C) at 0 cm (1), 10 cm (2), 20 cm (3), 30 cm (4) in a snow pack.

set was collected on April 23, 1986 under clear sky conditions (Figs. 5.3a and 5.3b). The extinction coefficients plotted in Figure 5.3a were obtained from data collected at depths of 2 to 18 cm. In Figure 5.3b, the extinction coefficients are plotted for depths from 18 to 30 cm.

A significant drop in the extinction coefficient was observed from A1 to A8, where A1 represents a depth of 2 cm and A8 a depth of 18 cm. The drop in the extinction coefficient is not uniform with depth. The maximum drop was observed in the top 10 cm. A lesser drop was observed for depths from 20 to 30 cm.

5.4 Depth of penetration of solar radiation in winter and spring respectively

5.4.1 Depth of penetration of solar radiation in winter

To illustrate the penetration of solar radiation during the winter, a data set that was collected on February 18, 1986 is used. Measurements were made at the snow surface and at 10 cm intervals for depths from 10 to 60 cm. The attenuation and the extinction coefficients at each depth are plotted in Figure 5.4 (Profile DA3). As in all other cases, the maximum energy on this day was transmitted in the spectral region around 580 nm. The solar radiation in the wavelengths from 880 to 1100 nm, 780 to 880 nm, 710 to 780 and 660 to 710 nm were completely attenuated between depths 0 to 10, 10 to 20, 20 to 30 and 30 to

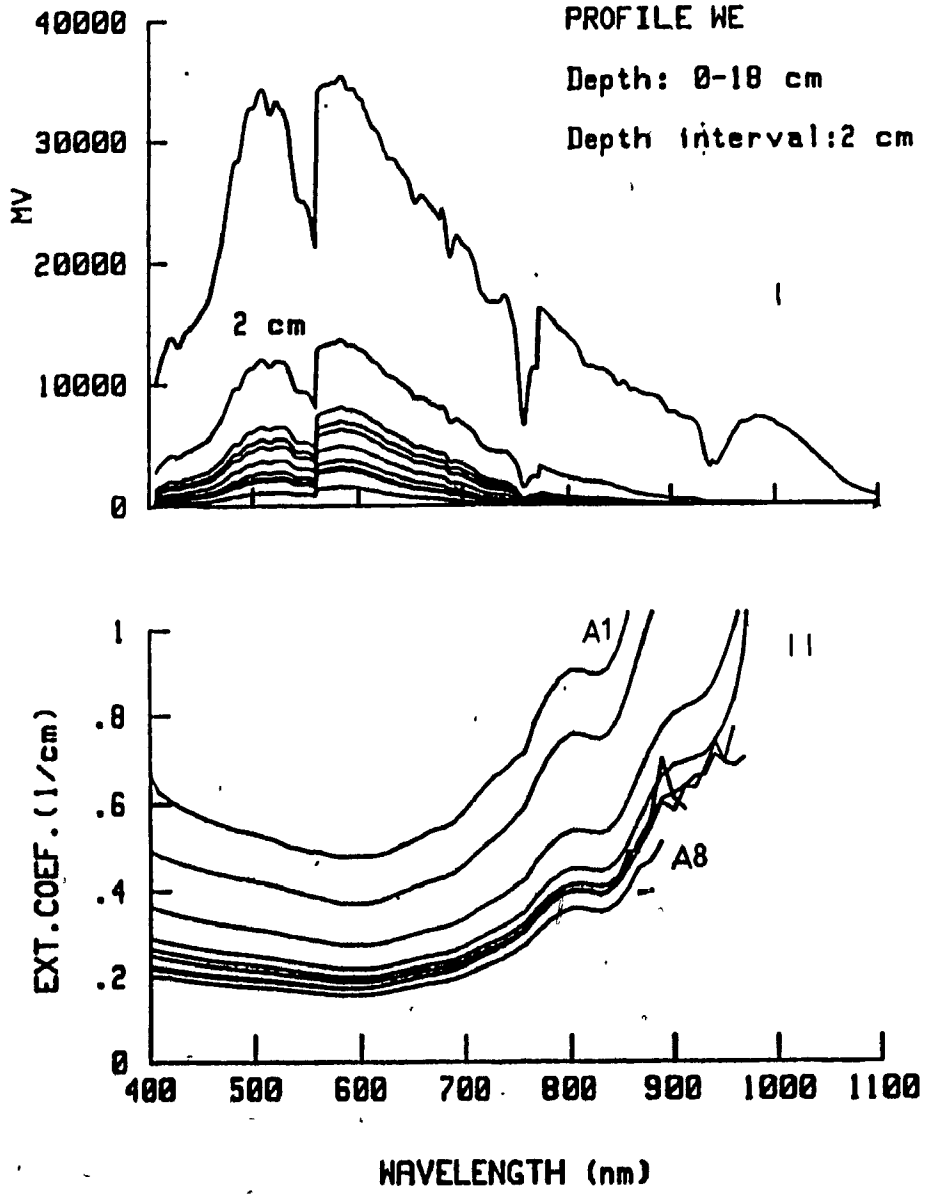

Fig. 5.3a: Variations in extinction coefficient due to depth of observation in a snow pack. Measured solar radiation (I) and extinction coefficient (II) from data 2 (A1) to 18 cm depth at intervals of 2 cm.

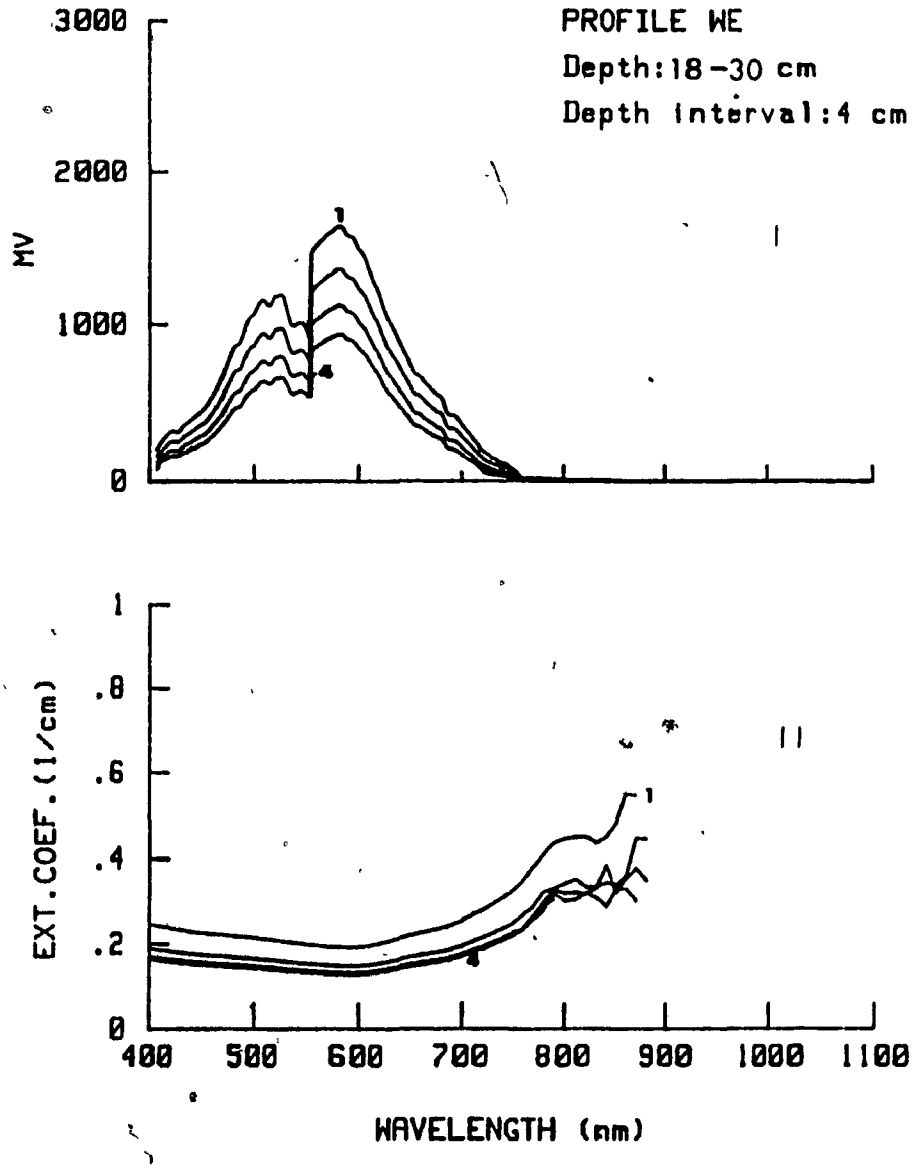

Fig. 5.3b: Variations in extinction coefficient due to depth of observation in a snow pack. Measured solar radiation (I) and extinction coefficient (II) from 18 (1) to 30 cm (4) at intervals of 4 cm.

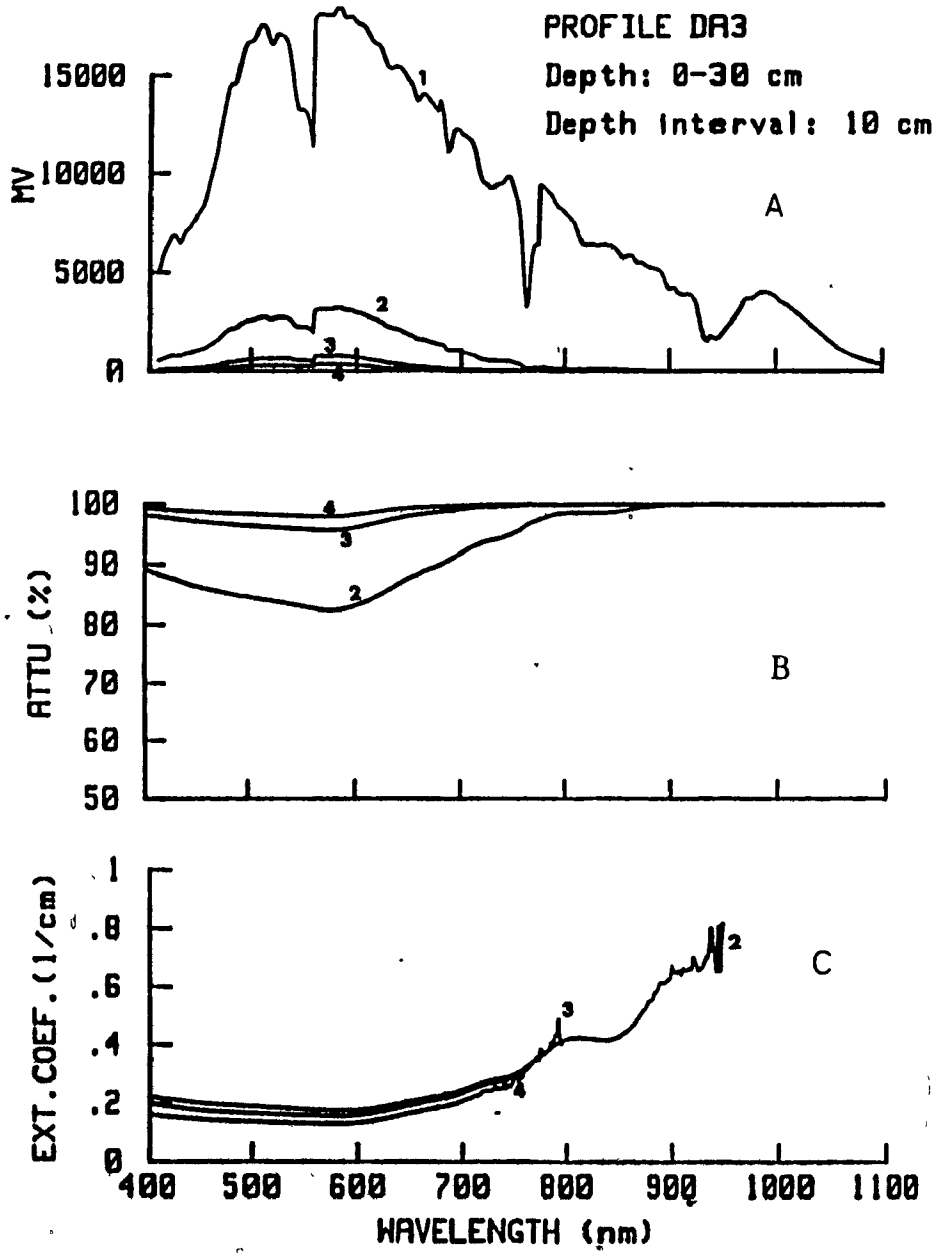

Fig. 5.4: Attenuation and extinction coefficient of solar radiation in winter. (A) Measured solar radiation at 0 cm (1), 10 cm (2), 20 cm (3) and 30 cm (4); (B) Attenuation and extinction coefficient (C).

40 cm respectively. A small quantity of energy was further transmitted to a depth of 60 cm at 580 nm. The amount of energy was very small, i.e. 25 mV as compared to 30,000 mV at the surface.

5.4.2 The depth of penetration of solar radiation in spring

The attenuation of solar radiation by snow in spring is illustrated by the MO2 profile (Fig. 5.5). The data were collected in April, 1986. The top graph of portion A represents the incoming solar radiation. The second and third graphs represent total radiation measured at 10 and 20 cm depth respectively.

The first graph from bottom represents the attenuation by snow at 10 cm and the second at 20 cm depth. The solar radiation from 900 to 1100 nm, 780 to 900, 760 to 780 and 700 to 780 nm were attenuated from depths of 0 to 10, 10 to 20, 20 to 30 and 30 to 40 cm respectively.

The extinction coefficient was estimated using equation 2.4. The variations in extinction coefficient with wavelength and depth are given in Figures 5.1 and 5.3. The results show that the lowest extinction coefficient occurs around 580 nm.

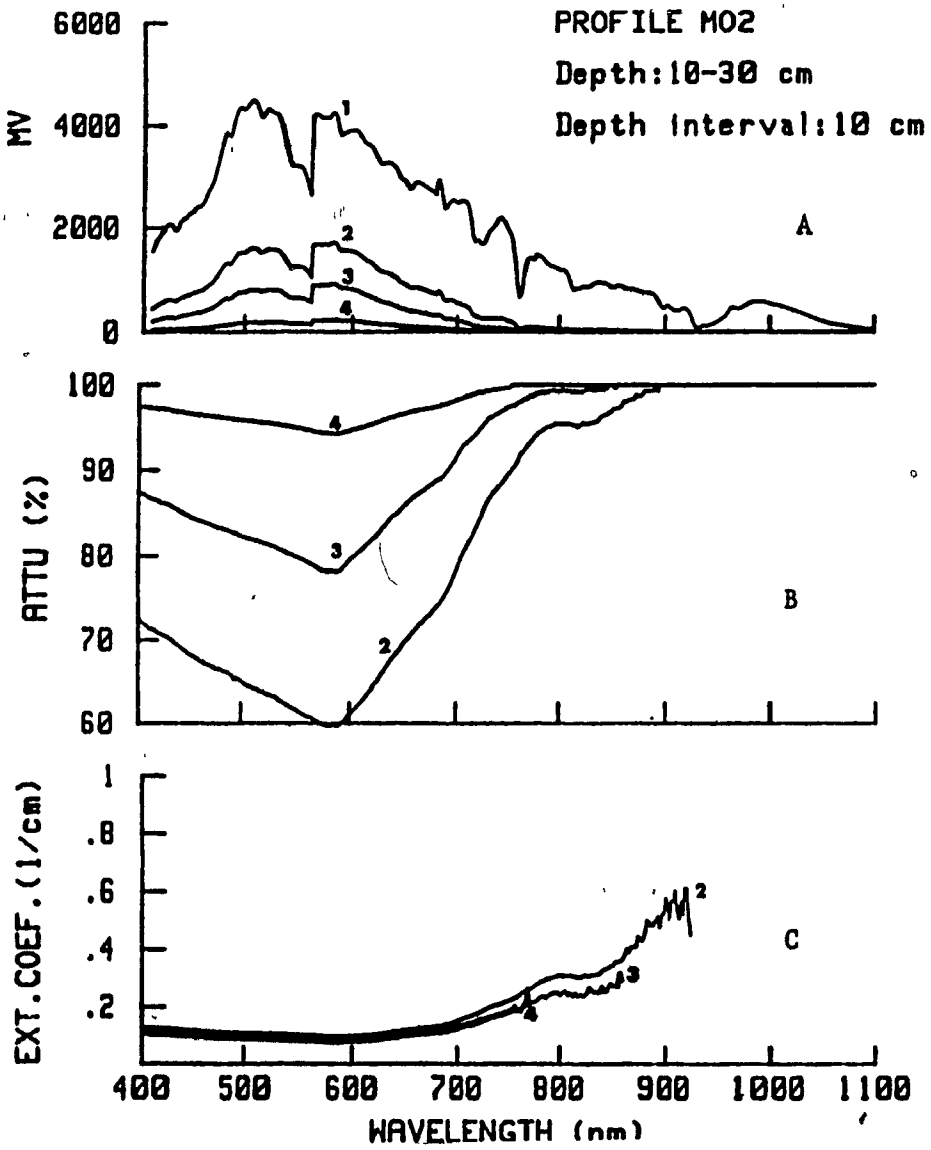

Fig. 5.5: Attenuation and extinction coefficient of solar radiation in spring. (A) Measured solar radiation at 0 (1), 10 (10), 20 (3) and 30 cm (4); (B) attenuation and (C) extinction coefficient.

5.4.3 Comparison of the depth of penetration of solar radiation in winter and spring

To compare the attenuation in winter and spring, the spectral attenuation and the extinction coefficient were plotted in Figures 5.6a and 5.6b. The attenuation at 10 and 20 cm and on the other hand 20 and 30 cm were plotted in Figures 5.6a and 5.6b, respectively. The basic pattern of attenuation from 400 to 1100 nm does not change from winter to spring. However, the amount of attenuation changes. In winter, the amount of attenuation measured at 580 nm and 10 cm depth was almost 81%. In spring, at the identical depth and wavelength, only 59 per cent of the incoming radiation was attenuated (Fig. 5.6a). Lower attenuation of solar radiation was observed in spring than in winter in all wavelengths and at all depths (Figs. 5.6a and 5.6b). These results are also reflected in a lower extinction coefficient observed in spring than in winter (Figs. 5.6a and 5.6b). These results in a general way support earlier predictions by Bohren and Barkstrom (1974), who predicted an extinction coefficient inversely proportional to the square root of grain size. Generally the grain size of the snow pack increases from winter to spring.

During the winter, radiation data in the top 10 cm layer was not collected. Therefore, it is not possible to compare the attenuation in the top layer for winter and spring. Usually contaminants accumulate in the top layer. Therefore, a higher

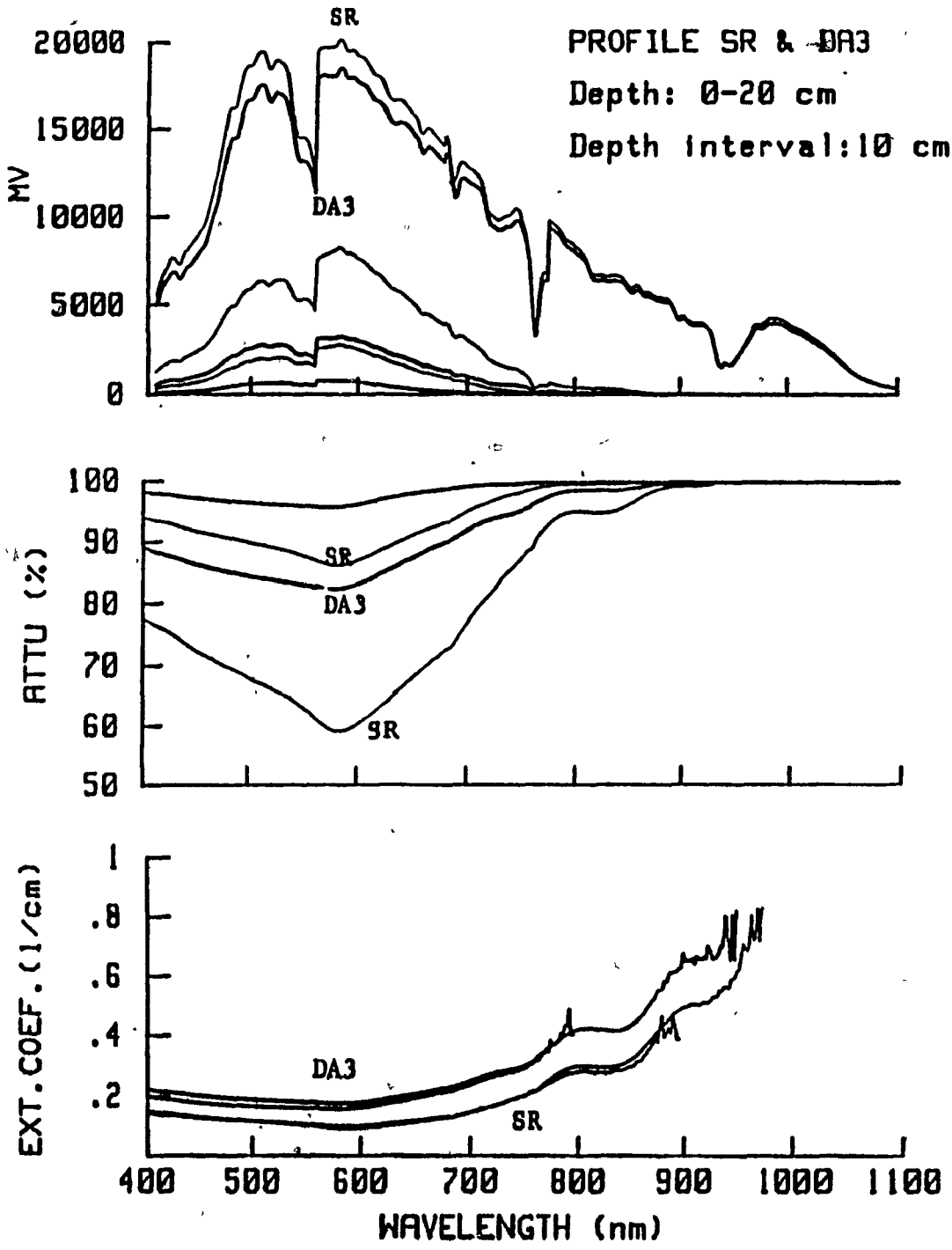

Fig. 5.6a: Comparison of attenuation and extinction coefficient between winter (DA3) and spring (SR).

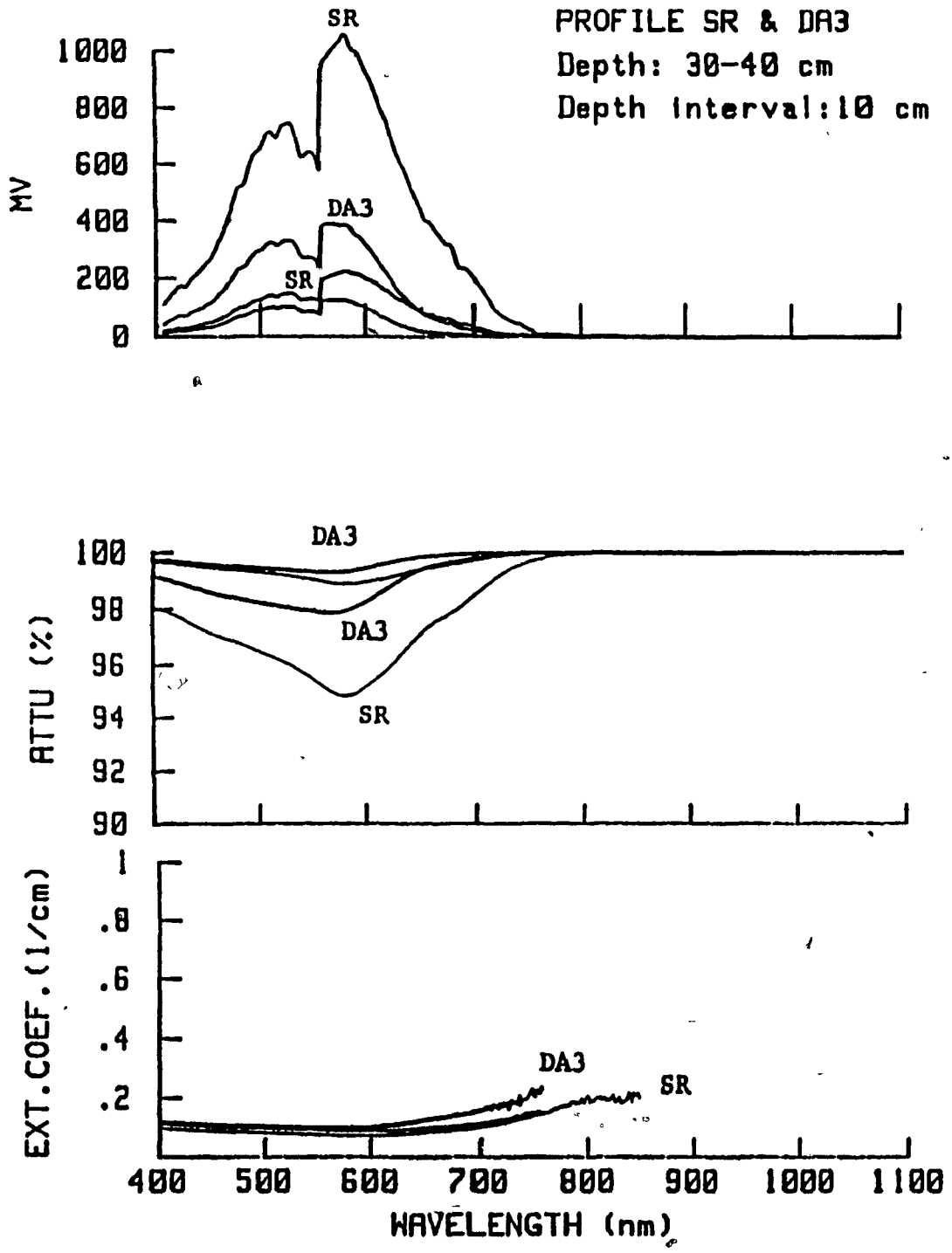

Fig. 5.6b: Comparison of attenuation and extinction coefficient between winter (DA3) and spring (SR).

extinction coefficient was expected in top layer during spring than during winter due to absorbtion by contaminants in wavelengths from 300 to 700 nm (Warren and Wiscombe, 1981; Maze, 1974). The present results show a decrease in extinction coefficient from winter to spring at depths from 10 to 40 cm.

5.5 The maximum penetration depth of solar radiation

The penetration depth of a snow pack, i.e. the maximum depth to which solar radiation can penetrate in a snow pack can be estimated using the observed extinction coefficient. The extinction coefficient was estimated using Equation 2.4. The depth of penetration into the snowpack can be estimated using the following relationship:

$$Z = - \ln(1/Io) * b \qquad (5.1)$$

where Z = Penetration depth of radiation (cm)

Io = Radiation intensity at snow surface (mV)

b = Extinction coefficient(1/cm)

Equation 5.1 is modified from equation 2.4. Iz, i.e. the radiation intensity at depth z is considered to be 1 mV. The radiation intensity at the snow surface, Io, measured on April 23, 1986 at 12:09 was used in all calculations. The sample Io was used in order to avoid errors due to different intensities at different times of day and year. The results are analysed

with respect to three main subjects: (i) the variation of penetration depth with wavelength, (ii) the variation in penetration depth due to variations in the extinction coefficient and (iii) the variation in maximum penetration depth from winter to spring.

5.5.1 Variations in penetration depth with wavelength

The variations in penetration depth with wavelength is given in Figure 5.7. This data set was collected in April, 1986. The penetration depth was estimated at intervals of 2 nm using equation 5.1.

The maximum penetration depth varies considerably from wavelength to wavelength. The range is from 140 cm to less than 3 mm (Fig. 5.7). The maximum penetration depth of 140 cm occurs around 580 nm. At 400 nm a penetration depth of 80 cm was observed and it increases with wavelength to 578 nm. From 584 nm, the penetration depth drops continuously to 1100 nm. The lowest value was observed between 1000 and 1100 nm, where the maximum penetration depth was less than 3 mm.

5.5.2 Variations in the penetration depth due to variations in the extinction coefficient.

As explained in section 5.3, the magnitude of the extinction coefficient can depend considerably upon the depth of

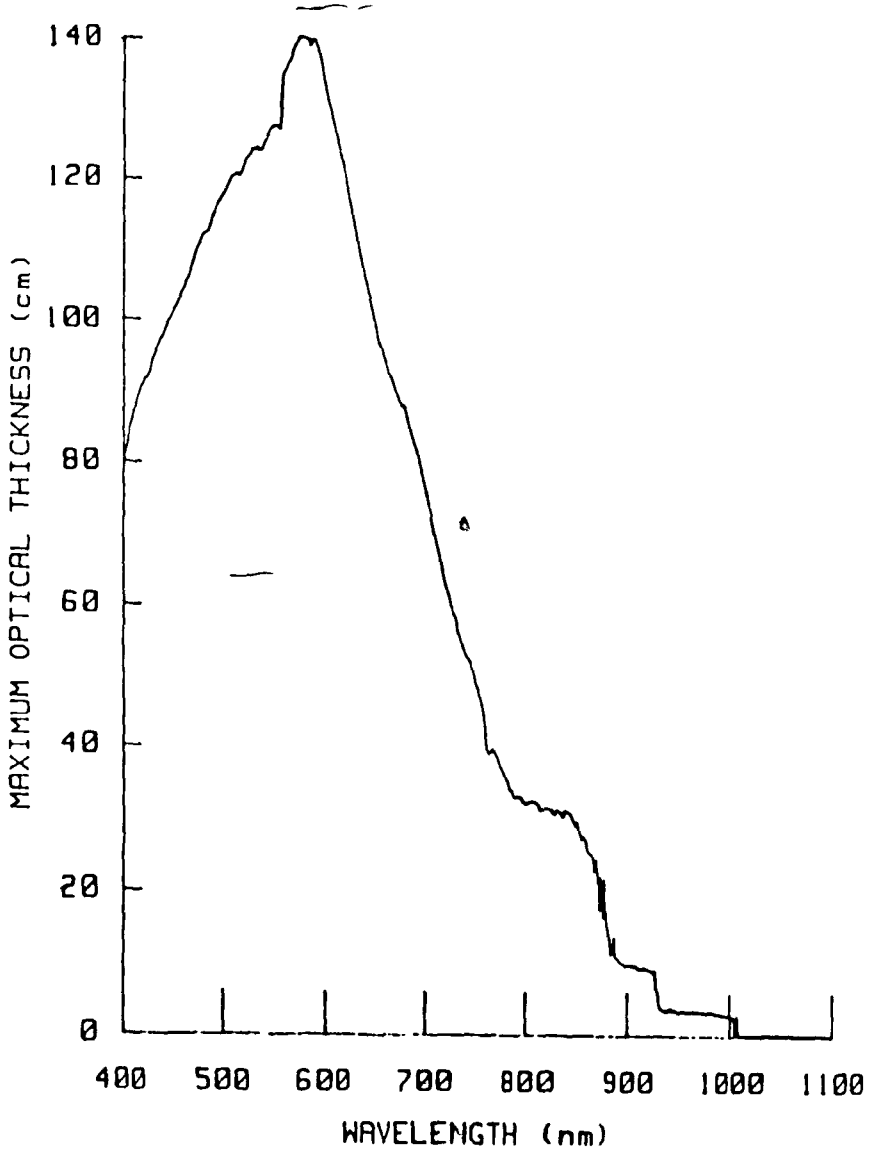

Fig. 5.7: Variations in optical thickness with wavelength

observation. Consequently, the depth of observation can also affect the penetration depth as is demonstrated in Figure 5.8. This data set was collected in February, 1986. The bottom graph represents the maximum penetration depth if Iz is collected at a depth of 10 cm. Each successive graph was estimated from Iz collected at further depth increments of 10 cm. The graph shows that during winter the maximum penetration depth can increase with the depth of the observation that was used to determine the extinction coefficient. This may not be true in the snow melt season as Figure 5.9 shows, possibly because of high concentration of contaminants at the top and slush at the bottom of the snow pack.

5.5.3 Changes in maximum penetration depth from winter to spring

The maximum penetration depth was estimated by taking the lowest extinction coefficient for each wavelength. For example in Figure 5.10, at a wavelength of 400 nm, the extinction coefficient was estimated from Iz collected at depths from 2 cm to 30 cm at an interval of 2 cm and at 35 and 40 cm. The lowest extinction coefficient was taken to estimate the maximum penetration depth. The same procedure was used to estimate the maximum penetration depth for wavelengths 400 to 1100 nm, at an interval of 2 nm in the spring and 4 nm in the winter.

In both winter and spring, the maximum penetration depth was

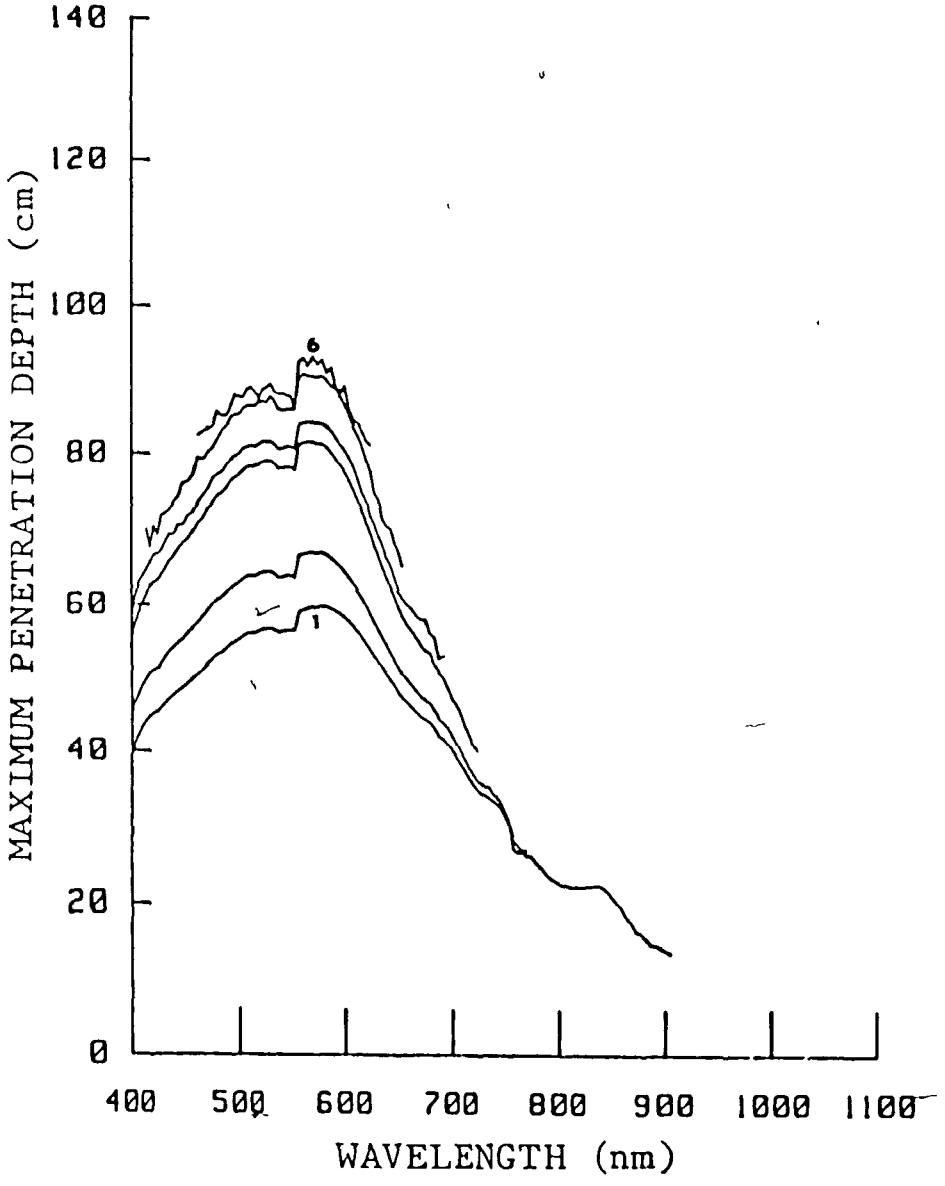

Fig. 5.8: Variations in penetration depth due to extinction coefficient. Depths of observation from 10 cm (1) to 60 cm (6) at intervals of 10 cm.

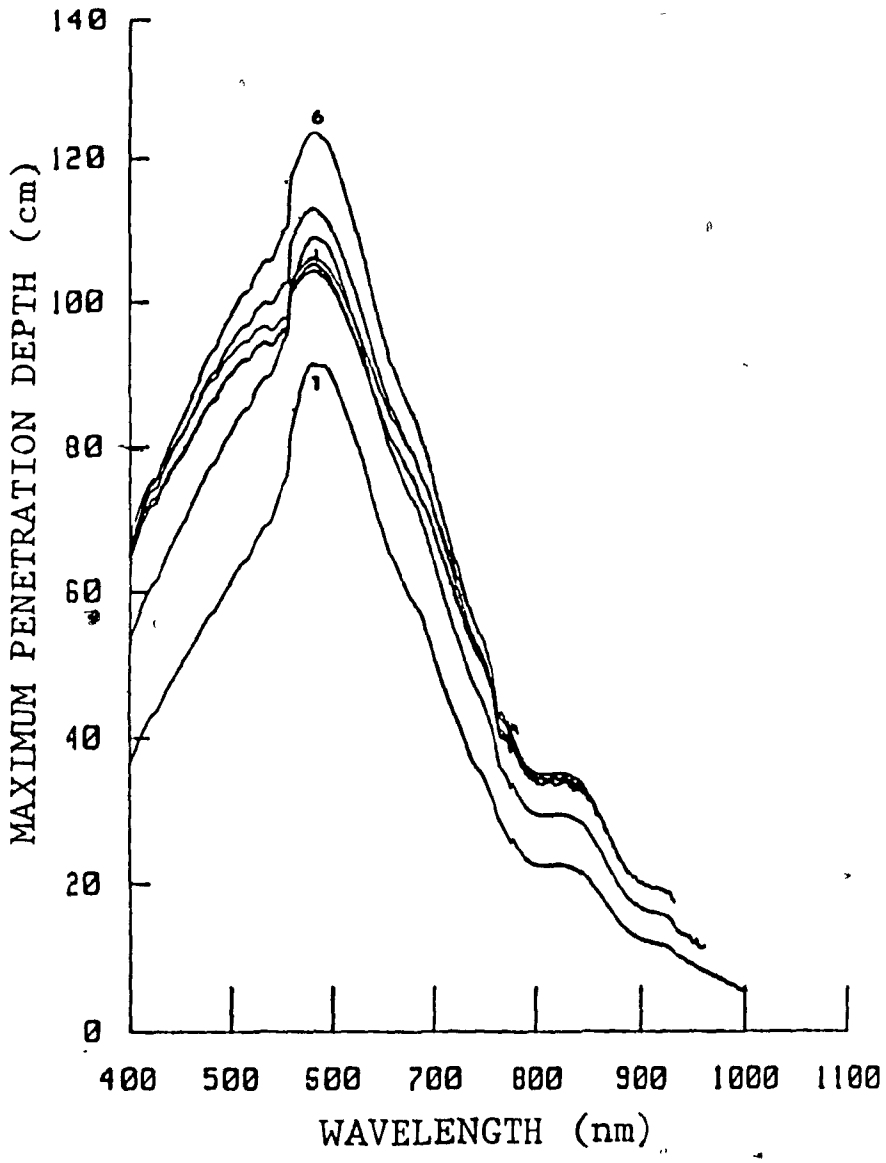

Fig. 5.9: Variations in penetration depth due to extinction coefficient. Depths of observation from 10 cm (1) to 60 cm (6) at intervals of 10 cm.

observed around 580 nm (Fig. 5.10). The maximum value in winter was observed to be less than 100 cm, whereas it was observed to vary from site to site from 120 to 175 cm in spring. The variations for different wavelengths are given in Figure 5.10.

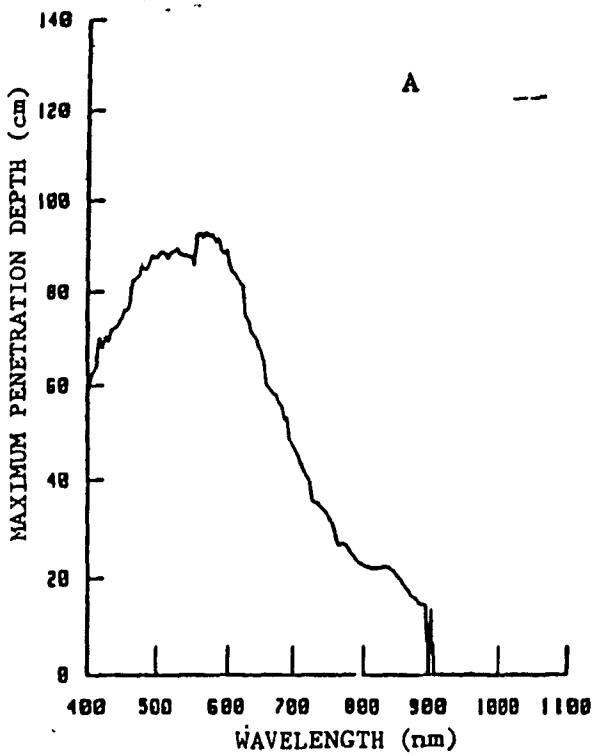

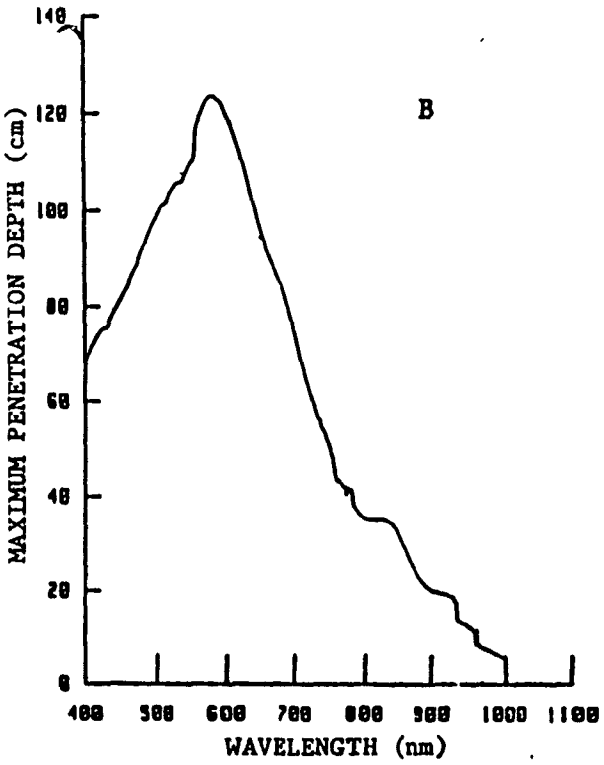

Fig. 5.10: Maximum penetration depth in (A) winter and (B) spring.

6. CONCLUSIONS AND RECOMMENDATIONS

6.1 Conclusions

6.1.1 Spectral reflectance

This investigation has examined the effects of grain size and liquid water content on the spectral reflectance and attenuation of solar radiation by the snow cover. Effects of liquid water content were monitored by measuring the change in spectral reflectance associated with changes from a melting to non-melting and again to a melting condition of the snow cover. A drop in reflectance of 18 per cent was observed around 960 nm when the snow changed from dry to wet and a rise of 9 per cent was observed for a change from wet to dry. This shows that the rise in reflectance upon refreezing, although significant, does not reach the premelting level. This observation is contrary to earlier observations of O'Brian and Munis (1975), who observed no increase in reflectance upon refreezing.

The ratios between the reflectance at 580-600 nm to the reflectance at 960-980 nm were more than 1.34 for melting snow and less than 1.30 for non-melting snow. These observations were repeated even after multiple freeze and thaw cycles suggesting that the wavelengths around 960 nm could be more sensitive to the liquid water content of snow than any other

region of the electromagnetic spectrum between 400 and 1100 nm. This is possibly because of the high absorption coefficient of water for wavelengths around 970 nm. Available data from the literature suggests that in the range 400-1100 nm the difference between the absorption coefficients of ice and water reaches a maximum near 970 nm (Irving and Pollack, 1968; Grenfell and Perovich, 1981).

The effects of grain size on spectral reflectance were examined using different size fractions of snow samples. For a change in grain size from 0.5-1 mm to 2-4 mm, a maximum difference of 16 per cent was observed around 1020 nm and a difference of 11 percent was observed at 960 nm. The reflectance showed an overall decrease with increasing grain size.

The significant rise in reflectance as the snow changes from wet to dry (even after multiple freeze and thaw cycles), the consistent difference in the ratio between reflectance at 580-600 and 960-980 nm for melting and non-melting snow and the relatively small influence of grain size as compared to liquid water content suggest that the spectral band around 960 nm could be useful in remote sensing of the liquid water content of snow.

Some of the results obtained in this study disagree with earlier models by Dozier et al (1981) and Wiscombe and Warren (1981), where a change in reflectance is considered to be due

only to an increase in grain size rather than changes in the liquid water content. However, the results of this investigation are based upon observations taken at one site only. In order to avoid the possibility of unknown errors due to local effects, further studies should be made in different locations and snow pack conditions to better assess the causes of this disagreement.

6.1.2 Spectral attenuation

Measurements of the attenuation of solar radiation by the snow pack show that the lowest attenuation occurs near 580 nm and the maximum attenuation between 990 and 1100 nm. Similarly, the lowest extinction coefficient was observed at 580 nm (< 0.1 per cm) and the maximum between 990 and 1100 nm (up to 2.5 per cm).

The extinction coefficient was observed to vary depending upon the depth of observation inside the snow pack. It generally decreased with increasing depth below the snow surface.

The attenuation of solar radiation by snow was greater in winter than in spring. At 580 nm wavelength, at a depth of 10 cm below the snow surface 60 percent of the incoming solar radiation were attenuated in spring, while almost 80 percent were attenuated in winter (Fig. 5.6a).

The maximum penetration depth was observed around 580 nm, where solar radiation can penetrate from 120 to 175 cm in spring, while it penetrates only to about 80 cm in winter. The lowest penetration of only a few millimeters occurs in wavelengths between 1000 and 1100 nm. These results are comparable with earlier estimates of Schwerdtfeger and Weller (1977) and Warren (1982), where penetration of visible radiation to a depth of 100 cm was predicted. The present results do not agree with the prediction of Warren (1982), where the maximum penetration was forecasted in the blue part of the spectrum (i.e. around 460 nm). In the present study the maximum penetration was observed at 580 nm which is in the green part of the spectrum.

6.1.3 Additional conclusions

The Li-1800 spectroradiometer performed satisfactorily under extreme temperature conditions at Schefferville. The data transfer from the radiometer to the TRS-80 model 100 computer and then to disk in the field greatly increased the throughput of the field data acquisition system.

6.2 Some recommendations for future research

The effects of the liquid water content of snow on the spectral reflectance were studied in the field under different sun elevations, changing physical characteristics of the snow cover and (not easily monitored) variations in its water

content. These measurements were also performed in only one location. It would be useful to undertake these studies under controlled laboratory conditions and to repeat some of the measurements at different locations and under different snow cover conditions. In addition, during this investigation the data used in the study of liquid water content were collected at a spectral interval of 10 nm. Additional investigations at narrower band width would help to locate more accurately the limits of the liquid water sensitive band near 960 nm.

The solar radiation data collected at the surface and in the snow pack were not converted into irradiance, because of lack of appropriate calibration of the fiber optics probe. Therefore, in this investigations only a relative analysis was done. It would be useful to convert the instrument response into irradiance values, so that the availability of solar radiation at each depth could be exactly known.

The present data set was collected at very high spectral resolution and at closely spaced depth intervals in the snow cover. Its usefulness has by no means been exhausted in this thesis. The data set and the field data acquisition system developed as part of this thesis could provide much additional service in further model development and testing.

REFERENCES

Bader,H. (1950): Note on the liquid water content of wet snow, Journal of Glaciology, Vol. 1, No. 8, pages 466-467.

Barnes,J.; Smallwood,C. and Michel,D. (1975): Synopsis of current techniques with emphasis on the application of near infrared data, NASA-SP-391, pages 199-213.

Barkstrom,B.R. (1972): Some effects of multiple scattering on the distribution of solar radiation in snow and ice, Journal of Glaciology, Vol. 11, pages 357-368.

Barkstrom,B.R. and Querfeld,C.W. (1975): Concerning the effect of anisotropic scattering and finite depth on the distribution of solar radiation in snow, Journal of Glaciology, Vol. 14, No. 70, pages 107-124.

Bohren,C.F. and Barkstrom,B.R. (1974): Theory of the optical properties of snow, Journal of Geophysical Research, Vol. 79, pages 4527-4535.

Bolsenga,S.J. and Kistler,R.D. (1982): A Dual Spectroradiometer System for Measuring Spectral Reflectances, Journal of Applied Meteorology, Vol. 21,

pages 642-647.

Choudhury,B.J. and Chang,A.T.C. (1981): The albedo of snow for partially cloudy skies, Boundary-Layer Meteorology, Vol. 20, pages 371-389.

Colbeck,S.C. (1982): An overview of seasonal snow metamorphism, Reviews of Geophysics and Space Physics, Vol. 20, No. 1, pages 45-61.

Colbeck,S.C. (1979): Grain clusters in wet snow, Journal of Colloid and Interface Science, Vol. 72, No. 3, pages 371-384.

Colbeck,S.C. (1978): The difficulties of measuring the water saturation and porosity of snow, Journal of Glaciology, Vol. 20, No. 82, pages 189-201.

Colbeck,S.C. (1975): Analysis of hydrological response of rain-on-snow, CRREL Research Report 340, pages 13.

Davis,R.E.; Dozier,J.; LaChapelle,E.R. and Perla, R. (1985): Field and laboratory measurements of liquid water by dilution, Water Resources Research, Vol. 21, No. 9, pages 1415-1420.

Davis, R.E. and Dozier,J. (1984): Snow wetness measurement by fluorescent dye dilution, Journal of Glaciogy, Vol. 30, No. 106, pages 362-363.

Dozier,J. (1984): Snow reflectance from Landsat-4 Thematic Mapper, IEEE Transactions on Geoscience and remote Sensing, Vol. GE-22, No. 3, pages 323-328.

Dozier,J., Schneider,S.R. and McGinnis Jr.,D.F. (1981): Effect of grain size and snow pack water equivalent on visible and nearinfrared satellite observations of snow, Water Resources Research, Vol. 17, No. 4, pages 1213-1221.

Dunkle, R.V. and Bevans,J.T. (1956): An approximate analysis of the solar reflectance and transmittance of a snow cover, Journal of Meteorology, Vol. 13, pages 212-216.

Fisk,D. (1986): Method of measuring liquid water mass fraction of snow by alcohol solution, Journal of Glaciology (in press).

Giddings,J.C. and LaChapelle,E.R. (1961): Diffuse theory applied to radient energy distribution and albedo of snow, Journal of Geophysical Research, Vol. 66, pages 181-189.

Granberg,H.B. and Kingsbury,C.M. (1984): Tests of new snow density samplers, Proc. of 41 st. Eastern Snow Conference, pages 224-228.

Granberg,H.B. (1984): Sieve analysis of snow, Instrument Report No.5, Terrain Analysis Group, Dept. of Geography, McGill University, Montreal, pages 20.

Grenfell,T.C. (1986): Determination of the liquid water content of snow by the dye dilution technique, Cold Regions Science and Technology, Vol. 12, pages 295-298.

Grenfell,T.C. and Perovich,D.K. (1977): Radiation absorption coefficients of polycrystalline ice from 400-1400 nm, Journal of Geophysical Research, Vol. 86, No. C8, pages 7447-7450

Grum,F and Luckey,G.W. (1968): Optical sphere paint and a working standard of reflectance, Applied Optics, Vol. 7, No. 11, pages 2289-2294.

Irving,W.M. and Pollack,J.B. (1968): Infrared optical properties of water and ice spheres, ICARUS, Vol. 8, pages 324-360.

Jones,E.B., Rango,A. and Howell,S. (1981): Measurements of liquid water content in a melting snow pack using cold calorimeter technique, Proc.of a workshop on microwave remote sensing of snow pack properties. NASA - CP 2153, pages 41-67.

Keeler,C.M. (1969): Some physical properties of Alpine snow. CRREL Research Report 271, 63 pages.

Keyser,J.H. (1981): Chemicals and abrasives for snow and ice control, Handbook of snow, principles, processes, management and use, Pergamon press, pages 580-609.

Kulkarni,A.V. and Navalgund,R. R. (1982): Snow Mapping, seminar cum workshop on application of Bhaskara-II TV and Samir data. Ahmedabad, India, pages CL.13.1-CL13.12.

LaChapelle,E.R. (1956): The centrifugal separation of free water from melting snow, Journal of Glaciology, Vol. 2, No. 20, pages 769-771.

Langham,E.J. (1973): The occurrence and movement of liquid water in the snow pack. Advanced concepts and Techniques in the study of snow and ice resources,National Academy of scicnce, Washington D.C., pages 67-75.

Langham, E.J. (1981): Physics and properties of snow cover. Handbook of snow, principles, processes, management and use, Pergamon press, pages 275-329.

Leaf,C.F. (1966): Free water content of snowpack in Subalpine areas, Proc.of the Western Snow Conference, pages 17-24.

Li,S. (1982): A model for the anisotropic reflectance of pure snow, Discussion paper #4, Dept. of Geography, University of California, Santa Barbara, 61 pages.

Linlor,I., Clapp,F.D., Meier,M.F. and Smith,J.L. (1975): Snow wetness measurements for melt forecasting, Operational Applications of satellite snowcover observations, NASA-SP 391, pages 375-397.

Male,D.H. and Granger,R.J. (1981): Snow surface energy exchange, Water Resources Research, Vol. 17, No. 3, pages 609-627.

Male,D.H. and Gray,D.M. (1981): Snow cover ablation and runoff, Handbook of snow, Principles, Processes, Management and use, Pergamon press,pages 360-430.

Mantis,H.T. et al. (ed.) (1951): Review of the properties of snow and ice, SIPRE Report Number 4, U. S. Army Corps of Engineers. 74 pages.

Manz,D.H. (1974): Interaction of solar radiation with snow, MSc thesis, University of Saskatchewan, Saskatoon (Unpublished).

Mellor,M. (1966): Some optical properties of the snow, Pub. No.69, de l'Association Internationale d'Hydrologic Scientifique, pages 128-140.

Mellor,M. (1977): Engineering properties of snow, Journal of Glaciology, Vol. 19, No. 81, pages 15-66.

Miller,M.N. (1972): Remote measurement of the ice and water content of clouds from Raman scattering, Image Technology, Vol. 14, No. 2, pages 17-23.

O'Brian,H.W.and Koh,G. (1981): Near-infrared reflectance of snow cover substrate, Cold Region Research and Engineering Laboratory, Research Report 81-21, 17 pages.

O'Brian,H.W. and Munis,R.H. (1975): Red and nearinfrared spectral reflectance of snow, Cold Region Research and Engineering Laboratory, Research Report 332, 18 pages.

O'Neill,A.D.J. and Gray, D.M. (1972): Solar radiation penetration through snow. Proc. of the International Symposium on the Role of Snow and Ice Hydrology, Banff, Canada, pages 277-241.

Petzold,D.E. (1974): Solar and net radiation over snow. Climatological Research Series, No. 9, Dept. of Geography, McGill University, Montreal, 77 pages.

Price,A.G. (1977): Snowmelt runoff processes in a subarctic area, Climatological Research Paper No. 10, Dept. of Geography, McGill University, Montreal, 104 pages.

Rango,A. (1985): Assessment of remote sensing input to hydrologic models, Water Resources Bulletin, Vol. 7, No. 1, pages 423-432.

Radok,U., Stephens,S.K., Sutherland,K.L. (1961): On the calorimetric determination of snow quality, Publication Number 54, de l'Association International d'Hydrologie Scientifique, pages 132-135.

Sauberer, F. (1938): Versuche uber spektrale messungen der Strahlungseigenschaften von Schnee und Eis mit Photoelementen, Meteorologische Zeitschrfit, 55(7), pages 250-255.

Schwerdtfeger,P. and Weller,G.E. (1977): Radiative heat transfer processes in snow and ice, Meteorological studies at plateau station, Antarctica, Antarct. Res. Ser., Vol. 25, edited by J.A.Businger, pages 35-39.

Slaughter,C.W. (1969): Snow albedo modification a review of literature, CRREL Technical Report 217, 24 pages.

Staenz,K. and Haefner,H. (1981): Spectral reflectance properties of snow in the Landsat MSS bands, Canadian Journal of Remote Sensing, Vol. 7, No. 1, pages 41-50.

Stiles,W.H. and Ulaby,F.T. (1980): Microwave remote sensing of snowpack, NASA-CR 3263, pages 157-172.

Trainor,L.E.H. (1947): The spectral reflectance and absorbtion of radiation by snow, M.A.Thesis, Dept. of Physics, University of Saskatchewan, Saskatoon, Saskatchewan. (Unpublished).

Wakahama,G. (1968): The metamorphism of wet snow, Publication No. 79 de l'Association International d'Hydrologie Scientifique, pages 370-379.

Warren,S.G. (1982): Optical properties of snow, Review of Geophysics and Space Physics, Vol. 20, No. 1, pages 67-89.

Warren,S.G. and Wiscombe,J.W. (1981): A model for the spectral albedo of snow II: snow containing atmospheric aerosoles, Journal of Atmospheric Science, Vol. 37, pages 2734-2744.

Weller,G.E. (1969): Radiation diffusion in Antarctic ice media, Nature, Vol. 221, No. 5178, pages 355-356.

Wiscombe,W.J. and Warren,S.G. (1981): A model for the spectral albedo of snow I: pure snow. Journal of Atmospheric Science, Vol. 37, pages 2712-2733.

Yoshida,Z. (1967): Free water content of wet snow, Proc. International Conference on Low Temperature Science, Vol. 1, Pt. 2, pages 80-87.

APPENDIX A

GRAPHS SHOWING SPECTRAL ATTENUATION AND EXTINCTION COEFFICIENT AT SITE 2

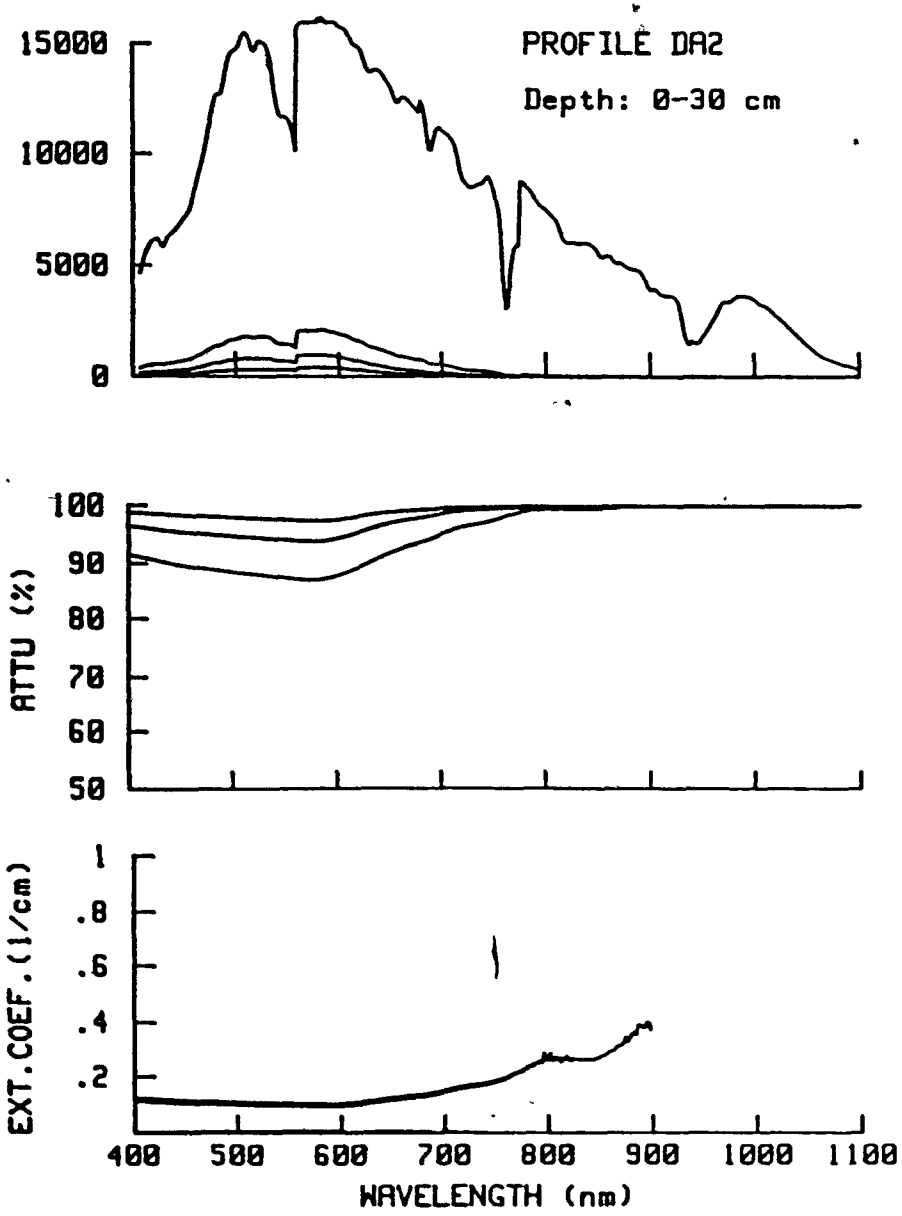
PROFILE DA2
Depth: 0-30 cm
15000
10000
5000
0
100
90
80
70
60
50
ATTU (%)
1
.8
.6
.4
.2
EXT.COEF.(1/cm)
400
500
600
700
800
900
1000
1100
WAVELENGTH (nm)

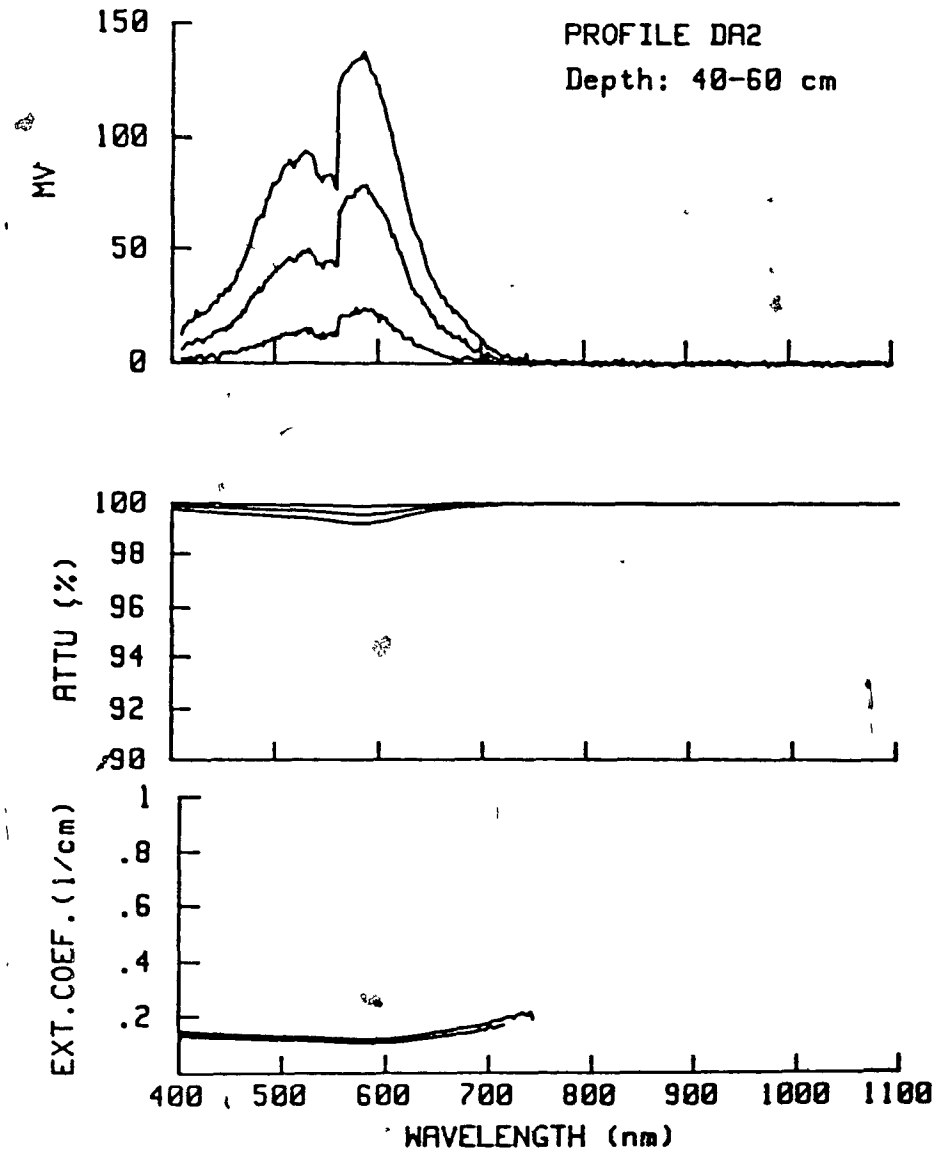
PROFILE DA2
Depth: 40-60 cm
150
100
50
0
MV
100
98
96
94
92
90
ATTU (%)
1
.8
.6
.4
.2
EXT.COEF.(1/cm)
400
500
600
700
800
900
1000
1100
WAVELENGTH (nm)

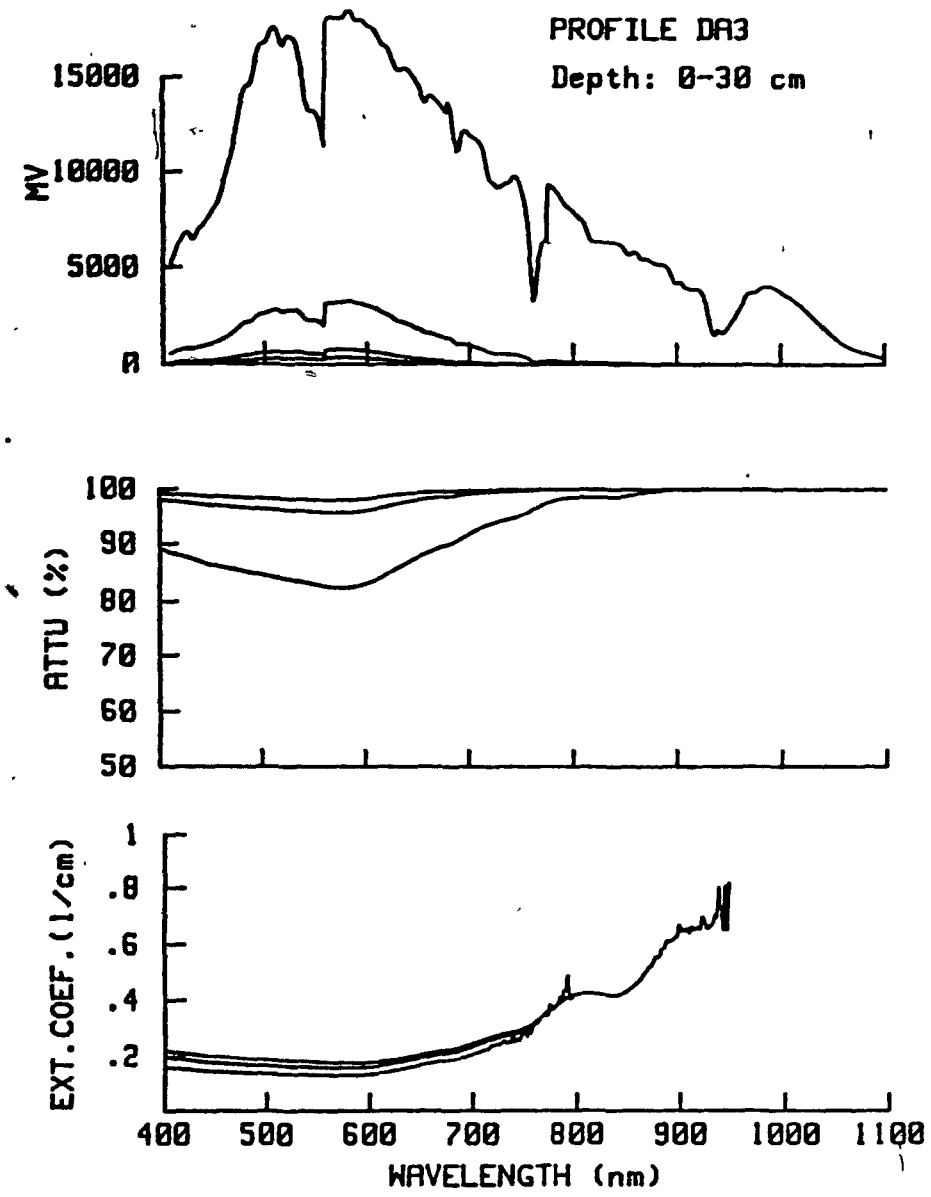
PROFILE DA3
Depth: 0-30 cm
MV
15000
10000
5000
0
ATTU (%)
100
90
80
70
60
50
EXT.COEF.(1/cm)
1
.8
.6
.4
.2
400
500
600
700
800
900
1000
1100
WAVELENGTH (nm)

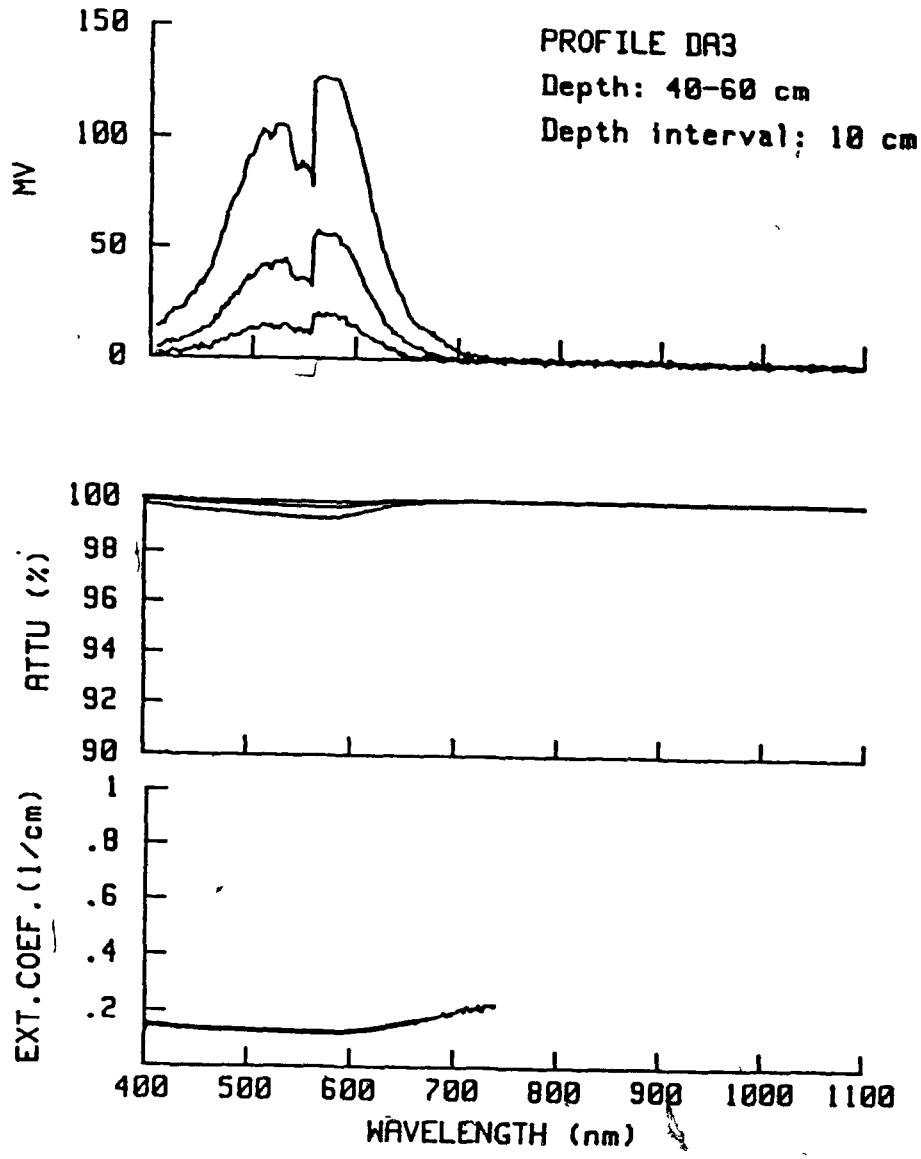
PROFILE DA3
Depth: 40-60 cm
Depth interval: 10 cm
MV
150
100
50
0
ATTU (%)
100
98
96
94
92
90
EXT.COEF.(1/cm)
1
.8
.6
.4
.2
400
500
600
700
800
900
1000
1100
WAVELENGTH (nm)

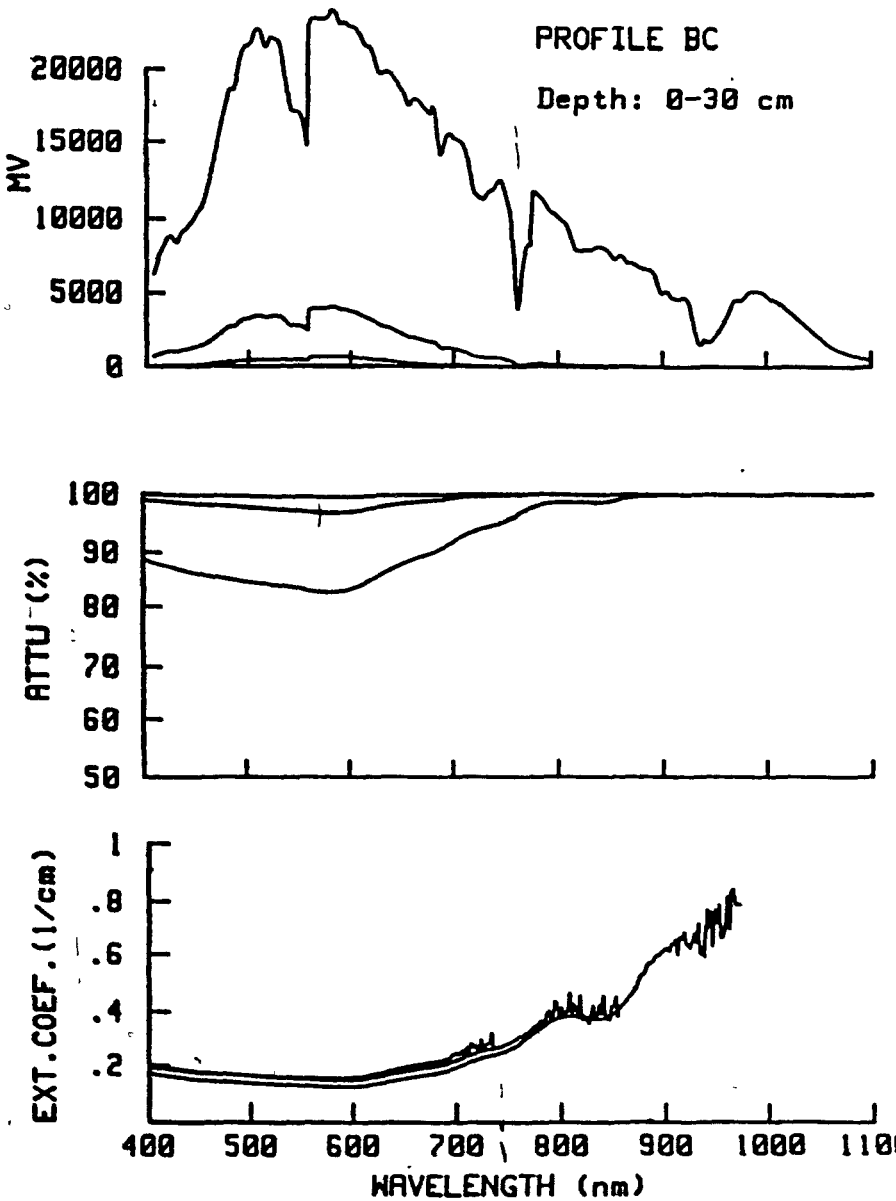
PROFILE BC
Depth: 0-30 cm
MV
20000
15000
10000
5000
0
ATTU (%)
100
90
80
70
60
50
EXT.COEF.(1/cm)
1
.8
.6
.4
.2
400
500
600
700
800
900
1000
1100
WAVELENGTH (nm)

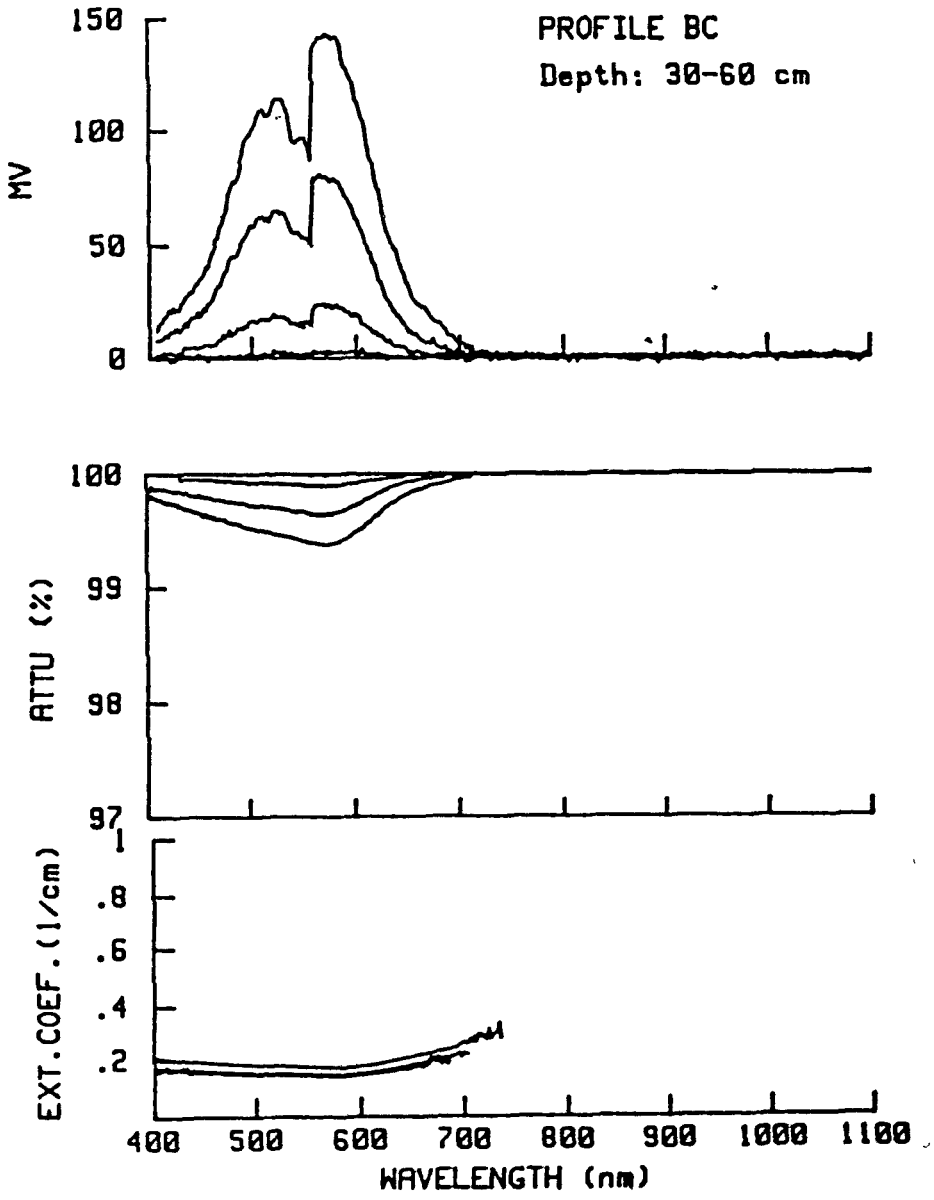
PROFILE BC
Depth: 30-60 cm
MV
150
100
50
0
ATTU (%)
100
99
98
97
EXT.COEF.(1/cm)
1
.8
.6
.4
.2
400
500
600
700
800
900
1000
1100
WAVELENGTH (nm)

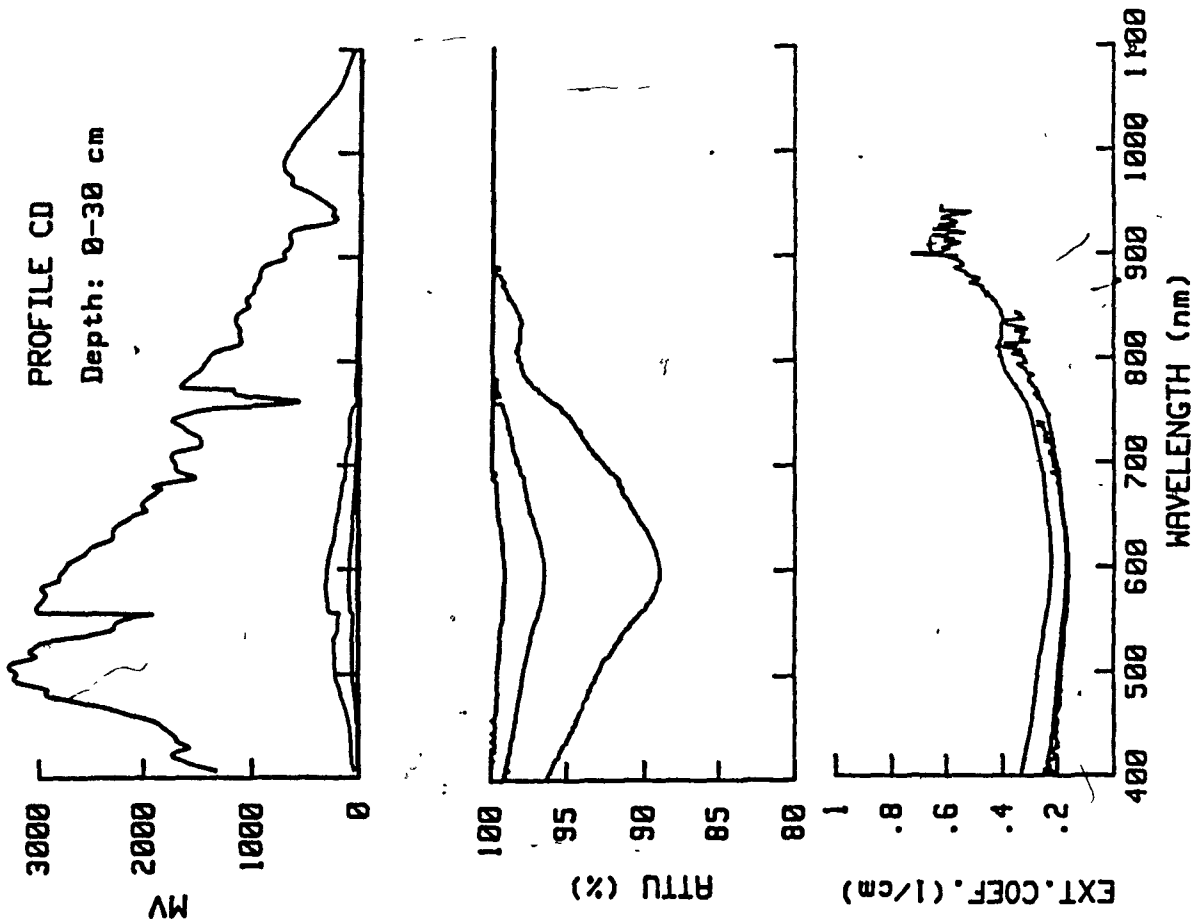
PROFILE CD
Depth: 0-30 cm
MV
3000
2000
1000
0
RTTU (%)
100
95
90
85
80
EXT.COEF. (1/cm)
1
.8
.6
.4
.2
400
500
600
700
800
900
1000
1100
WAVELENGTH (nm)

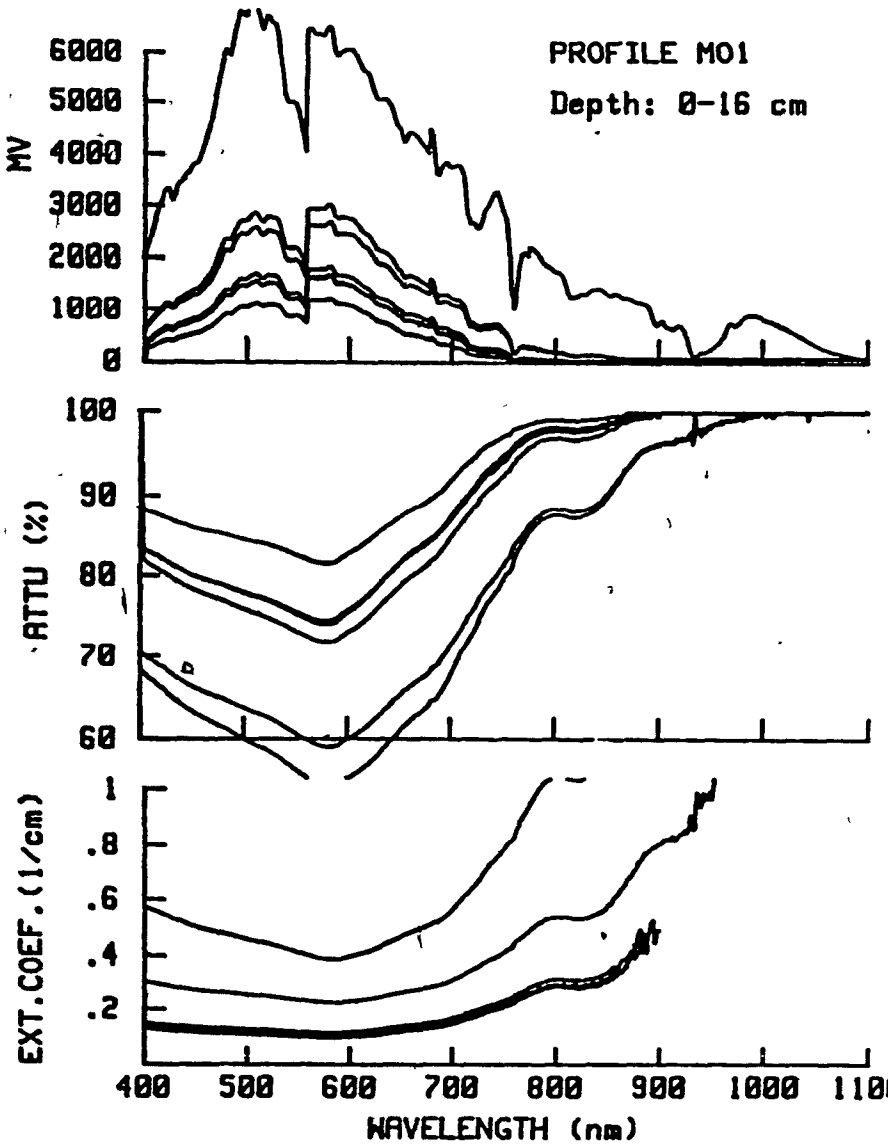
PROFILE M01
Depth: 0-16 cm
MV
6000
5000
4000
3000
2000
1000
0
ATTU (%)
100
90
80
70
60
EXT.COEF.(1/cm)
1
.8
.6
.4
.2
400
500
600
700
800
900
1000
1100
WAVELENGTH (nm)

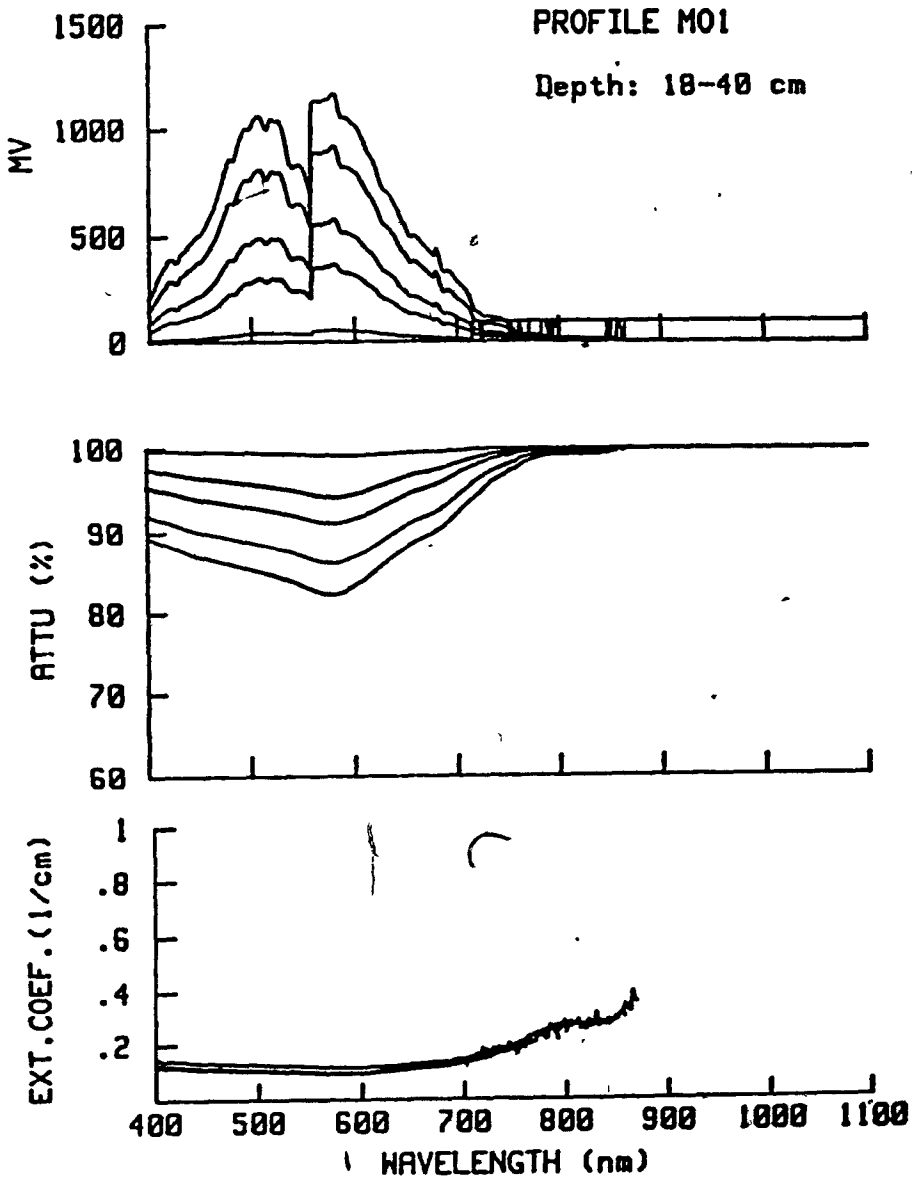
PROFILE M01
Depth: 18-40 cm
MV
1500
1000
500
0
ATTU (%)
100
90
80
70
60
EXT.COEF.(1/cm)
1
.8
.6
.4
.2
400
500
600
700
800
900
1000
1100
WAVELENGTH (nm)

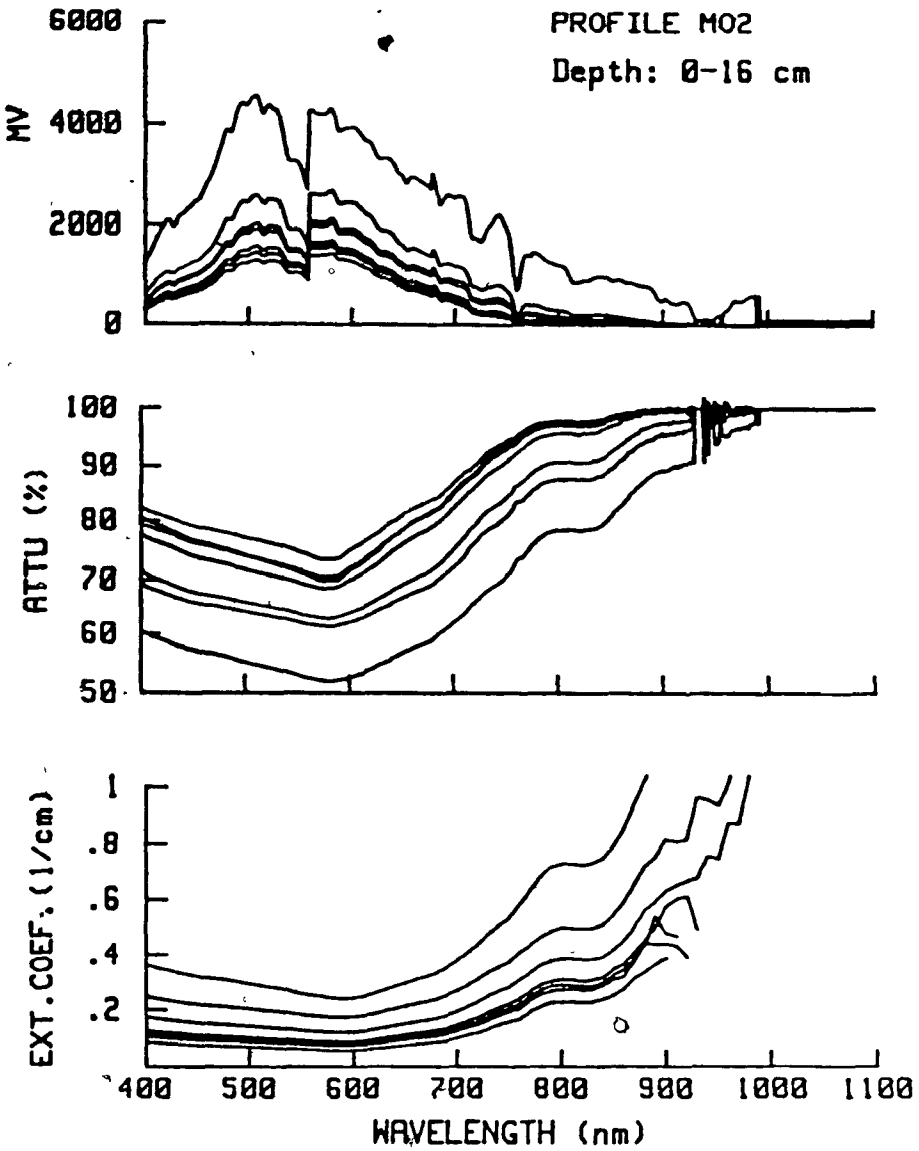
PROFILE M02
Depth: 0-16 cm
MV
6000
4000
2000
0
ATTU (%)
100
90
80
70
60
50
EXT.COEF.(1/cm)
1
.8
.6
.4
.2
400
500
600
700
800
900
1000
1100
WAVELENGTH (nm)

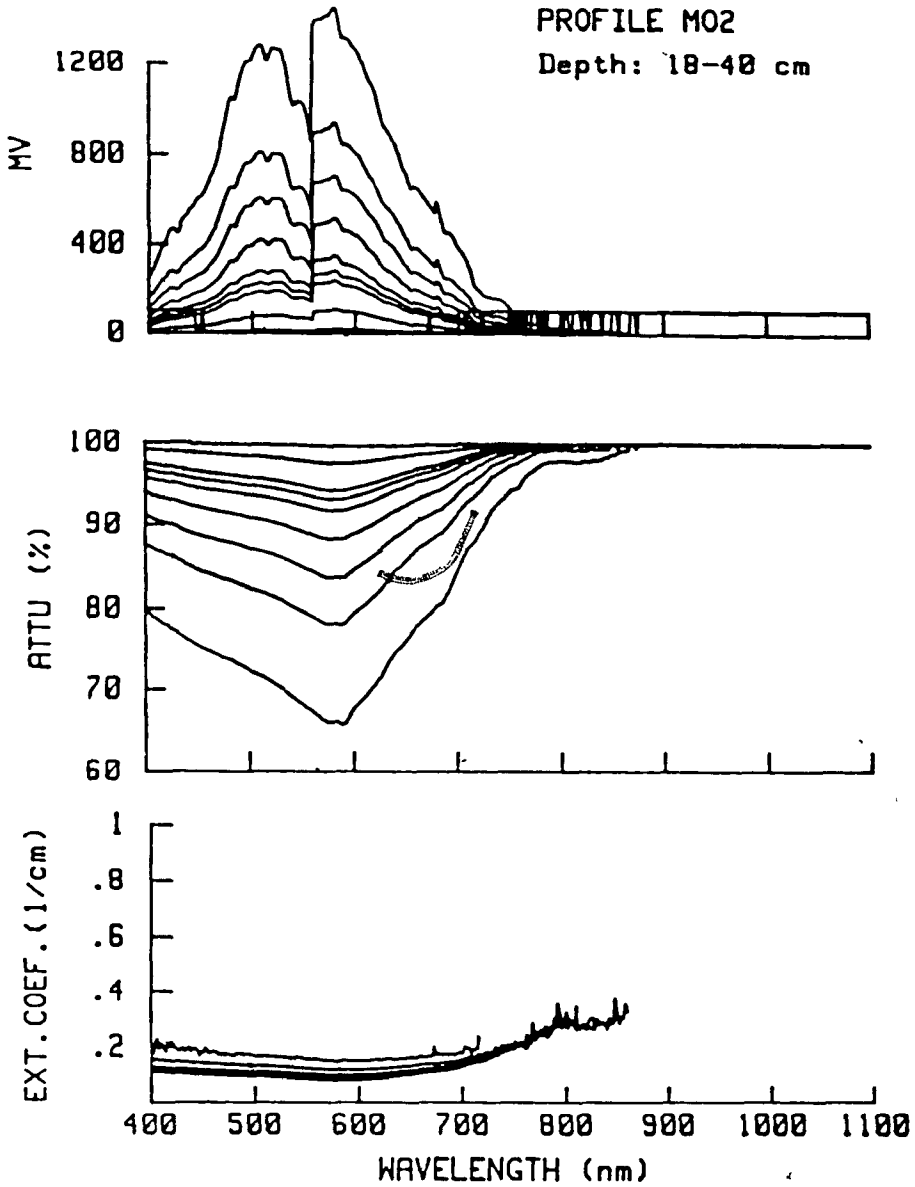
PROFILE M02
Depth: 18-40 cm
MV
1200
800
400
0
ATTU (%)
100
90
80
70
60
EXT.COEF.(1/cm)
1
.8
.6
.4
.2
400
500
600
700
800
900
1000
1100
WAVELENGTH (nm)

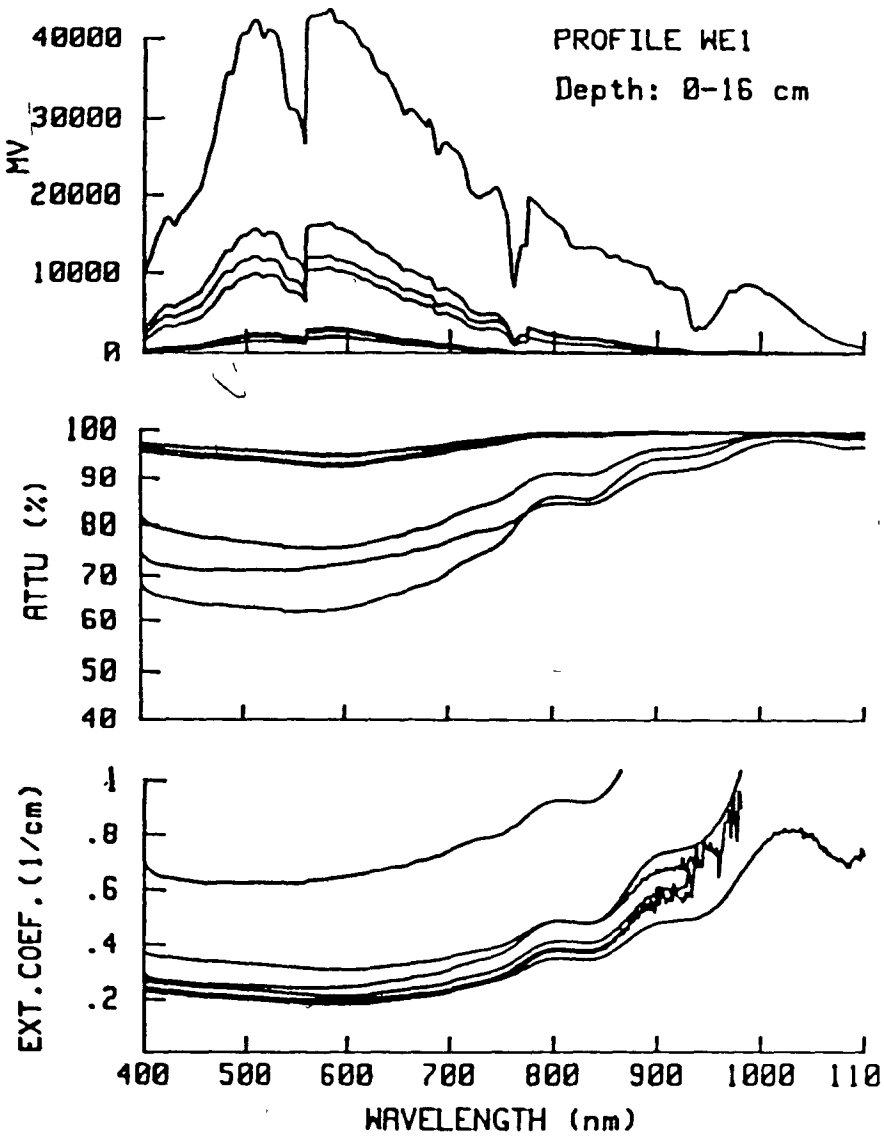
PROFILE WE1
Depth: 0-16 cm
MV
40000
30000
20000
10000
0
ATTU (%)
100
90
80
70
60
50
40
EXT.COEF.(1/cm)
1
.8
.6
.4
.2
400
500
600
700
800
900
1000
1100
WAVELENGTH (nm)

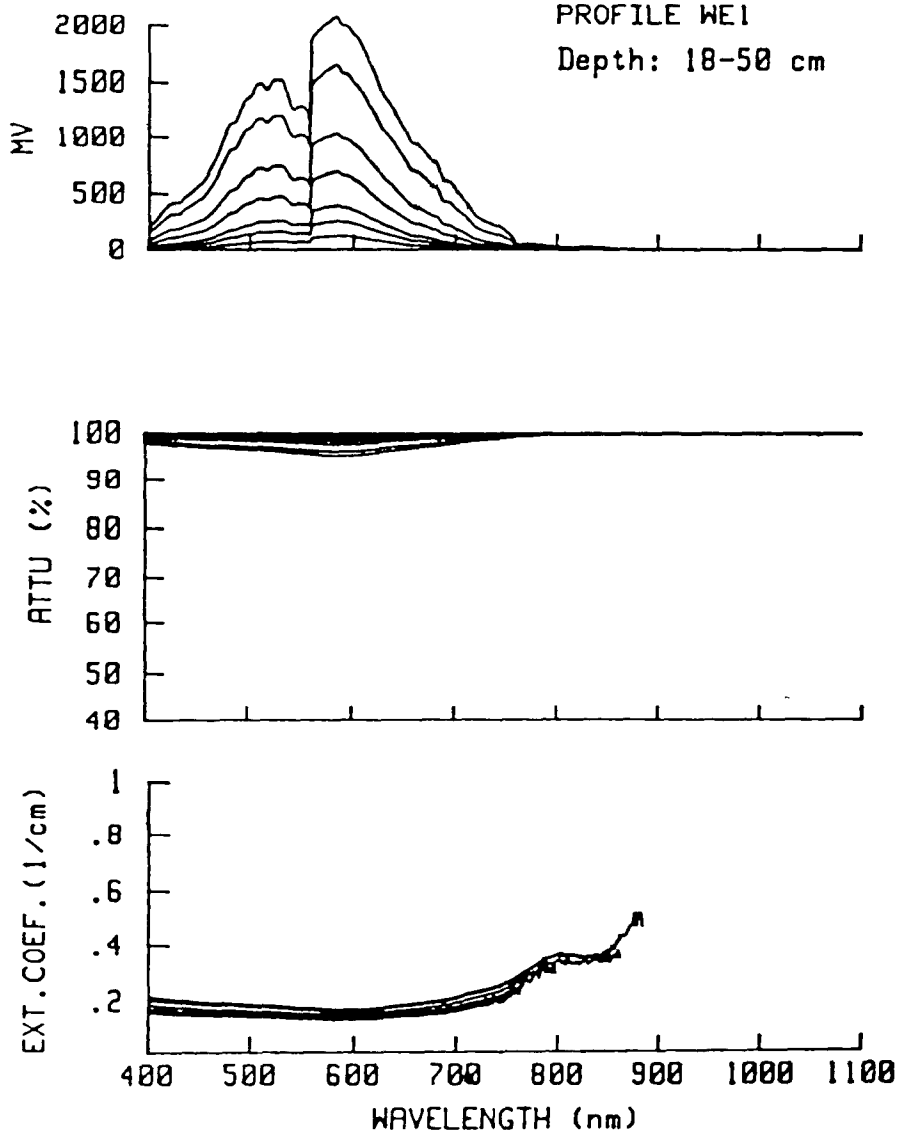
PROFILE WE1
Depth: 18-50 cm
MV
2000
1500
1000
500
0
ATTU (%)
100
90
80
70
60
50
40
EXT.COEF.(1/cm)
1
.8
.6
.4
.2
400
500
600
700
800
900
1000
1100
WAVELENGTH (nm)

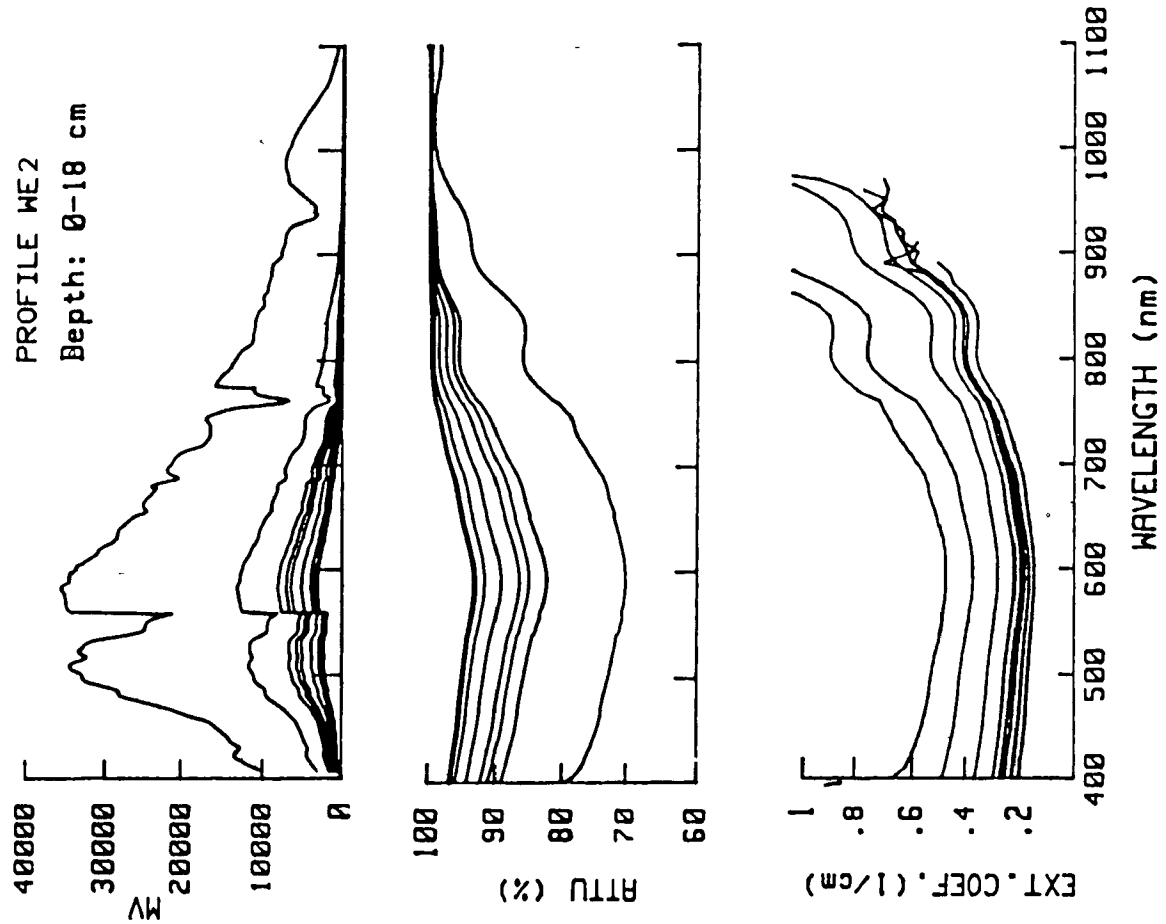
PROFILE WE2
Depth: 0-18 cm
40000
30000
20000
10000
0
MV
100
90
80
70
60
RTTU (%)
1
.8
.6
.4
.2
EXT.COEF.(1/cm)
400
500
600
700
800
900
1000
1100
WAVELENGTH (nm)

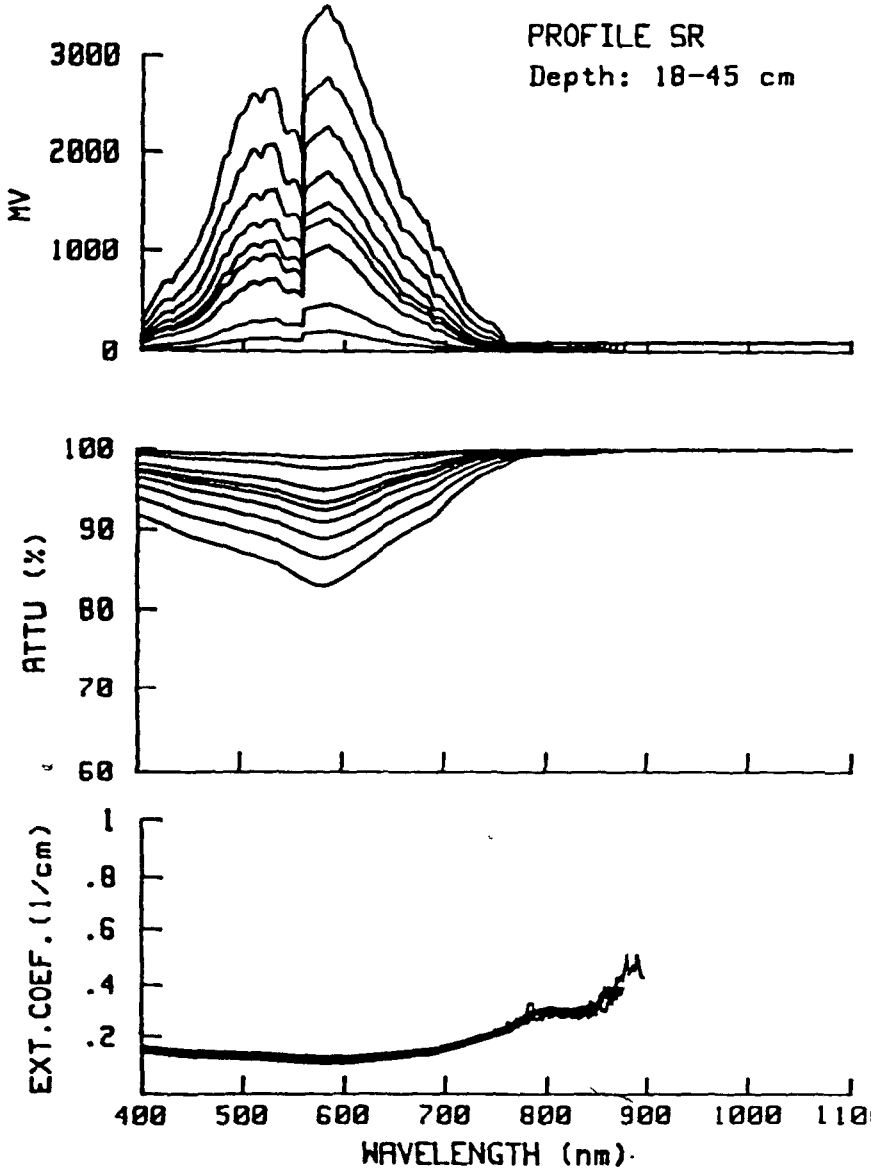
PROFILE SR
Depth: 18-45 cm
MV
3000
2000
1000
0
ATTU (%)
100
90
80
70
60
EXT.COEF.(1/cm)
1
.8
.6
.4
.2
400
500
600
700
800
900
1000
1100
WAVELENGTH (nm)

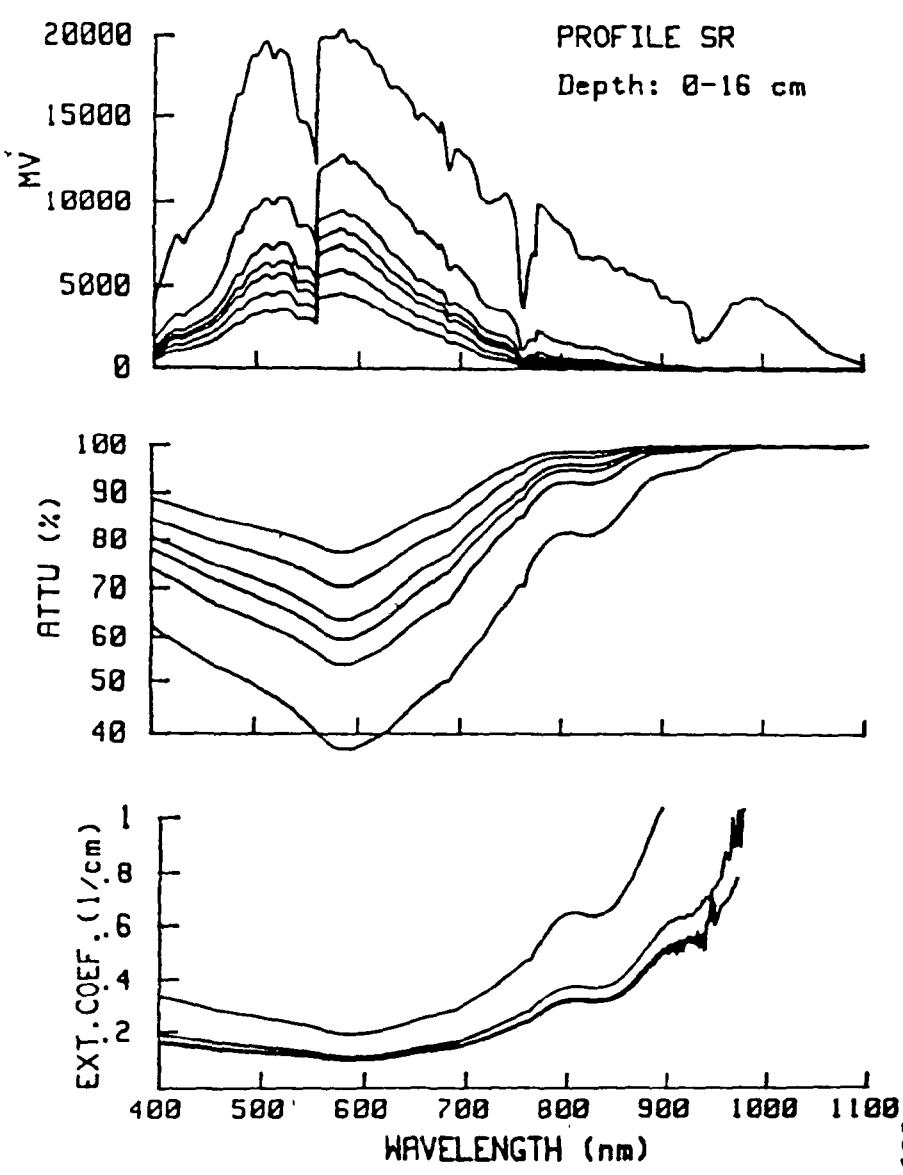
PROFILE SR
Depth: 0-16 cm
MV
20000
15000
10000
5000
0
ATTU (%)
100
90
80
70
60
50
40
EXT.COEF.(1/cm)
1
.8
.6
.4
.2
400
500
600
700
800
900
1000
1100
WAVELENGTH (nm)

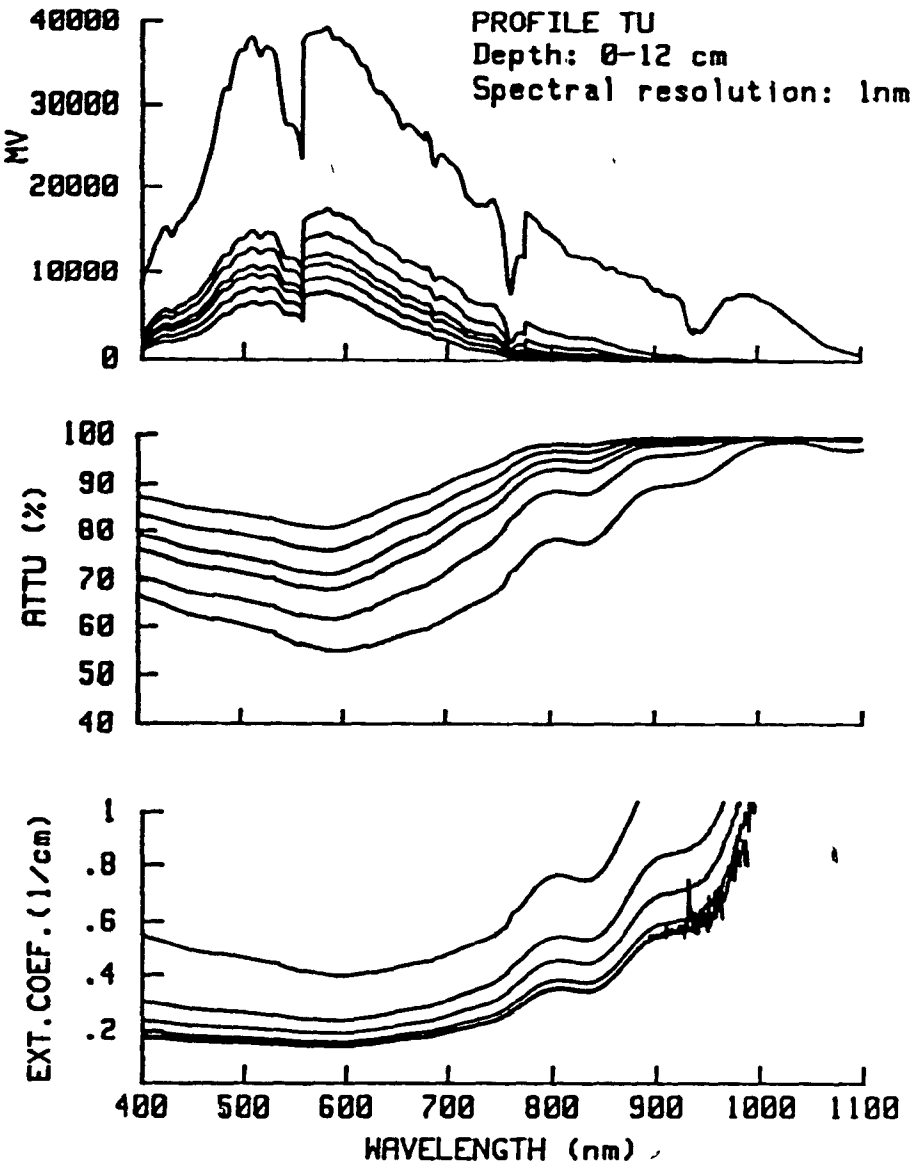
PROFILE TU
Depth: 0-12 cm
Spectral resolution: 1nm
MV
40000
30000
20000
10000
0
ATTU (%)
100
90
80
70
60
50
40
EXT.COEF.(1/cm)
1
.8
.6
.4
.2
400
500
600
700
800
900
1000
1100
WAVELENGTH (nm)

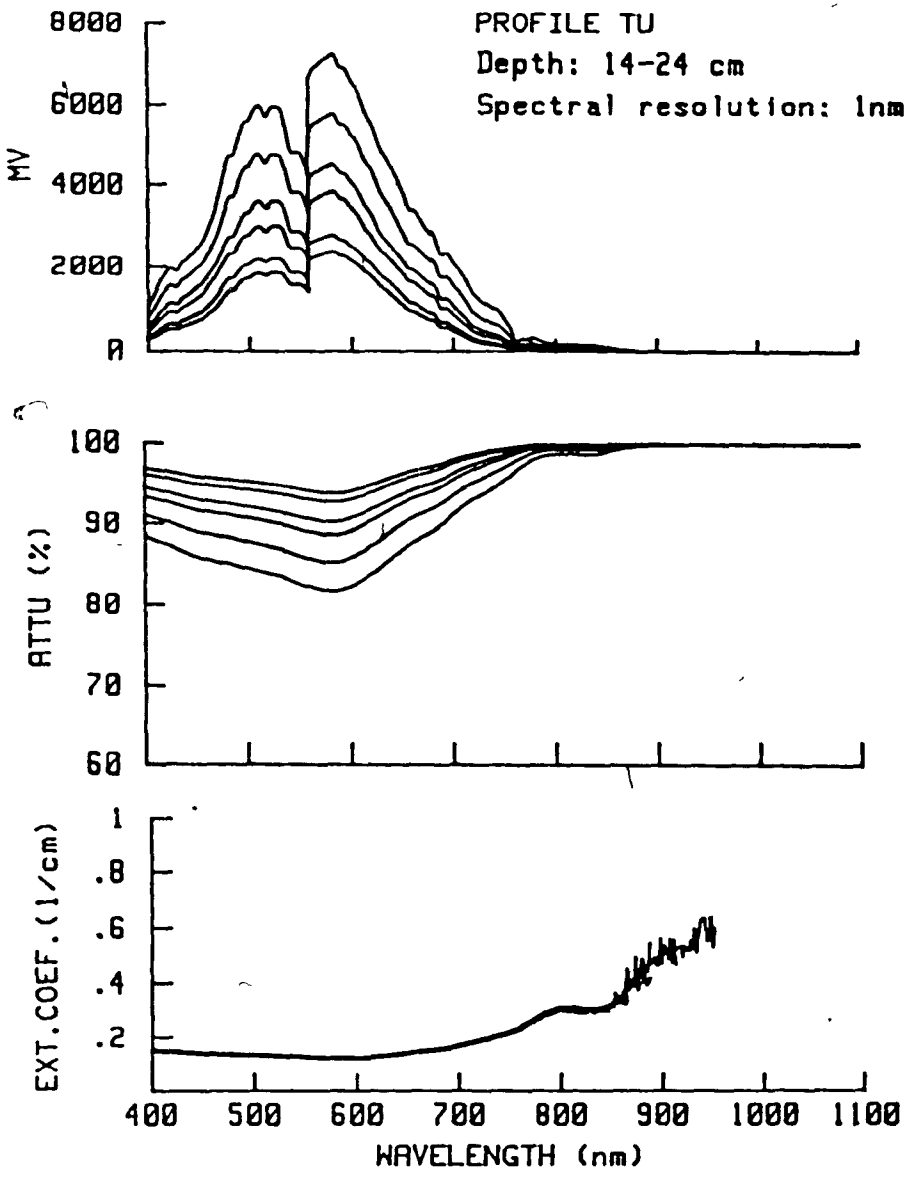
PROFILE TU
Depth: 14-24 cm
Spectral resolution: 1nm
MV
8000
6000
4000
2000
0
ATTU (%)
100
90
80
70
60
EXT.COEF.(1/cm)
1
.8
.6
.4
.2
400
500
600
700
800
900
1000
1100
WAVELENGTH (nm)

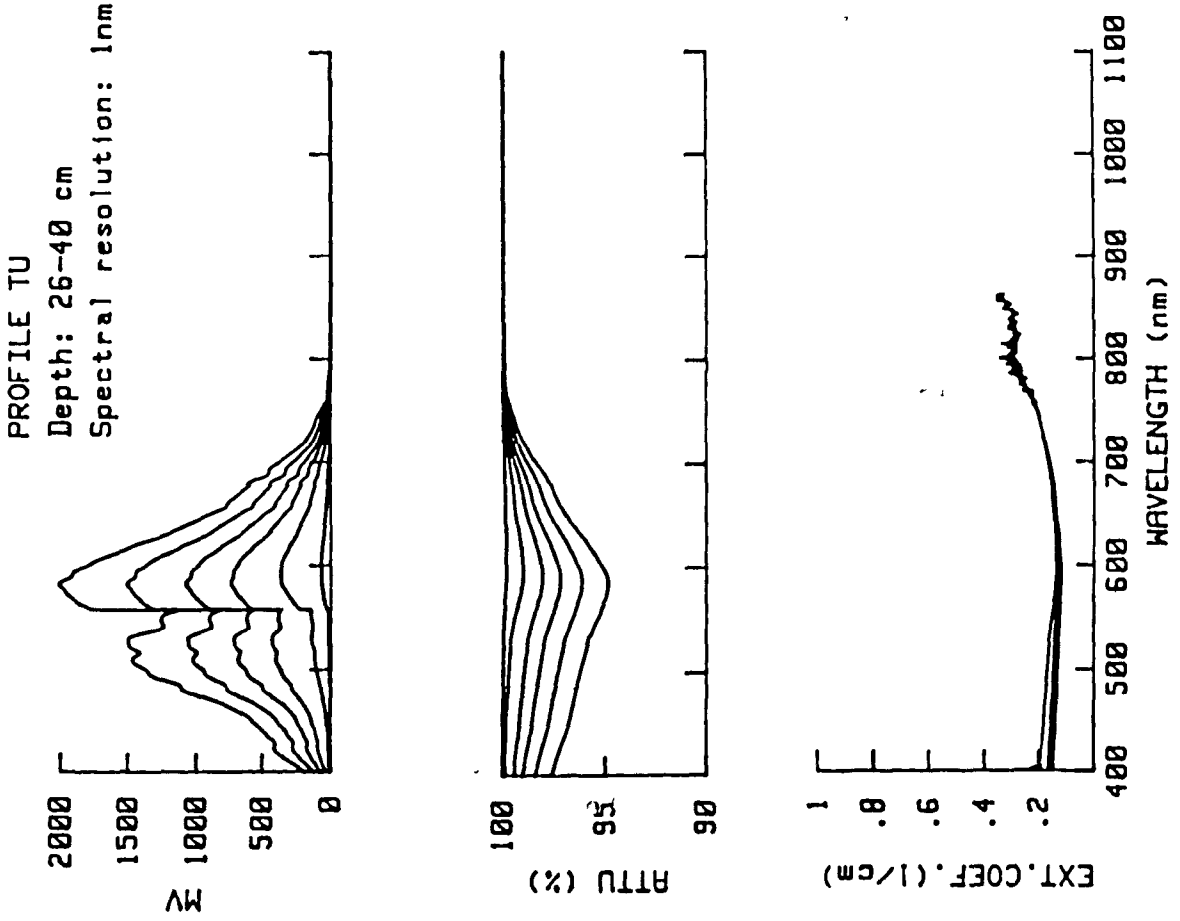
PROFILE TU
Depth: 26-40 cm
Spectral resolution: 1nm
MV
2000
1500
1000
500
0
RTTU (%)
100
95
90
EXT.COEF.(1/cm)
1
.8
.6
.4
.2
400
500
600
700
800
900
1000
1100
WAVELENGTH (nm)